Dear Editor and Referees,

Thank you for your review of our manuscript. We greatly appreciate the substantial amount of time and effort that you dedicated to this review process.

We have revised the manuscript according to your comments and the point-by-point response is also attached in this file. The marked-up manuscript version showing the changes made is also provided as follow. Please note that the numbers of tables and figures mentioned in this revised manuscript are different from those in the former manuscript.

In order to facilitate access to the response, the corresponding page number ranges are listed below and you can also link to the corresponding section by clicking the hyperlink:

Thanks again.

Kind regards.

Songhua Wu

----------Reviewer Comments----------

1. Reviewer 1

General comments:

This manuscript presents the results of wind measurements by coherent Doppler lidar from a ship in the Yellow Sea. The authors give a description of the algorithm for processing lidar data, which makes it possible to compensate for the measurement error associated with the motion of the ship. The results of joint measurements of height wind profiles by lidar and radiosonde are analyzed. The paper may be of interest to the readers of AMT. However, when describing the experiment and the data processing procedure, excessive attention is paid to secondary issues, and important details are ignored. Sometimes

the terminology used by the authors makes it difficult to understand what they mean and how they obtained results presented in the manuscript. Some results raise doubts about their correctness:

1) The authors assume that the bias of lidar estimate of the wind velocity is associated only with errors in determination of the ship speed and direction and with the pointing angle knowledge errors (Section 3.3). One can agree with this, if lidar estimates of the radial velocity are obtained at a sufficiently high signal-to-noise ratio (SNR, ratio of the signal spectrum peak to the standard deviation of noise component of the spectrum estimate), when the probability (or fraction) of a bad (unreliable) estimate of the radial velocity is practically zero. However, results shown in Fig.9 for heights above 2 km were obtained at SNR =2 dB when the probability of bad estimate b = 0.3. As shown in Fig.4, true wind speed V = 5 m/s at a height of 2 km. According to the theory (Frehlich, R.G. and Yadlowsky, M.J.: Performance of mean-frequency estimators for Doppler radar and lidar, Journal of Atmospheric and Oceanic Technology 11(5), 1217-1230, 1994), the bias of velocity estimate BIAS = <Vˆ> - V, where <...> is ensemble averaging and Vˆ is the velocity estimate, is determined by the equation: BIAS = -b*V. Therefore at b = 0.3 and V = 5 m/s the bias equals -1.5 m/s. Nevertheless, in Fig. 9(Ñ ¸ A) we see that the bias is about zero at SNR = 2.

R: I did not explain it clearly. The random error of radial velocity e_V in an individual Doppler Lidar velocity estimate is dependent on the signal-to-noise ratio (SNR) of the measurement. It can be evaluated based on the frequency spectrum of the retrieved velocity, which is applied for vertical velocity random error estimation in this paper, and we can also use the velocity differences from even- and odd-numbered pulses to estimate the random error (Frehlich 2001). As for the random error of horizontal velocity, we need firstly obtain the random error of each radial velocity that is used for 4-DBS wind profile. Then the radial velocity error should be scaled into the horizontal velocity error based on the relationship between horizontal velocity components U, V and the radial velocity.

As for the bias in this paper, we deal with the derivation of systematic errors (bias) to the horizontal wind retrieval. The error sources from the knowledge of the ship velocity and the lidar pointing angle are systematic part, and it is assumed that the random error part of the ship velocity and the lidar pointing angle is zero, which is reasonable and robust for horizontal wind retrieval according to the specific parameters of lidar, GNSS and INS. The small bias at SNR=2 in Fig.9 actually represents the bias from the contribution of knowledge error of ship velocity and lidar pointing angle.

However, the bias of velocity estimates BIAS= <Vˆ> - V, as the referee mentioned, is different from the definition in this paper. The definition of bias in this paper is $bias_v = \hat{V} - V_{truth} - e_V$, where $\hat{V}$ is the measured velocity estimate, V_{truth} is the desired or true wind measurement and e_V is the random error. It can be seen that the BIAS referee mentioned is the sum of

$bias_v$ and e_V. As for the BIAS = -b*V=-0.3*5=-1.5 m/s, the referee mentioned, actually I really wonder how the b=0.3 is determined. It is mentioned in Frehlich's paper that the empirical model for the fraction of bad estimates b as a function of Φ for fixed Ω and M is: $b(\Phi) = [1 + (\frac{\Phi}{b_0})^{\alpha}]^{-\gamma}$. It is noted that the in this paper SNR is defined as the ratio of the peak value of FFT spectral signal in each range bin to the Root-Mean-Square (RMS) of background noise signal, which is different from Frehlich's paper definition and need to be treated carefully when determining those parameters. It would be possible to compare bias of two systems if we know the details of Frehlich's empirical model.

2) Fig.9 (b) shows the random error of wind velocity. On the other hand, the second term on the right-hand side of Eq. (11) is defined as the random error with zero mean. It is unclear how the result shown in Fig.9 (b) was obtained. It is necessary to describe in more detail the procedure for obtaining this result. The results shown in Fig. 4 and Fig. 9 are obtained from the same lidar data (measurements from 15:52 to 16:02 on May 9, 2014)?

R: Various methods of estimating the magnitude of the random error of Doppler Lidar velocity measurements have been introduced (Frehlich 2001). The measurements of error from velocity spectrum are used in this paper. A 50 % window overlap factor, a Hamming window is used in order to reduce the leakage in the spectra. A zero-padding of the missing values were applied to each window for each spectrum calculation to improve the frequency resolution. The constant high-frequency region of velocity spectrum higher than 0.2 Hz, shown in Figure 1 below, represents uncorrelated random error contribution, which is departing from the Kolmogorov's -5/3 law. The random error of vertical wind velocity is estimated as the standard deviation of the measured signal after high-pass filter.

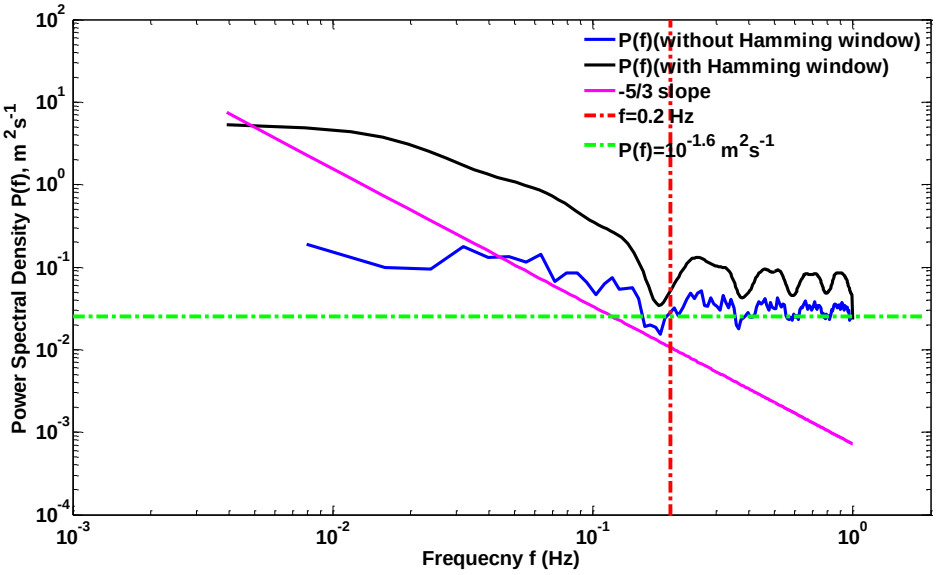

Figure 1: Power spectral density P(f) without and with Hamming window for the CDL measured vertical speed between 15:52 and 16:02 LST on 09 May and for an altitude of 1495 m (blue and black solid line, respectively). The expected spectral behavior according to the Kolmogorov's−5/3 law (pink solid line), the noise frequency threshold (red dotted line) and the derived noise floor for the CDL (green dotted line) are shown.

The results shown in Fig. 4 and Fig. 9 are obtained from the same lidar data (measurements from 15:52 to 16:02 on May 9, 2014).

3) How can SNR be determined below 2 dB, if in this case with a high degree of probability the peak in the measured spectrum is associated with the noise, but not with the signal?

R: The SNR in this study is defined as the ratio of the peak value of FFT spectral signal in each range bin to the Root-Mean-Square (RMS) of background noise signal. Figure 1 shows the array of the spectral $S(l\Delta f;k\Delta R)$, where $l=0,1,2,3,...,L-1$ is the spectral channel number and $L=100$. In this case the frequency resolution $\Delta f \approx 0.98$ MHz and the corresponding velocity resolution is $\Delta V = 0.76$ ms^{-1}. The bandwidth $B_{100}=(L-1)\Delta f = 97.68$ MHz, and the corresponding radial velocity measurement range is ± 37.5 ms^{-1}. Figure 1a shows the last 10 range gates raw array of spectral in green line. We estimate the averaged background noise spectrum

$$\overline{S}_N(l\Delta f)=\frac{1}{10}\sum_{k=94}^{103}S(l\Delta f;k\Delta R) \tag{8}$$

Subtracting the background noise spectral $\overline{S}_N(l\Delta f)$ from the raw spectral array $S(l\Delta f;k\Delta R)$, the unnoisy array of spectral $S(l\Delta f;k\Delta R)$ can be obtained and shown in red line in Fig. 1. The peak value index l_{peak} from the $S(l\Delta f;k\Delta R)$ can be firstly obtained and thus the absolute signal power $P_s(k\Delta R)$ at various ranges $k\Delta R$ can be represented as:

$$P_s(k\Delta R)=S(l_{peak}\Delta f;k\Delta R)-\frac{1}{12}\left(\sum_{l_{peak}-20}^{l_{peak}-15}S(l\Delta f;k\Delta R)+\sum_{l_{peak}+15}^{l_{peak}+20}S(l\Delta f;k\Delta R)\right) \tag{9}$$

Replacing integration by summation and taking into account that the zero velocity point in one channel is $l_{zero}=50$, we estimate the noise power P_N as

$$P_N=\frac{1}{10}\sum_{k=94}^{k=103}\sqrt{\frac{1}{21}\sum_{l=l_{zero}-10}^{l_{zero}+10}\hat{S}_N(l\Delta f;k\Delta R)^2} \tag{10}$$

Finally, we obtain the range profile of the $SNR(k\Delta R)$ using the equation

$$SNR(k\Delta R) = 10\log_{10}\left(\frac{P_s(k\Delta R)}{P_N}\right) \quad (11)$$

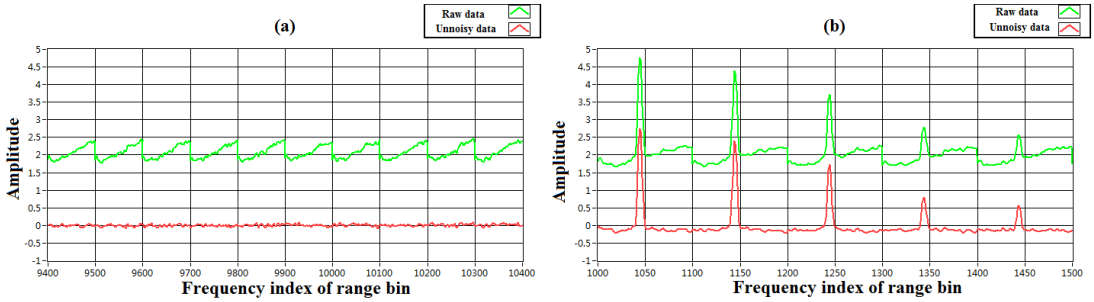

Figure 1: The CDL measured array of the FFT spectra (a) the last 10 range gates spectra for background noise spectrum estimation (b) the 1st – 5th range gates (150 m – 270 m, range resolution is 30 m) spectrum.

The SNR from Banakh et al. 2013 is defined as the ratio of the averaged heterodyne signal power P_s to the average detector noise power P_n in a 50-MHz bandwidth. The power P_s and P_n are integrals of the spectral densities $S_s(f)$ and $S_n(f)$, respectively, in frequency f within a band of width B_{50}, that is:

$$P_s = \int_{B_{50}} S_s(f)df \quad (5)$$

$$P_n = \int_{B_{50}} S_n(f)df \quad (6)$$

Comparing the definition from Banakh et al. 2013, the SNR in this paper is simpler and also indicates the CDL detection capability, data accuracy and atmospheric tracer particle relative intensity. In this sense, the SNR threshold value in this paper is higher than the one in previous studies (Banakh et al. 2013; Achtert et al 2015) for the same signal power spectrum.

Specific comments

1) Page 3, lines 27-30: The pulse energy depends on the pulse width? If so, what is the pulse energy (and pulse repetition rate) for pulse durations of 100, 200 and 400 ns?

R: I did not explain it clearly. The pulse energy is fixed and the pulse width is configurable. Pulse width is the full width at half maximum of the laser pulse waveform. A wider pulse width results in a larger measurement blind spot, but increases the average power and detection distance of the laser. Narrower pulse width can reduce the measurement of blind spots, but must also reduce the average power of the laser in order to control the laser peak power within the maximum range of the fiber, that is, will reduce the detection range.

The description in the revised manuscript is: “The achieved pulsed energy is approximately 150 μJ and the pulse repetition frequency is 10 kHz .”

2) In section 2 the following information should be added:

a) width of the time window (T) for obtaining the lidar signal power spectrum (T equals probing pulse duration of 200 ns?);

R: T=200 ns.

“The pulse width produced by the modulation, which is also the width of time window for obtaining the lidar signal power spectrum, is adjustable from 100 ns to 400 ns , thus the spatial resolution can be varied from 15 m to 60 m . We typically operate the CDL with a pulse width of 200 ns in this study.”

b) width of the frequency band (B) within which the radial velocity was estimated from the lidar signal power spectrum (B = 50 MHz?);

R: The bandwidth $B_{100} = (L-1)\Delta f = 97.68$ MHz is used for radial velocity estimation. The specific introduction can be seen in the answer to general comment question 3.

c) number of laser shots used for the spectral accumulation;

R: N=5000

d) number of radial velocity estimates (for each range) that were obtained from lidar measurement for 10 minutes and then they were used for obtaining one estimate the wind vector.

R: Both the determination of the ship-induced Doppler shift and the radial velocity have the same temporal resolution of 0.5 s. Figure 4 in the revised manuscript shows the flowchart of shipborne CDL data processing. Specifically, the LOS velocity and Signal to Noise Ratio (SNR) can be firstly determined using lidar data and FFT analysis. After the data pre-processing including the quality control based on SNR threshold, the attitude transformation is then used to obtain the azimuth and elevation in each LOS vector in Earth coordinate system with temporal resolution of 0.5 s. The LOS velocity detected by lidar is the atmosphere motion relative to ship coordinate system, thus the removal of the along-beam platform velocity due to ship motion is needed. In this study, the horizontal wind profile with 2-min temporal resolution will be retrieved for vertical velocity correction. Basically, the LOS velocities from N, S, E, and W direction after SNR quality control during the chosen 2-min interval are collected firstly. Then the procedure of filtration of reliable estimates of each radial velocity based on SNR threshold is used to obtain “good” speed estimates. The selected radial velocities and corresponding ship condition information in each radial direction are averaged and the averaged ship condition will be used for the removal of platform velocity effect. Finally, the horizontal with 2-min temporal resolution can be retrieved using modified 4-DBS mode. The vertical wind measurement has a temporal resolution of 0.5 s, the horizontal wind whose retrieved time is closest to vertical wind measured time will be used for vertical velocity correction.

3) Add the tele-scope diameter and beam diameter (1/e**2) to Table 1

R: The parameters have added to the Table 1 in revised version.

Telescope diameter	3 inches
Beam effective diameter	60 mm
Focal length	290 mm

4) Page 8, lines 25-28: "It can been seen that the discrepancies in wind profile above 1 km between the radiosonde and lidar measurement are significant due to the multipath effect at the ship platform and decrease in collocation of the measurement." Another reason for the discrepancy between the results of the measurement of the wind by the lidar and the radiosonde at heights above 1 km is quite possible: the bias of the corrected lidar estimate of the wind due to the low SNR. It would be nice to add high profiles of the SNR in Figures 4 and 5. By the way, using some known procedure of filtration of good (reliable) estimates of the radial velocity obtained from 10-min lidar (4-DBS) measurements, the authors could obtain an unbiased wind speed estimate even in the case when the SNR is about 0 dB (if the percentage of good estimates is not below 20%).

R: It can be seen that the discrepancies in wind profile above 1 km between the radiosonde and lidar measurement are significant. On the one hand, the random error of the corrected CDL estimation of the wind due to the low SNR shown in Fig. 6a contributes to this discrepancy. On the other hand, the drift of radiosonde is affected by atmospheric turbulence perturbations and the CDL detection volume is changing during cruising observation. The spatial separation between radiosonde and CDL which can be called multipath effect, can cause larger discrepancy with increasing altitude.

Thanks for your suggestions, the SNR profile has added to the Fig 5 and 6 in the revised version, as shown below:

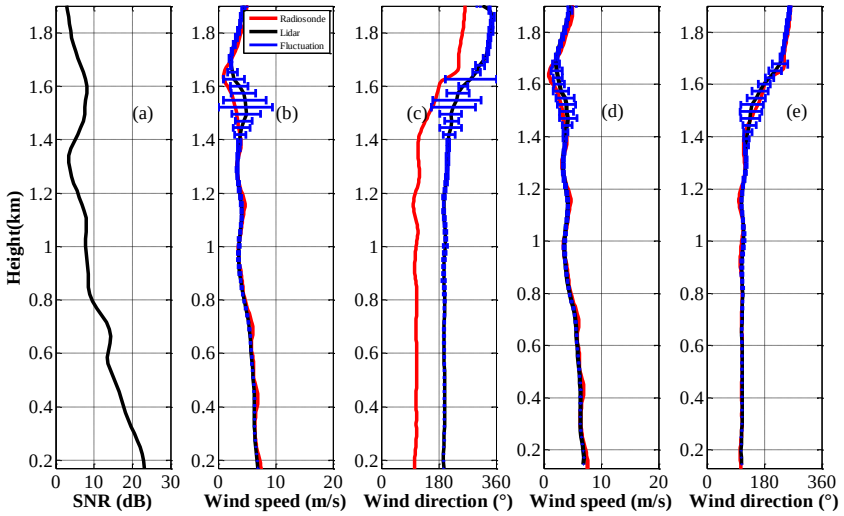

Figure 1: Anchored observation: (a) SNR profile (b) (c) wind speed and (d) (e) wind direction measured by CDL (blue line) before and after attitude correction, respectively. The simultaneous radiosonde data is shown in red line. The blue bars represent the sampling fluctuations from 15:52 to 16:02 LST, 09 May, 2014.

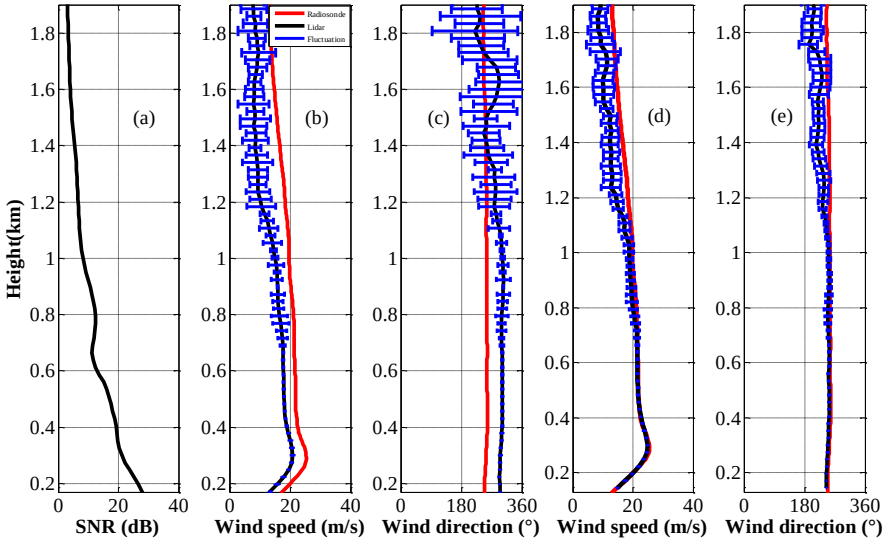

Figure 2: As Fig. 1, but for 07:44 to 07:54 LST 13 May, 2014 in cruising observation.

2. Reviewer 2

Summary:

A newly developed ship-borne wind lidar, consisting of a coherent wind lidar from a Chinese manufacturer is presented in this manuscript. There are a few other papers on ship-borne wind lidars (e.g. Achtert et al. 2015 and from NOAA, e.g. Tucker et al. 2009) and thus this kind of application with its specific challenges (ship movement and environment) is challenging and still provides some novelty. In contrast to other earlier reports (e.g. Achtert et al. 2015), no active stabilisation of the complete lidar is performed, but the movement and angles are measured and corrected in post-processing. Some comparisons to radiosondes from a cruise in the Yellow Sea are shown in addition to two cases with vertical and horizontal wind measurements. Thus the topic of the manuscript fits to AMT. Major comments from my side are related to the description of the motion correction approach with GPS/INS, which is not clear at some places and lacks details to assess its novelty. Indeed the manuscript is very similar to the one of Achtert et al. (2015) in terms of description of methodology (correction algorithms), statistical comparison and evaluation with radiosonde, assessment of errors (spectral approach). Also numerous minor comments are related to the presentation of the topic. Thus I would recommend that the manuscript can be only accepted after major revisions of text, figures and additional material is included.

General and Major Comments:

1) The differences to the NOAA HRDL and the system by Achtert et al. 2015 should be mentioned more explicitly in the introductory paragraph (p. 3, 1st paragraph "it can be seen .." is not clear) Achtert et al. (2015) use an active motion-stabilized platform; so the difference to the described system here is clear. The NOAA HRDL uses a SDS to point the scanner LOS direction. But all systems need a motion-correction in the post-processing afterwards due to the limited accuracy of the active systems. So it is understood that the described system in the paper is neither on a motion-stabilized platform nor the scanner LOS pointing direction is controlled by use of the ship attitude angles. Is this correct? If yes, then also the limitations of this approach (e.g. high ship movements, rough sea) should be discussed in the main part and summary more explicitly. On the other hand it is mentioned on p. 9, ch. 3.2 that, "the hemispherical scanner maintains the pointing of the lidar beam to zenith stare mode..". Does that mean that the scanner direction is controlled by the information from the INS?

R: The described system in the paper is neither on a motion-stabilized platform nor the scanner LOS pointing direction is controlled by use of the ship attitude angles. The LOS velocity measured by CDL in ship coordinate system $\vec{V}_{LOS\_measure}$ is unaffected by the ship movement, therefore the approach is available under high ship movement. $\vec{V}_{LOS\_measure}$. Since the bandwidth $B_{100} = (L-1)\Delta f = 97.68$ MHz, the corresponding radial velocity measurement range is ± 37.5 ms^{-1}. As for the feasibility under different sea condition, generally, except for the extremely rough sea condition, the LOS velocity component from vertical velocity in different directions is assumed to be identical. Then the u, v can be calculated using a modified 4-DBS formula. Under extremely rough sea condition, the difference of elevation angle in different directions is significant, and

the contribution of vertical velocity to LOS velocity needed to be treated carefully. In this case, the height interpolation of radial velocity can be used, and if three or more radial velocities at the same height are obtained, the horizontal and vertical velocity can be retrieved. But if the elevation angle in one direction is too small, the detectable height will be limited. Figure 1 shows the statistical distribution of the lidar pitch and roll angle from 09 May 2014 to 19 May 2014. In most cases the sea condition is less rough and the approach can be used reasonably.

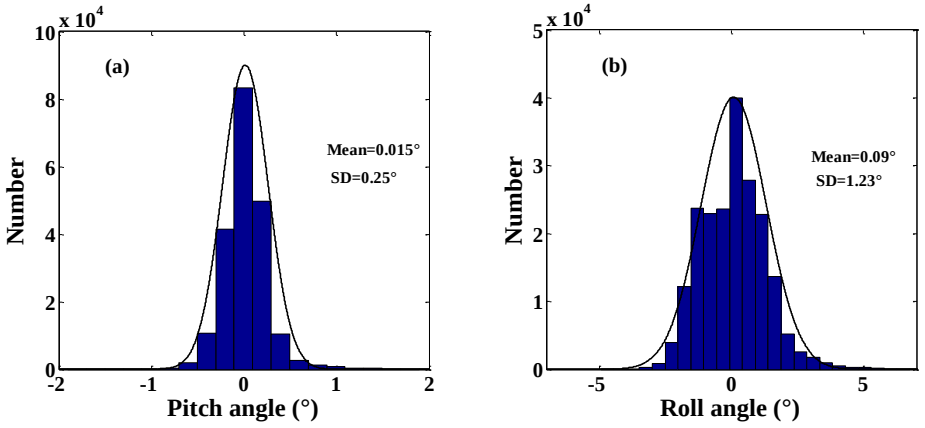

Figure 1. Statistical distribution of the lidar pitch and roll angle from 09 May 2014 to 19 May 2014.

I didn't explain it clearly, "the hemispherical scanner maintains the pointing of the lidar beam to zenith stare mode", in this sentence, the "zenith stare mode" represents the measurement in Lidar coordinate system, not the scanner direction in ECS controlled by the information from the INS

2) The main part of the manuscript deals with the motion correction. Thus relevant parameters of the used GPS and INS system (type, accuracy, precision, data acquisition rate) should be provided and discussed. Why are 2 antennas shown in Fig. 1? Also the limitations of this approach, e.g. for high wind speeds or high angular rates during rough see conditions need to be discussed in the main text. Why did the authors not chose an approach the control the scanner LOS direction, especially for the vertical pointing mode, by using the attitude angles from the INS (or is this applied)? Also details of the hard-target calibration need to be discussed. Is this performed once (before the cruise)? What angular offsets are determined, are different hard-targets in different direction used (range, elevation)? It is stated that "It can be seen that there exists no laser direction error." How do you come to this conclusion? Can you provide more details on that (e.g. data, Figure)?

R: The CDL scanner is mounted on the roof of the cabinet container with two fixed Global Navigation Satellite System (GNSS) antennas. Double antennas are used for determining the exact heading angle with accuracy of 0.1° when the ship is anchored. The attitude correction system uses XW-GI5651 MEMS Inertial/Satellite Integrated Navigation System. It is equipped with

MEMS gyroscope, accelerometer, and multi-mode and multi-frequency GNSS receiver. It can realize single antenna dynamic alignment or double antenna auxiliary fast and high-precision orientation. The specification are listed in Table 2. Generally, the attitude correction system uses GNSS to define earth coordinate system (ECS), where the ship speed, heading angle and earth location including the longitude and latitude in ECS can be obtained. Another important part of attitude correction system is the inertial navigation system. The inertial navigation system is rigidly mounted on the base of the scanner within the cabinet container, instead of the deck of the ship, to keep constant relative angles with reference to the lidar coordinate system. It records the lidar motion angles in real time including pitch, roll, laser beam azimuth and elevation even when the GNSS is sheltered or disturbed, and the recorded information is the exact lidar itself attitude in lidar coordinate system.

Table 2: Component Parameters of the XW-GI5651 MEMS Inertial/Satellite Integrated Navigation system.

System real-time precision						
Heading		0.1° (double antenna mode, baseline length ≥ 2 m)				
		0.1° (single antenna, speed > 10 ms^{-1})				
Attitude		0.1°				
Position		Single point positioning ≤ 5 m				
		RTK 2 cm + 1 ppm (CEP)				
Data updating rate		200 Hz (configurable)				
Starting time		≤ 10 s				
Alignment time		1~2 min (depending on dynamic maneuvering mode)				
		Double antenna aided orientation time ≤ 1 min				
Post-processing precision						
Heading		0.05°				
Attitude		0.05°				
Position precision	Time to lose lock	0 s	10 s	60 s	300 s	600 s
	Position	0.02 m	0.04 m	3 m	20 m	60 m

Physical properties	
Power consumption	< 7 W
Working temperature	-40 °C ~ 80 °C
Overall size	100 mm × 90 mm × 50 mm
Weight	< 500 g

The limitation of this approach has been discussed in *General and Major Comments Question 1*. We didn't use any actively stabilized compensation device in order to simplify mechanical system and to easily place CDL on ship platform. What's more, the scanner control system needs higher accuracy, especially for vertical mode measurement.

In our system, the inertial navigation system is rigidly mounted on the base of the scanner, instead of the deck of the ship, to keep constant relative angles with reference to the transmitting laser beam. It records the Lidar motion angles including pitch, roll, laser beam azimuth and elevation, thus the recorded attitude information is the exact Lidar itself feature in Lidar coordinate system. After installation, a hard target calibration is firstly performed to determine the misalignment between the ship and laser beam axes. Specifically, the buildings near the wharf where there is no occlusion issue between the CDL and the candidate buildings can be chosen as the hard target. As shown in Fig.1, when the laser beam direction points to the hard target, the azimuth angle φ_{lidar} in Lidar coordinate system is recorded, meanwhile the azimuth angle φ_g in Earth Coordinate System can be obtained using the Google Earth software if the exact longitude and latitude of hard target is determined. According to the ship heading angle ψ, we can get the azimuth angle $\varphi_s = \varphi_g - \psi$ between ship heading and the hard target in Ship Coordinate System. So far, the misalignment angle between the ship and laser beam axes $\Delta\varphi = \varphi_s - \varphi_{Lidar}$ can be corrected using the geometrical relationship between these three angles. And then the standard ship attitude definition can be determined based on the relationship between Lidar and ship coordinate system, which will be used in the following ship motion correction process. It can be seen that there exists no laser direction error determined by misalignment between the ship and laser beam axes since the Lidar is considered to be relative static during field experiment.

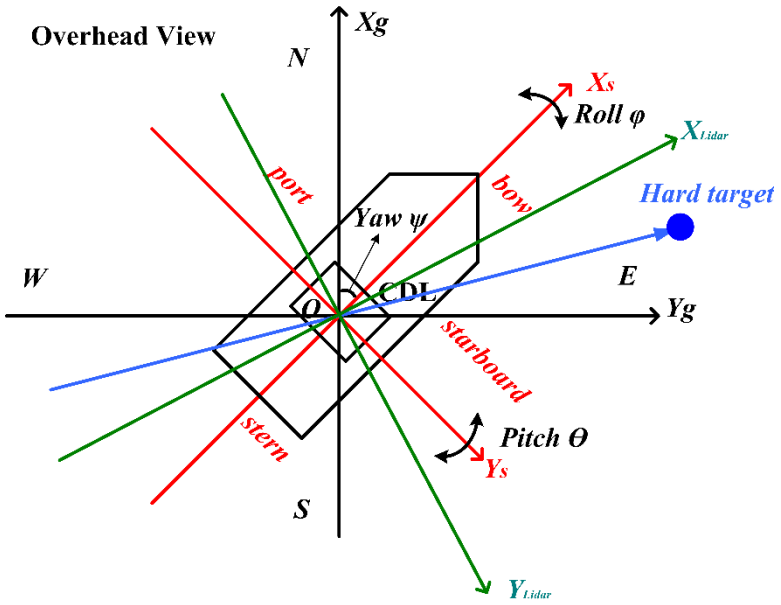

Figure 1. The overhead view of Lidar, ship and Earth coordinate system and corresponding hard target calibration.

3) The temporal resolution of the determination of the ship-induced Doppler shift (eq. 6) and the correction of the LOS velocity (eq. 7) needs to be stated and discussed. A figure showing a time-series of raw-data from the sensors (angles, velocity) could illustrate this to provide an impression about the time scales of the ship movement during anchored and cruising measurements. Also the timing of the DBS is not clear: How long is 1 LOS obtained, how long for the vertical velocity, and how long is the averaging time for the horizontal wind? Especially for the vertical pointing measurements the variability of the off-zenith angle should be shown in a Fig. The vertical velocity determination does need a correction for the horizontal wind. What is the time separation between the horizontal and vertical wind measurement?

Reply: Both the determination of the ship-induced Doppler shift and the radial velocity have the same temporal resolution of 0.5 s. Figure 4 in the revised version shows the flowchart of shipborne CDL data processing. Specifically, the LOS velocity and Signal to Noise Ratio (SNR) can be firstly determined using lidar data and FFT analysis. After the data pre-processing including the quality control based on SNR threshold, the attitude transformation is then used to obtain the azimuth and elevation in each LOS vector in Earth coordinate system with temporal resolution of 0.5 s. The LOS velocity detected by lidar is the atmosphere motion relative to ship coordinate system, thus the removal of the along-beam platform velocity due to ship motion is needed. In this study, the horizontal wind profile with 2-min temporal resolution will be retrieved for vertical velocity correction. Basically, the LOS velocities from N, S, E, and W direction after SNR quality control during the chosen 2-min interval are collected firstly. Then the procedure of filtration of reliable estimates of each radial velocity based on SNR threshold is used to obtain "good" speed estimates. The selected radial velocities and corresponding ship condition information in each radial direction are averaged and the averaged ship condition will be used for the removal of platform

velocity effect. Finally, the horizontal with 2-min temporal resolution can be retrieved using modified 4-DBS mode. The vertical wind measurement has a temporal resolution of 0.5 s, the horizontal wind whose retrieved time is closest to vertical wind measured time will be used for vertical velocity correction. A time-series of raw-data from the sensors (angles, velocity) and corrected angles can be seen in Fig.1 and Fig 2 as below:

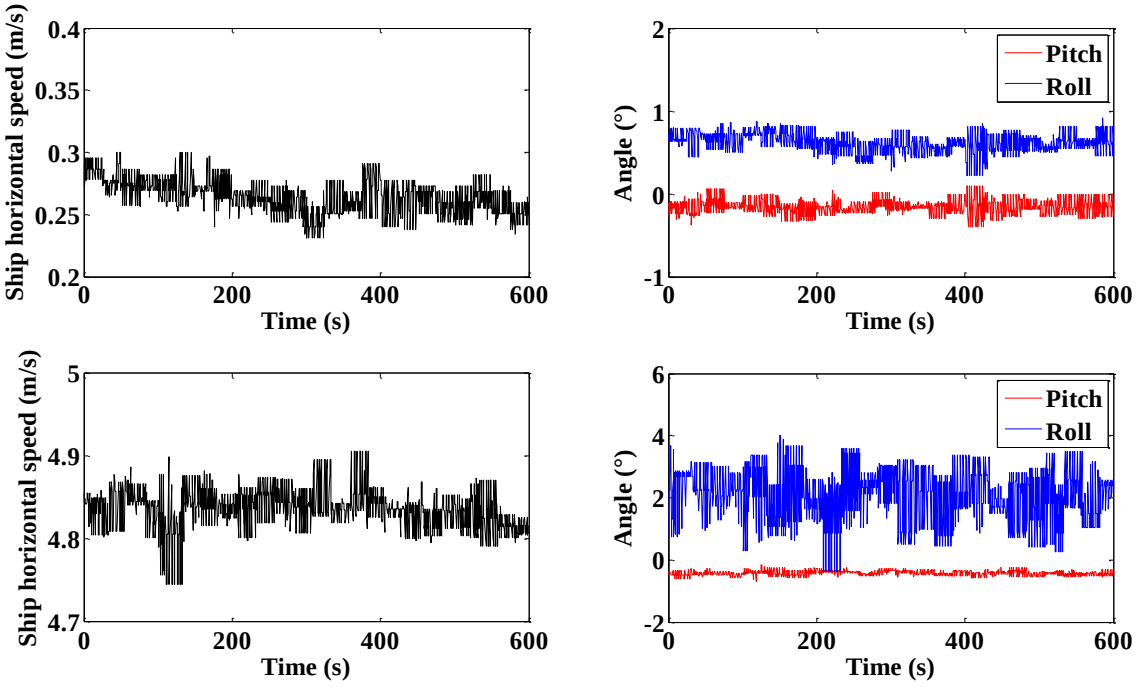

Figure 1: (a) Time series of ship horizontal speed and (b) pitch and roll angles on 09 May 2014 (15:52-16:02) during anchored measurement, (c) Time series of ship horizontal speed and (d) pitch and roll angles on 13 May 2014 (07:44-07:54) during cruising measurement.

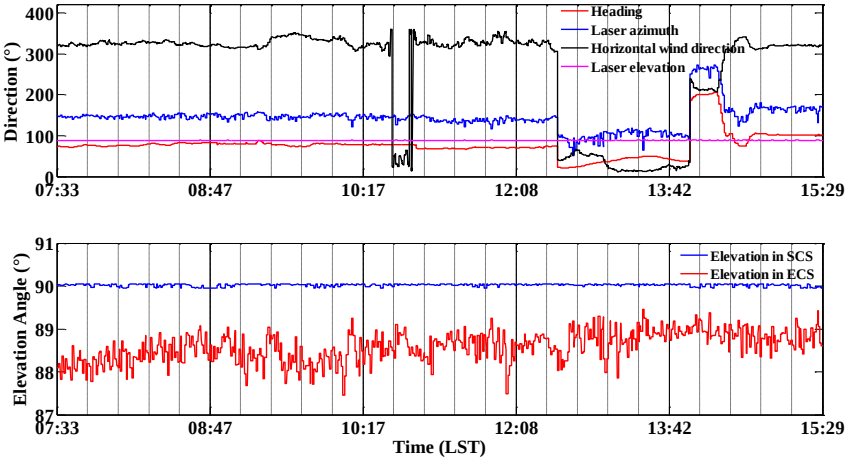

Figure 2: Example measurement from 07:33 to 15:29 LST 14 May 2014: (a) Time series of ship heading, CDL laser beam azimuth and elevation in the Earth coordinate system, and horizontal wind direction at 0.4 km. (b) Elevation angle in zenith stare mode in Ship Coordinate System and Earth Coordinate System.

4) In Achtert et al. (2015) the influence of the distortion of the flow due to the ship is discussed and modelled. In this manuscript this issue is only mentioned in 1-2 sentences on p. 9. What was the geometry/height of the ship? What would be the maximum height for a flow distortion, taking some numbers and scaling from the approach of Achtert et al (2015)? The lidar and radiosonde data is shown only above 150 m for this manuscript, but you conclude from your statistical comparison that the height of 200 m might be still affected by the flow distortion. So some more discussions on the geometry/height of the ship and the expected flow distortion around is needed.

R: The height of Dongfanghong-2 is 84 m. The relative height between CDL and the highest building on ship is about 15 m shown in Figure 1. When the strong wind blows from the ship bow, the building and experimental setups on ship have an important effect on CDL lower-level detection volume where the induced-turbulence may cannot meet the assumption of homogeneous isotropic atmosphere for 4-DBS retrieval. On the other hand, the blind area of CDL is 150 m and corresponds to the height of 129.9 m when laser beam elevation angle is 60°, meaning that less data points are available below 200 m with effective comparison. Therefore, whether the flow distortion around the ship is the main reason for the discrepancies in the lower part measurement or not is yet unclear. Further study, especially focused on the CFD model, needs to be used to the assess the potential effects on turbulent flow and wind field analysis.

In Achtert's paper, it is concluded that the normalized bias in horizontal wind speed is less than 2% for all wind directions at altitudes above 75m. But the specific geometric parameters of the ship in CFD simulation domain are not mentioned, which is important for determination of the maximum height for a flow distortion induced by ship. However, it surely provides us a new sight for Lidar data quality assessment, especially for the correction of the wind measurements used for turbulence fluxes exchange from Marine-Atmosphere interface.

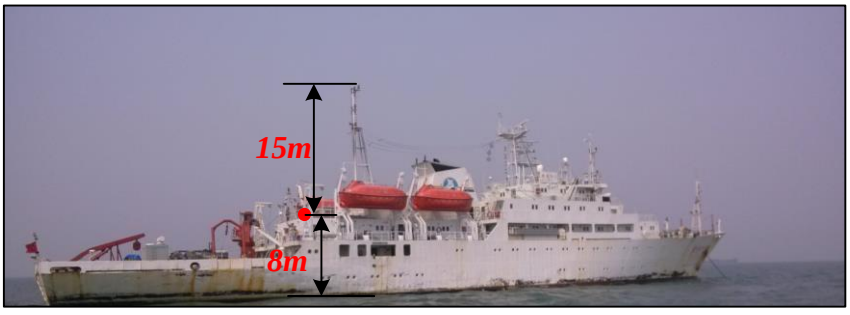

Figure 1. The Dongfanghong-2 research vessel during 2014 Yellow Sea Campaign. The red solid dot represents the CDL position.

5) Ch. 3.3. Error analysis: The authors deal here with the derivation of systematic errors (bias) to the horizontal wind retrieval I am wondering, if the error sources from the knowledge of the ship velocity and the lidar pointing angle are really systematic (over longer timescales) or random, and would add to the random error of the wind retrieval. A clear distinction needs to be made in the underlying assumption for the ship velocity and lidar pointing wrt systematic and random errors. Are the provided numbers for ship velocity and pointing only the systematic part? What would be the random error of these quantities?

R: It is noted that the knowledge error of the ship velocity and lidar pointing angle mentioned in Part 3.3 are systematic part and it is assumed that the random error of these parameters is zero, which is reasonable and robust for horizontal wind retrieval.

6) The authors could consider moving some of the equations related to the correction algorithms (Ch. 2) and error analysis (Ch. 3.3) to an appendix. At least for these parts, which are well known (e.g. coordinate transformations, descriptions of angles, DBS technique). I would restrict the description in ch. 2 and 3.3 to the novel aspects of this work.

R: Thanks for your suggestion. The motion-correction algorithm including Eq. 1-5 in the manuscript has moved to Appendix A.

7) I am missing a description of the overall objective of the deployment in the Yellow Sea in 2014 in the introduction. Was this only for technical demonstration, or were further atmospheric-oceanic processes studied. I am also missing a discussion of the open questions for turbulent flux measurements or wind vector measurements over the sea, which would need a shipborne Doppler wind lidar. One should discuss some objectives for the development of a shipborne wind lidar in the introduction. Also it might be useful to provide a paragraph in the Summary about future plans and campaigns.

R: Thanks for your suggestion. The description of the objectives has been added to the last paragraph in the Introduction part. It is described below:

"The experimental investigation was undertaken by Dongfanghong-2 research vessel affiliated with Ocean University of China in 2014 over the Yellow Sea. The Yellow Sea, a marginal sea of the Pacific Ocean, is the northern part of the East China Sea. It is located between mainland China and the Korean Peninsula. There is seldom study on boundary layer dynamics study based on CDL in this region. As one of the main objectives, the CDL was deployed on the ship in this campaign to demonstrate the feasibility of the algorithm-based attitude correction method. The obtained accurate three-dimensional wind information can provide significant preparation for further studies on characteristics of dynamics and thermodynamics in the MABL and turbulence flux exchange over sea surface. In addition to CDL, as another important part of this campaign, a High Spectral Resolution Lidar (HSRL) and a CL31 ceilometer were also deployed on the ship platform in order to detect MABL height spatial-temporal evolution and to retrieve the aerosol and cloud optical characteristics such as extinction coefficient and backscatter ratio and so forth. It will help us to understand the complex behavior of MABL and the aerosol cloud forcing

characteristics over sea region and the impact on climate change. This paper focuses on CDL performance and gives a thorough analysis of the attitude correction for lidar velocity measurement."

The description of the further plan has been added to the last paragraph in the Summary part. It is described below:

"Overall, combining a CDL with attitude correction system and accurate motion correction process as presented here forms a reliable and autonomous set-up that could be placed on mobile platform to provide more detailed, higher spatial and temporal resolution view of three-dimensional wind field information. It will be further validated and improved under different sea conditions using CFD model simulation and field campaign. More specific studies are being carried out or prepared, including atmospheric turbulence characteristics statistics and multi-scale wind field observation in MABL, wind turbine wake and atmospheric turbulence interaction over offshore wind power field (Wu et al., 2016; Zhai et al., 2017), mass transport and flux analysis in MABL with combination of CDL and Multi-wavelength Polarization Raman Lidar (Wu et al., 2016).

Specific Comments

1) p.1 Intro: A number of studies are referenced for turbulent fluxes over the sea surface (Axford, 1968). Could these studies be grouped by objective, technology or geographical region to be more specific. Otherwise this long list of references is not very informative.

R: Thanks for your suggestion. The references has been grounded according to different platforms and geographical region. It is shown below:

"There are many studies on the turbulent fluxes measurement over the sea surface. Various motion sensing technique on the moving platform has been developed in the field of airborne (Axford, 1968), space-borne (Hawley et al., 1993) and shipborne observations (Fujitani, 1992; Song et al., 1996; Edson et al., 1998; Miller et al., 2008). Many shipborne field experiments have been widely carried out over Pacific Oceanic area (Mitsuta et al., 1974; Bradley et al., 1991; Shao, 1995; Tsukamoto et al., 1995)."

2) p.3, line 15: "Few studies .. in this region". Are there any references for these studies?

R: As far as we know, there is seldom study on boundary layer dynamics study based on CDL in this region.

3) p. 5, L 11: The different elevation angles are probably due to ship rotation and movement during the time period of measuring different LOS directions, which should be stated here. Thus it is important to mention the duration of the measurement of each

LOS direction, and the complete 4 beams, and the relevant movements of the ship during these periods. How is the expected elevation angle _0 obtained?

R: Thanks for your suggestion, the description has been added in the manuscript. It is shown below:

But for the shipborne platform, the elevation θ_g in four directions (north, south, west and east in ship coordination system) may have slightly difference (see Eq. (A5)) due to ship rotation and movement during the time period of measuring different LOS directions, thus a conversion of $\vec{V}_{LOS}$ from real elevation θ_g to the expected elevation θ_0 is firstly processed, that is,

$$\vec{V}'_{LOS} = \vec{V}_{LOS} \cos\theta_0 / \cos\theta_g \quad (4)$$

It is noted that θ_0 can be set any value from 0° to 90°, and in this paper $\theta_0 = 60^\circ$ is set for horizontal wind profile retrieval. During the experiment, each radial direction will take 5 s to obtain 10 measured LOS velocity for accumulation and average. In this sense, the highest temporal resolution of horizontal wind velocity using 4-DBS mode is 20 s. The recorded ship condition information has the same update rate of 0.5 s as radial velocity's, which can be averaged to remove the platform motion effect on radial velocity.

4) p. 7, 1st paragraph: It should be stated, how the background noise signal is obtained, e.g. via the recorded signal after a sufficiently long laser travel time, or via a separate measurement w/o laser pulse emission. Do the authors see an advantage of their SNR definition over the one from Banakh et al. 2013?

R: The SNR in this study is defined as the ratio of the peak value of FFT spectral signal in each range bin to the Root-Mean-Square (RMS) of background noise signal. Figure 1 shows the array of the spectral $S(l\Delta f; k\Delta R)$, where $l = 0,1,2,3,...,L-1$ is the spectral channel number and $L = 100$. In this case the frequency resolution $\Delta f \approx 0.98$ MHz and the corresponding velocity resolution is $\Delta V = 0.76$ ms^{-1}. The bandwidth $B_{100} = (L-1)\Delta f = 97.68$ MHz, and the corresponding radial velocity measurement range is ± 37.5 ms^{-1}. Figure 1a shows the last 10 range gates raw array of spectral in green line. We estimate the averaged background noise spectrum

$$\bar{S}_N(l\Delta f) = \frac{1}{10}\sum_{k=94}^{103} S(l\Delta f; k\Delta R) \quad (8)$$

Substracting the background noise spectral $\bar{S}_N(l\Delta f)$ from the raw spectral array $S(l\Delta f; k\Delta R)$, the unnoisy array of spectral $S(l\Delta f; k\Delta R)$ can be obtained and shown in red line in Fig. 1. The peak value index l_{peak} from the $S(l\Delta f; k\Delta R)$ can be firstly obtained and thus the absolute signal power $P_s(k\Delta R)$ at various ranges $k\Delta R$ can be represented as:

$$P_s(k\Delta R) = S(l_{peak}\Delta f; k\Delta R) - \frac{1}{12}\left(\sum_{l_{peak}-20}^{l_{peak}-15} S(l\Delta f; k\Delta R) + \sum_{l_{peak}+15}^{l_{peak}+20} S(l\Delta f; k\Delta R)\right) \quad (9)$$

Replacing integration by summation and taking into account that the zero velocity point in one channel is $l_{zero} = 50$, we estimate the noise power P_N as

$$P_N = \frac{1}{10}\sum_{k=94}^{k=103}\sqrt{\frac{1}{21}\sum_{l=l_{zero}-10}^{l_{zero}+10} \hat{S}_N(l\Delta f; k\Delta R)^2} \quad (10)$$

Finally, we obtain the range profile of the $SNR(k\Delta R)$ using the equation

$$SNR(k\Delta R) = 10\log_{10}\left(\frac{P_s(k\Delta R)}{P_N}\right) \quad (11)$$

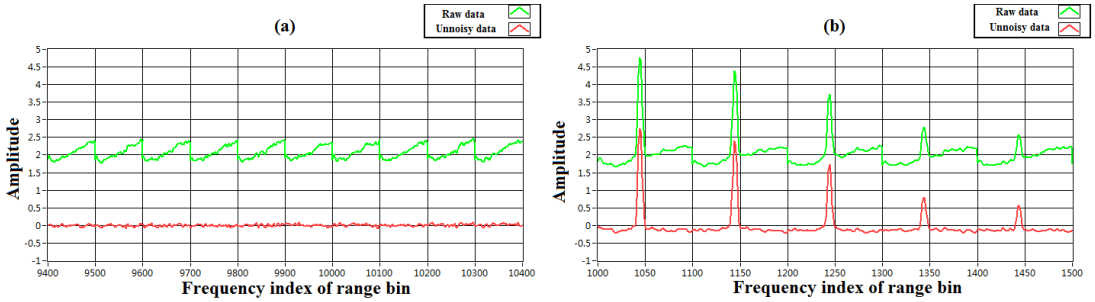

Figure 1: The CDL measured array of the FFT spectra (a) the last 10 range gates spectra for background noise spectrum estimation (b) the 1st – 5th range gates (150 m – 270 m, range resolution is 30 m) spectrum.

The SNR from Banakh et al. 2013 is defined as the ratio of the averaged heterodyne signal power P_s to the average detector noise power P_n in a 50-MHz bandwidth. The power P_s and P_n are integrals of the spectral densities $S_s(f)$ and $S_n(f)$, respectively, in frequency f within a band of width B_{50}, that is:

$$P_s = \int_{B_{50}} S_s(f)df \quad (5)$$

$$P_n = \int_{B_{50}} S_n(f)df \quad (6)$$

Comparing the definition from Banakh et al. 2013, the SNR in this paper is simpler and also indicates the CDL detection capability, data accuracy and atmospheric tracer particle relative intensity. In this sense, the SNR threshold value in this paper is higher than the one in previous studies (Banakh et al. 2013; Achtert et al 2015) for the same signal power spectrum.

5) p. 7, L24: It should be described how the wind fluctuations are determined. Is it the standard deviation of wind measurements of higher temporal resolution (resolution?) during the 10 min.? Why are bars shown only for part of the profile in Fi.g 4 and 5? Is it smaller than a specific value below 1.4 km in Fig. 4? Do the fluctuations represent instrument noise or atmospheric fluctuations? What could be the reason that there are higher fluctuations in the layer of 1.4-1.6 km in Fig. 4?

R: The black line indicates the mean measurement by CDL during the 10-min period, and the red line shows the result which is obtained from simultaneous radiosonde data. The blue bars represent the standard deviation of CDL wind measurement from the 2-min temporal resolution results during the chosen analyzed period, representing the atmospheric fluctuations.

The standard deviation of wind speed and direction below 1.4 km are less than 0.5 m/s and 5°, respectively, showing that the atmospheric condition is relative stable below 1.4 km. While there are higher fluctuations in the height of 1.4 – 1.6 km. The higher SNR in the layer of 1.4 – 1.6 km shown in Fig. 5a implies the existence of cloud or aerosol layer, more active and complex atmospheric movement in this layer may results in higher fluctuations.

6) p. 7, L27: Same question related to the method to determine the STD for the angles. Determined from the variability during the 10 min using raw data with of temporal resolution of xx s?

R: I didn't explain it clearly. The related description has added to the manuscript, and it is shown below:

It is noted that the standard deviation of the angles is determined from the variability during the 10 min period using N=1200 raw data with temporal resolution of 0.5 s, which is shown in Fig. 7b.

7) p.7, L28: Which SNR threshold was used here?

R: The SNR threshold in this study is 8 dB. The reason why SNR threshold is 8 dB has been analyzed in Sect. 3.3.

8) p.8, L26, last sentence: What is a "multipath effect"? This should be clarified. Also the difference in radiosonde and lidar location should be stated quantitatively. What is the difference in mean wind speed and direction between radiosonde and lidar above 1 km? Can a lidar instrumental effect excluded to explain the difference? I am not convinced that it is only colocation.

R: The difference in mean wind speed and direction between radiosonde and CDL above 1 km is about 3.4 ms^{-1} and 15.2°, respectively, showing significant discrepancy. On the one hand, the random error of the corrected CDL estimation of the wind due to the low SNR shown in Fig. 6a contributes to this discrepancy. On the other hand, according to the recorded information, the mean heading angle and cruising speed of the ship is 75.86° and 4.84 ms^{-1}, respectively, and the mean wind speed and direction above 1 km is 255° and 18.4 ms^{-1}, respectively. Since the drift of radiosonde is affected by atmospheric wind, and turbulence perturbation and the CDL detection volume is changing during cruising observation, the result discrepancy between radiosonde and CDL caused by different observation location, also called the multipath effect, is larger with increasing height.

9) p.8 and Fig. 6: I would propose to plot the radiosonde on the x-axis and the lidar on the y-axis and also perform the linear least square fit with these coordinates. I consider the radiosonde as more accurate and the usual linear LSF procedures assume that the x-parameter is without errors (minimization of vertical differences). I also consider the criteria of excluding data with 1*SD as too strict. Only gross outliers – deviating from a Gaussian distribution – could be excluded. This would typically result in a criteria of >3*SD.

It needs also to be stated, how many data-pairs were excluded from the statistical comparison in order to judge the numbers of gross outliers. Also the SD typically refers to the SD of the difference (lidar-radiosonde). I am wondering how the SD of the lidar data ydata was obtained here. It is clear that the statistical parameters for bias, SD, R, and RMSE need to be calculated without a rigorous excluding of the data (with 1*SD). This point needs to be revisited and clarified.

R: I agree with your suggestion, the radiosonde on the x-axis and the lidar on the y-axis has been used in the manuscript. Figure 1 shows the distribution of difference (lidar-radiosonde) and fitted Gaussian distribution. The total number of wind speed and direction dataset is 1062 and 951, respectively. The 1*SD, 2*SD, 3*SD are plotted in red, black and blue dotted-line, respectively. The SD is the standard deviation of the difference of (lidar-radiosonde). It can be seen from figure 1 that the criteria of excluding data with 2*SD is more reasonable for gross outliers. Figure 2-4 shows the comparison of lidar and radiosonde using different criteria. The excluded data-pair using the different criteria are listed in Table 1 below:

Table 1. Excluded data-pair and corresponding % using different criteria

	Excluded wind speed data-pair (%)	Excluded wind direction data-pair (%)
3*SD	14 (1.3%)	12 (1.3%)
2*SD	62 (6%)	56 (5.9%)
1*SD	252 (21%)	225 (24%)

The statistical parameters for bias, SD, R, and RMSE after data quality control with different criteria are shown in figure 2-figure 4.

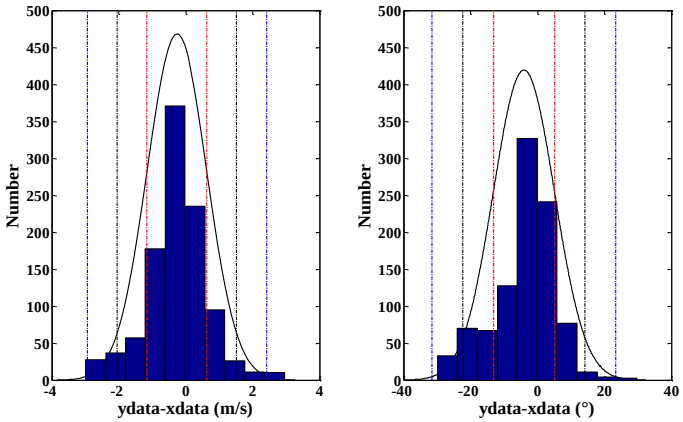

Figure 1: Distribution of difference (lidar-radiosonde) (a) wind speed (m/s) (b) wind direction (°)

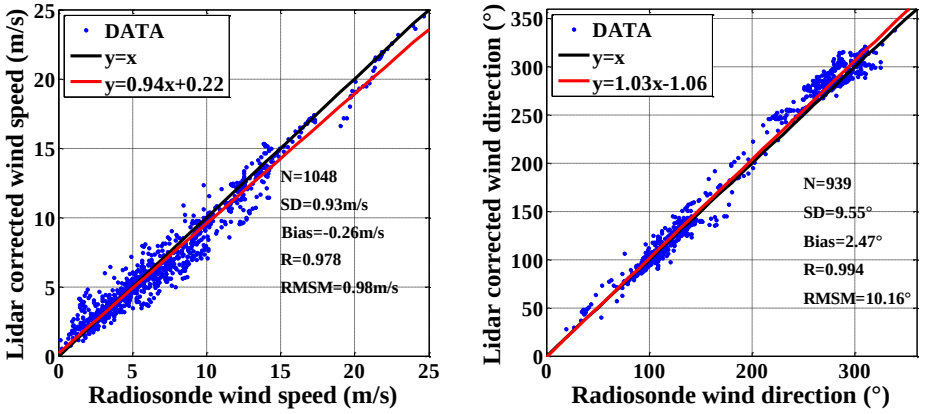

Figure 2: Comparison of (a) wind speed and (b) wind direction between CDL and radiosonde data using 3*SD threshold

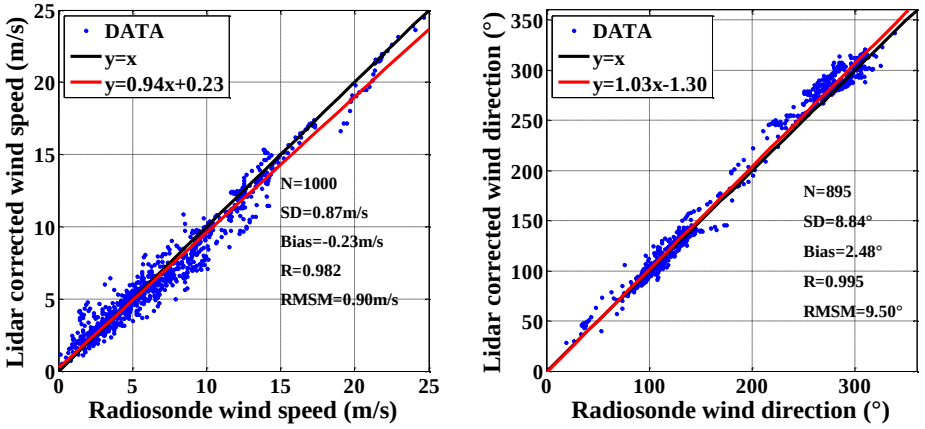

5

Figure 3: Comparison of (a) wind speed and (b) wind direction between CDL and radiosonde data using 2*SD threshold

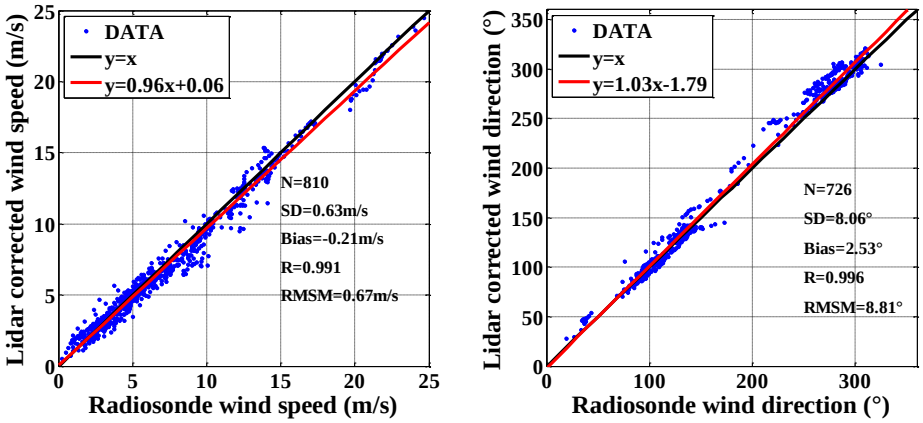

Figure 4: Comparison of (a) wind speed and (b) wind direction between CDL and radiosonde data using 1*SD threshold.

10) p.9, ch. 3.2 and Fig. 7: The dots for MABL height are shown for the first 1/3 of Fig. 7 in a region of SNR around 10, where no obvious gradients can be seen, whereas for the second 2/3 it is more in the region between 10 dB (light blue) and 0 dB (dark blue). Please check and comment. Is there a reference about the ABL height determination using the first negative gradient?

R： We didn't explain it clearly. The MABL height has been retrieved and compared using different instruments such as the CDL, radiosonde, and CL31 ceilometer during this campaign (Wang et al., 2016). Many papers have discussed the use of backscatter signal of Lidar for boundary layer height estimation, assuming that the boundary layer has higher aerosol concentrations than the free troposphere above. In this paper, the SNR, representing the relative aerosol backscatter profiles, were used and two common methods includes thresholding SNR to determine MABL height (Melfi et al. 1985) and finding the height of the first strong negative gradient (White et al. 1999; Hennemuth and Lammert 2005) in SNR. Figure 1a shows the Time-Height-Intensity of SNR and the retrieved MABL height marked with black and red solid circles. The radiosonde data during 17:34 LST 14 May 2014 and corresponding MABL height using the gradient of potential temperature and relative humidity are also shown in Fig. 2. It can be seen that diurnal variation of MABL height is less obvious within 1.0 km - 1.5 km, consistent with the mixing layer height retrieved from the radiosonde potential temperature and relative humidity profile.

The related references have been added to the manuscript:

1. Hennemuth, B., and Lammert, A.: Determination of the atmospheric boundary layer height from radiosonde and lidar backscatter, Boundary-Layer Meteorol., 120(1), 181-200, 2006.

2. Menut, L., Flamant, C., Pelon, J., and Flamant, P. H.: Urban boundary-layer height determination from lidar measurements over the Paris area, Appl. Opt., 38(6), 945-954, 1999.

3. Wang, D., Song, X., Feng, C., Wang, X., and Wu, S.: Coherent Doppler Lidar Observations of Marine Atmospheric Boundary Layer Height in the Bohai and Yellow Sea, Acta Opt. Sin., 35(A01), 1-7, 2015.

4. White, A. B., Senff, C. J., and Banta, R. M.: A comparison of mixing depths observed by ground-based wind profilers and an airborne lidar, J. Atmos. Oceanic. Technol., 16(5), 584-590, 1999.

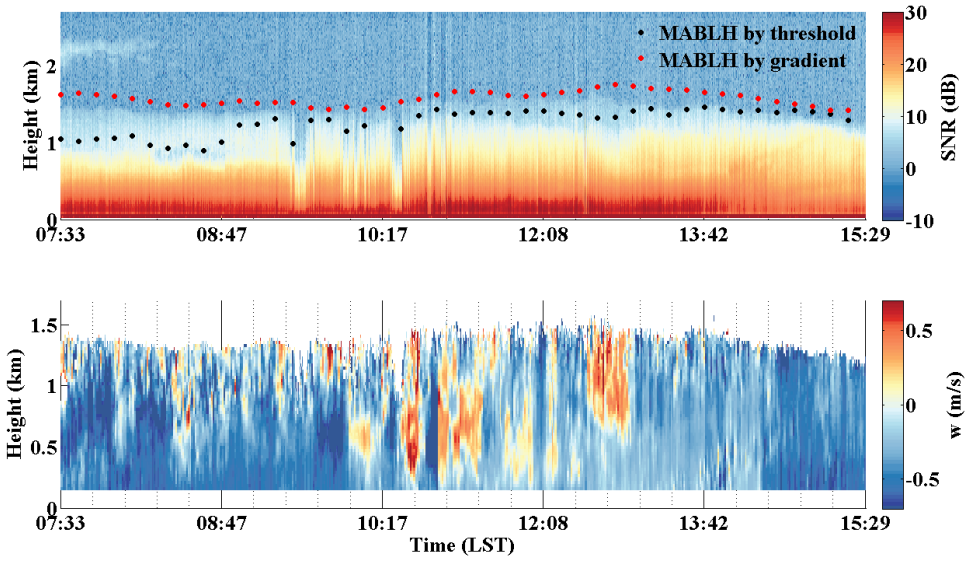

Figure 1: Example measurement from 07:33 to 15:29 LST 14 May 2014: (a) Time-Height-Intensity of SNR and retrieved MABL height using SNR threshold and gradient method (black and red solid circles, respectively). (b) Time-Height-Intensity of vertical velocity after attitude correction.

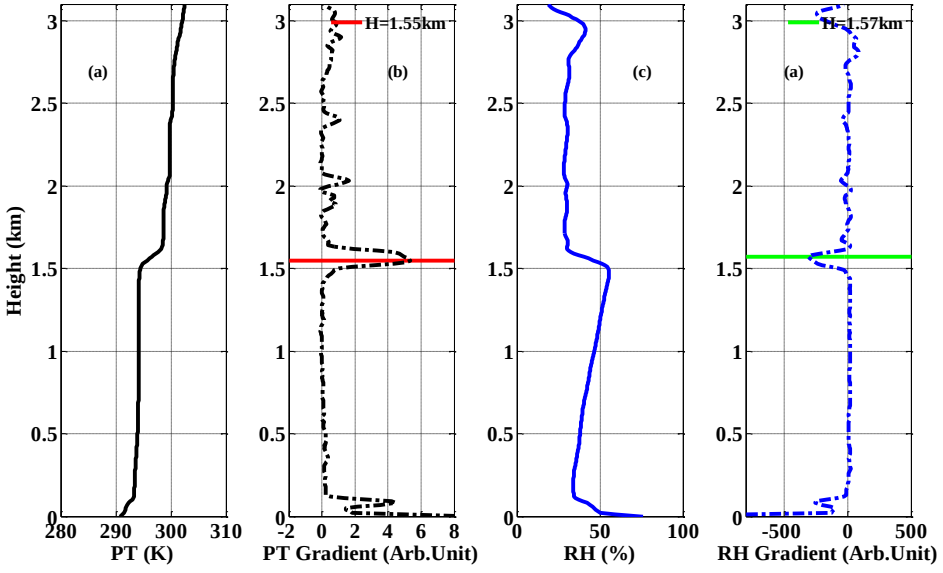

Figure 2: Radiosonde profiles of (a) potential temperature (K) (b) the gradient of potential temperature (c) relative humidity (%) and (d) the gradient of relative humidity at 12:00, LST 14 May 2014. The horizontal red and green lines in (b) and (c) stand for MABL height retrieved from potential temperature and relative humidity, respectively.

11) p.11, L5: I consider an error of only 0.1_ for the ship heading as very small. Is this justified by the hard-target measurements?

R: The error of 0.1 for ship heading comes from the accuracy of Global Navigation Satellite System.

12) p.11, L8: What quantity is derived in eq. (14) in comparison to eq (13); Both are called "bias" LOS_N but eq. (14) with a "N"". Text should clearly state, the difference. What eq. (13 or 14) is then used in the estimates for the bias (eq. 17 and 18)?

R: The $\vec{V}_{LOS}$ is the LOS velocity in Earth coordination system with elevation θ_g. The $\vec{V}'_{LOS}$ is the LOS velocity in Earth coordination system with elevation $\theta_0 = 60^\circ$ in this study. The relationship between $\vec{V}_{LOS}$ and $\vec{V}'_{LOS}$ is $\vec{V}'_{LOS} = \vec{V}_{LOS}\cos\theta_0 / \cos\theta_g$. The bias of $\vec{V}_{LOS}$ is derived using eq (13) and the bias of $\vec{V}'_{LOS}$ is affected by $\vec{V}_{LOS}$ and θ_g according to the error propagation theory, as shown in eq. (14). The estimation for horizontal wind bias shown in eq. 17 and 18 are related to $bias_{b1}$ and $bias_{b2}$. According to $b_1 = (\vec{V}'_{LOS\_N} - \vec{V}'_{LOS\_S})/\cos\theta_0$ and $b_2 = (\vec{V}'_{LOS\_E} - \vec{V}'_{LOS\_W})/\cos\theta_0$, the bias of $\vec{V}'_{LOS}$ will be used.

13) p.11, eq. 15/16: These eq. could be moved to ch. 2 after eq (10), because it deals with u, and v retrieval and not with error estimates as in ch. 3.3.

R: Thanks for your suggestion, the eq 15-16 has moved to ch.2 after eq.10.

14) p.11, L13: Here it is stated, that the lidar pointing angles are very small (and assumed to be perfect), but on p.12, L2 it is stated the errors are dominated by ship velocity and lidar pointing errors. This is in contradiction.

R: I did not explain it clearly. Because of the requirement for small bias in the radial velocity measurements, the error in the laser beam direction must be very small and one can assume perfect knowledge of the coefficient a_i.

The dominant source of bias of the horizontal velocity estimates come from the biases of the radial velocity estimates, which are determined by the error in the ship velocity $\vec{V}_{ship\_horizontal}$, $\vec{V}_{ship\_vertical}$ and heading angle ψ and lidar pointing knowledge errors $\Delta\varphi$ and $\Delta\theta$ (see Eq. 13).

15) p.12, L6ff: Here the method of obtaining the random error is described ("In this case, a"). But no resulting spectrum is shown in Fig. 9. This needs to be added or reformulated.

R: Various methods of estimating the magnitude of the random error of Doppler Lidar velocity measurements have been introduced (Frehlich 2001). The measurement of error from velocity spectrum were used in this paper. A 50 % window overlap factor, a Hamming window is used in order to reduce the leakage in the spectra. A zero-padding of the missing values were applied to each window for each spectrum calculation to improve the frequency resolution. The constant high-frequency region of velocity spectrum higher than 0.2 Hz, shown in figure below, represents uncorrelated random error contribution, which is departing from the Kolmogorov's -5/3 law. The random error of vertical wind velocity is estimated as the standard deviation of the measured signal after high-pass filter.

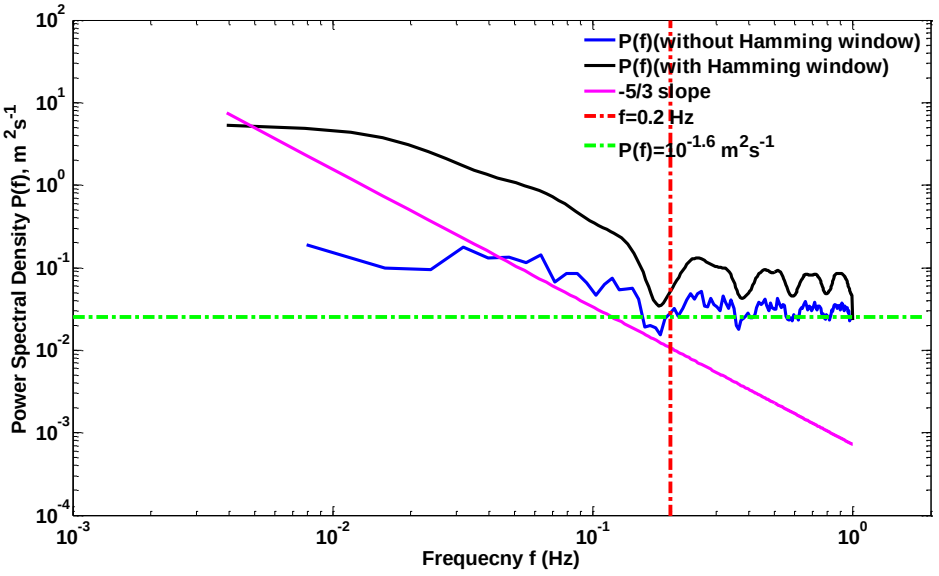

Figure 1: Power spectral density P(f) without and with Hamming window for the CDL measured vertical speed between 15:52 and 16:02 LST on 09 May and for an altitude of 1495 m (blue and black solid line, respectively). The expected spectral behaviour according to the Kolmogorov's−5/3 law (pink solid line), the noise frequency threshold (red dotted line) and the derived noise floor for the CDL (green dotted line) are shown.

16) P12: L12: Are you sure that it is an elevated aerosol layer and not a cloud, which provides the high SNR around 1.5 km?

R: Thanks for your suggestion. Actually, we cannot judge whether it is an elevated aerosol layer or cloud only using the SNR intensity signal. We searched the recorded information from Vaisala CL31 ceilometer software screenshot, as shown below:

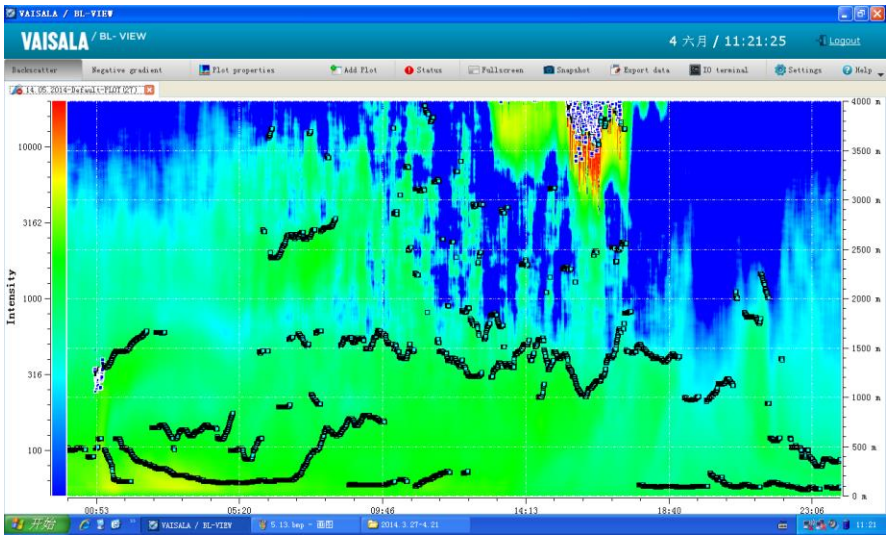

Figure 1: CL31 ceilometer software real-time results on 14 May 2014.

In this figure, the candidate boundary layer height and cloud base height can be marked with black squares and white squares, respectively. The high SNR around 1.5 km during 07:33 – 08:40 LST is an aerosol layer, not cloud layer. The description has been corrected in the manuscript.

17) p.12, L23: speckle-induced phase noise is not discussed in Achtert et al. 2015. Another reference needs to be provided

R: The related references have been added to the manuscript.

1. Frehlich, R.: Effects of wind turbulence on coherent Doppler lidar performance, J. Atmos. Oceanic. Technol., 14(1), 54-75, 1997.
2. Frehlich, R.: Estimation of velocity error for Doppler lidar measurements, J. Atmos. Oceanic. Technol., 18(10), 1628-1639, 2001.

18) p.13 Summary: The limitations of the approach in comparison to existing systems need to be mentioned in the summary. Also I am missing an outlook about future algorithm or hardware improvements or future deployment during ship cruises.

R: The limitation of the approach has been discussed in General and Major Comments Question 1.

The outlook has been described in General and Major Comments Question 7.

19) p.13, L14: The number for the bias and the STD from the statistical comparison of all radiosondes should be stated here.

R: The total number of wind speed and direction dataset for comparison is 1062 and 951, respectively.

20) Ref. Liu et al. 2010: More details should be provided for this reference, which is not really accessible, or the reference should be removed or replaced. Also Achtert et al. (2015) provide these transformations.

R: In Liu et. al 2010 paper, a mobile Doppler lidar had been developed for 3D wind measurements by Ocean University of China. In order to further improve the mobility of the mobile Doppler lidar for lidar calibration and validation, both GPS and inertial navigation system were integrated on the vehicle for performing measurements during movement. The modifications of the system and the results of the moving measurements were presented. This work simplifies the construction of the mobile Doppler system and makes the lidar more flexible for ground-based wind measurements and validation with the ADM-Aeolus spaceborne Doppler lidar.

21) Fig. 1: An additional Figure should be shown of the ship to illustrate the location of the CDL on the ship and possible disturbances of the flow.

R: Revised

22) Fig. 1: The location of the INS on the CDL should be indicated in the Figure.

R: Revised

23) Fig. 2: The symbols used for the angles pitch, roll, yaw should be placed also in the Figures.

R: Revised

24) Fig. 7: the legend within Fig. 7b is too small

R: Revised

%%==========%%

Editorial: A large number of editorial comments were directly added to the PDF-Version of the manuscript. In addition the term “et al” needs to be replaced by “et al.”. The manuscript needs thorough proof-reading after revision.

1) P2 L27: “High Resolution Doppler Lidar (HSRL)” needs to be corrected also at other places

R: Revised

2) P4 L25: Check style file or other papers, if "," or ";" is needed to separate coordinates.

R: Revised, X_g, Y_g, Z_g

3) P5 L3: This is not clear: why is the azimuth angle changing, when looking downward.

R: From the top view, the φ_s increases in a clockwise direction during 4-DBS mode operation.

4) P5 L4: This must be the Xs-Zs plane.

R: we have checked the definition, it is the Xs-Ys plane.

5) P5 L8: Here the indices "g" are missing.

R: the “g” has added to the manuscript

6) P6 L10: "homogenous" flow instead "cellular"

R: revised

7) P6 L17: N, S, E and W, not uppercase style.

R: revised

8) P8 L15: sentence not completed: “What’s more, the fluctuation in wind speed and direction above 1 km is more severe.”

R: What’s more, the fluctuation in wind speed and direction above 1 km is more severe than the results below 1 km.

9) P9 L3: “the coefficient of determination of 0.96”, I assume this value is R^2. I consider it sufficient to provide R.

R: Yes, the coefficient of determination of 0.96 is R^2, the description is delated in the manuscript.

10) P20 Fig 7. This text is too small; also the quantities should be plotted with differetn y-scales to see more details.

R: revised, please see figure 11 in the revised vision.

11) P23 Table 1 could be replaced by power consumption.

R: revised

12) P24 Table 2 are these numbers accuracy and precision?

R: Yes, revised.

13) P24 Table 3: I would consider only 2 significant digits for normalized RMSE and direction values as sufficient, e.g. 4.6 (instead 4.55) or 4.3 (instead 4.27)

R: revised.

14) In addition the term “et al” needs to be replaced by “et al.”. The manuscript needs thorough proof-reading after revision.

R: revised.

3. Reviewer 3

Summary:

This manuscript describes a study that is relevant to Atmospheric Measurement Techniques. The authors describe procedures and measurement performance of a coherent Doppler wind lidar (CDWL) from ship. The manuscript proposes an algorithm to compensate for error of wind measurement due to the motion of the ship and provides contributions for lidar communities using shipborne applications. The manuscript has some issues that need clarification. There are numerous specific comments. A major revision of manuscript is needed before it can be accepted for publication.

General comments:

1) Although details of a CDWL WindPrintS4000 are not described in the previous papers, in my opinion, details of the CDWL are not described well. The authors use an AOM for the heterodyne detection and a FPGA for FFT analysis. But there is no information about the sampling frequency and points used for FFT. The information is related to range-resolution for the time-domain, frequency-resolution for the frequency-domain and observable wind speed range. In the manuscript, bandwidth of 50MHz is used for data processing. Do you use a FPGA operating at a sampling frequency of 100MHz? Is it correct? In the previous paper, a AOM of 80MHz is used for the heterodyne detection. Therefore, frequency range of 60-100 MHz at center of 80MHz is detection range to determine LOS wind speed. 20MHz corresponds to be LOS wind speed of 15.5 m/s. ±50 m/s is “speed measurement range” shown in the previous paper. It is not consistent each other. It is puzzled to me. I might be missing something...and if so, please describe technical details and other aspects of the CDWL for better understanding the manuscript.

R: The SNR in this study is defined as the ratio of the peak value of FFT spectral signal in each range bin to the Root-Mean-Square (RMS) of background noise signal. Figure 1 shows the array of the spectral $S(l\Delta f;k\Delta R)$, where $l=0,1,2,3,...,L-1$ is the spectral channel number and $L=100$. In this case the frequency resolution $\Delta f \approx 0.98$ MHz and the corresponding velocity resolution is $\Delta V = 0.76$ ms^{-1}. The bandwidth $B_{100}=(L-1)\Delta f = 97.68$ MHz, and the corresponding radial velocity measurement range is ± 37.5 ms^{-1}. The elevation angle for 4-DBS is normally set as 60°, so the detectable maximum horizontal wind speed is ± 106 ms^{-1}.

2) Definition of SNR is given in the manuscript. SNR=0dB means the signal power equals to noise power (NEP). Is it correct? Do you mean that the minus values are bad estimates? Minus values of SNR are shown in Figures 7 and 9. Why? Please describe details and derivation of SNR and search procedure by adding explanation sentences and figure.

R: The SNR in this study is defined as the ratio of the peak value of FFT spectral signal in each range bin to the Root-Mean-Square (RMS) of background noise signal. Figure 1 shows the array of the spectral $S(l\Delta f;k\Delta R)$, where $l=0,1,2,3,...,L-1$ is the spectral channel number and $L=100$. In this case the frequency resolution $\Delta f \approx 0.98$ MHz and the corresponding velocity resolution is $\Delta V = 0.76$ ms^{-1}. The bandwidth $B_{100}=(L-1)\Delta f = 97.68$ MHz, and the corresponding radial velocity measurement range is ± 37.5 ms^{-1}. Figure 1a shows the last 10 range gates raw array of spectral in green line. We estimate the averaged background noise spectrum

$$\overline{S}_N(l\Delta f)=\frac{1}{10}\sum_{k=94}^{103}S(l\Delta f;k\Delta R) \tag{8}$$

Subtracting the background noise spectral $\overline{S}_N(l\Delta f)$ from the raw spectral array $S(l\Delta f;k\Delta R)$, the unnoisy array of spectral $S(l\Delta f;k\Delta R)$ can be obtained and shown in red line in Fig. 1. The peak value index l_{peak} from the $S(l\Delta f;k\Delta R)$ can be firstly obtained and thus the absolute signal power $P_s(k\Delta R)$ at various ranges $k\Delta R$ can be represented as:

$$P_s(k\Delta R)=S(l_{peak}\Delta f;k\Delta R)-\frac{1}{12}\left(\sum_{l_{peak}-20}^{l_{peak}-15}S(l\Delta f;k\Delta R)+\sum_{l_{peak}+15}^{l_{peak}+20}S(l\Delta f;k\Delta R)\right) \tag{9}$$

Replacing integration by summation and taking into account that the zero velocity point in one channel is $l_{zero}=50$, we estimate the noise power P_N as

$$P_N=\frac{1}{10}\sum_{k=94}^{k=103}\sqrt{\frac{1}{21}\sum_{l=l_{zero}-10}^{l_{zero}+10}\hat{S}_N(l\Delta f;k\Delta R)^2} \tag{10}$$

Finally, we obtain the range profile of the $SNR(k\Delta R)$ using the equation

$$SNR(k\Delta R)=10\log_{10}\left(\frac{P_s(k\Delta R)}{P_N}\right) \tag{11}$$

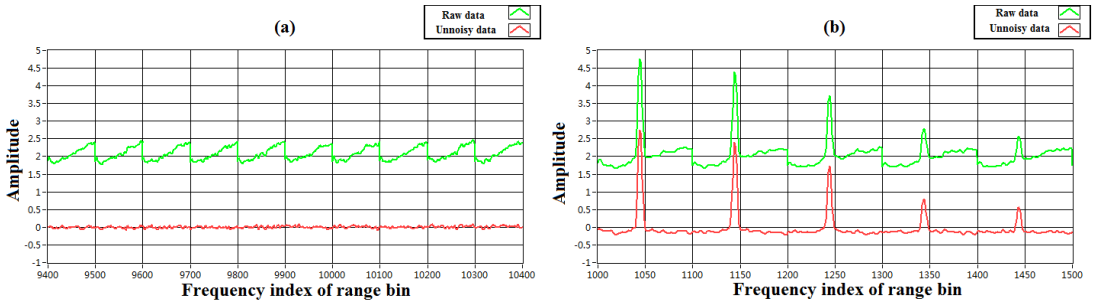

Figure 1: The CDL measured array of the FFT spectra (a) the last 10 range gates spectra for background noise spectrum estimation (b) the 1st – 5th range gates (150 m – 270 m, range resolution is 30 m) spectrum.

The SNR from Banakh et al. 2013 is defined as the ratio of the averaged heterodyne signal power P_s to the average detector noise power P_n in a 50-MHz bandwidth. The power P_s and P_n are integrals of the spectral densities $S_s(f)$ and $S_n(f)$, respectively, in frequency f within a band of width B_{50}, that is:

$$P_s = \int_{B_{50}} S_s(f)df \tag{5}$$

$$P_n = \int_{B_{50}} S_n(f)df \tag{6}$$

Comparing the definition from Banakh et al. 2013, the SNR in this paper is simpler and also indicates the CDL detection capability, data accuracy and atmospheric tracer particle relative intensity. In this sense, the SNR threshold value in this paper is higher than the one in previous studies (Banakh et al. 2013; Achtert et al 2015) for the same

3) It is also necessary to describe here the statistical process of these measures. How did you calculate LOS wind speed error and bias? How many radiosondes did you launch? What is the vertical resolution of the radiosonde? How do you interpolate to the CDWL data to for compare with the radiosonde? Ex. vertical resolution of the CDWL is 60m, while the vertical resolution of the radiosonde is 30m. The tow data points measured by the radiosonde are used for comparison with the CDWL. Or, one data averaged using two data points are used for that. Are data in the altitude range between 150m and 4000m used for the statistical comparison show in the Figure 6. A question comes for the difference between number N of 990 shown in Figure 6 and number points (wind speed: 84, 106...65; wind direction: 89,93...88) shown in Table 4. Why are the numbers used for the wind speeds and wind directions are different? Please add explanation related to spatial and temporal difference between the DBS and the radiosonde measurements.

R: The bias of the LOS wind is calculated using Eq. 12-15 in the revised manuscript, and it is based on the error propagation theory. The error of LOS wind at specific azimuth and elevation angle is difficult for shipborne measurement since the ship

motion results in measurement from various directions. It is different from the error analysis of vertical velocity. The corrected vertical velocity is the velocity from zenith stare direction. Thus the error of vertical velocity can be obtained from the time series of corrected vertical velocity using frequency spectrum analysis.

In order to assess the accuracy of the shipborne lidar wind measurement, a comparison of the lidar measurement and 11-radiosonde dataset during the experiment has been made. It is noted that the range resolution of lidar in this study is 30 m, and the corresponding vertical resolution with elevation angle of 60° is about 26 m. The vertical resolution of radiosonde is 10 m. During the comparison, the wind profile of radiosonde should be interpolated to the common height grid with finer resolution of 2 m firstly, and then the data point closest to height point of lidar will be chosen for comparison. The measurement range in this study is between 150 m and 3240 m (corresponding to the 104th range bin), thus the altitude range between 130 m and 2806 m are used for the statistical comparison shown in the Fig. 8.

The dataset for comparison in Fig.8 in the revised manuscript excludes the data where $|ydata - xdata| > 2 * SD$. The $ydata$ and $xdata$ is the Lidar and corresponding radiosonde data, respectively, and SD represents the standard deviation of the difference of $ydata - xdata$. According to the distribution of difference of $ydata - xdata$ and fitted Gaussian distribution shown below, the criteria of excluding data with $2 * SD$ is reasonable for gross outliers. The excluded data-pair number and proportion is 62, 6% for wind speed and 56, 5.9% for wind direction, respectively. The number used for the wind speeds and wind directions are different since the $|ydata - xdata| > 2 * SD$ in wind speed and direction comparison is different from each other.

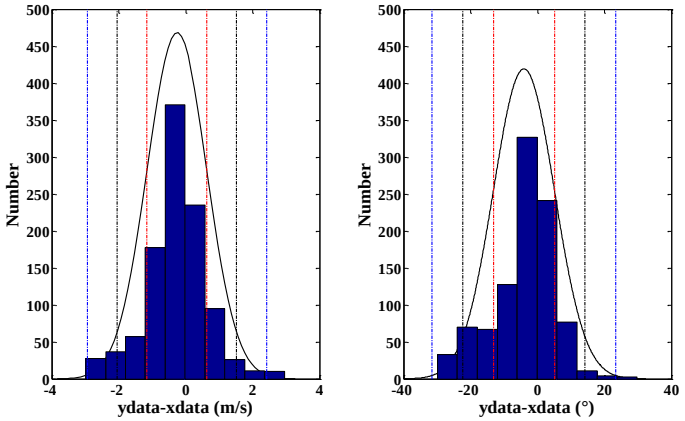

Figure 1: Distribution of difference (lidar-radiosonde) (a) wind speed (m/s) (b) wind direction (°)

4) How did you determine misalignment and angle between the ship and laser beam axes? Although explanation sentences using a hard target are descried in the manuscript, technical details and other aspects of this are not described well. More details should be provided.

R: In our system, the inertial navigation system is rigidly mounted on the base of the scanner, instead of the deck of the ship, to keep constant relative angles with reference to the transmitting laser beam. It records the Lidar motion angles including pitch, roll, laser beam azimuth and elevation, thus the recorded attitude information is the exact Lidar itself feature in Lidar coordinate system. After installation, a hard target calibration is firstly performed to determine the misalignment between the ship and laser beam axes. Specifically, the buildings near the wharf where there is no occlusion issue between the CDL and the candidate buildings can be chosen as the hard target. As shown in Fig.1, when the laser beam direction points to the hard target, the azimuth angle φ_{lidar} in Lidar coordinate system is recorded, meanwhile the azimuth angle φ_g in Earth Coordinate System can be obtained using the Google Earth software if the exact longitude and latitude of hard target is determined. According to the ship heading angle ψ, we can get the azimuth angle $\varphi_s = \varphi_g - \psi$ between ship heading and the hard target in Ship Coordinate System. So far, the misalignment angle between the ship and laser beam axes $\Delta\varphi = \varphi_s - \varphi_{Lidar}$ can be corrected using the geometrical relationship between these three angles. And then the standard ship attitude definition can be determined based on the relationship between Lidar and ship coordinate system, which will be used in the following ship motion correction process. It can be seen that there exists no laser direction error determined by misalignment between the ship and laser beam axes since the Lidar is considered to be relative static during field experiment.

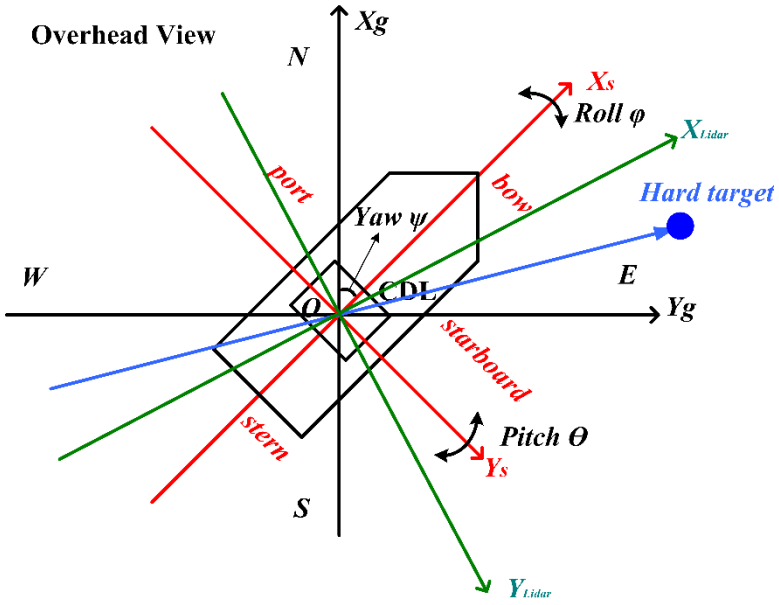

Figure 1. The overhead view of Lidar, ship and Earth coordinate system and corresponding hard target calibration.

Specific Comments:

1) P. 2 line 22, “wind speed”. Do you mean “wind vector”?

R: Yes, revised

2) P. 3 line 4, “the CDL”. a CDL

R: revised

3) P. 3 line 4, “vertical wind”. horizontal wind

R: revised

4) P. 3 line 11, “In order to ...the Yellow sea”. What is main purpose of the experimental investigation? Scientific or Engineering?

R: The main objective and further plan is described in the revised version Introduction and Summay, see below:

Introduction part:

As one of the main objectives, the CDL was deployed on the ship in this campaign to demonstrate the feasibility of the algorithm-based attitude correction method. The obtained accurate three-dimensional wind information can provide significant preparation for further studies on characteristics of dynamics and thermodynamics in the MABL and turbulence flux exchange over sea surface. In addition to CDL, as another important part of this campaign, a High Spectral Resolution Lidar (HSRL) and a Vaisala CL31 ceilometer were also deployed on the ship platform in order to detect MABL height spatial-temporal evolution and to retrieve the aerosol and cloud optical characteristics such as extinction coefficient and backscatter ratio and so forth. It will help us to understand the complex behaviour of MABL and the aerosol cloud forcing characteristics over sea region and the impact on climate change. This paper focuses on CDL performance and gives a thorough analysis of the attitude correction for lidar velocity measurement.

Summary part:

Overall, combining a CDL with attitude correction system and accurate motion correction process as presented here forms a reliable and autonomous set-up that could be placed on mobile platform to provide more detailed, higher spatial and temporal resolution view of three-dimensional wind field information. It will be further validated and improved under different sea conditions using CFD model simulation in further field campaign. More specific studies are being carried out or prepared, including atmospheric turbulence characteristics statistics and multi-scale wind field observation in MABL, wind turbine wake and atmospheric turbulence interaction over offshore wind power field (Wu et al., 2016; Zhai et al., 2017), mass transport and

flux analysis in MABL with combination of CDL and Multi-wavelength Polarization Raman Lidar (Wu et al., 2016), and the forthcoming ADM-Aeolus wind data validation over China Sea in 2018.

5) P.3 line 30, "200ns". Is the number for 150μJ at 10 KHz?

R: The pulse width produced by the modulation is adjustable from 100 ns to 400 ns. In this study, the pulse width of 200 ns, corresponding to the range resolution of 30 m, is used. The pulsed energy is approximately 150 μJ and the pulse repetition frequency is 10 kHz.

6) P.4 line 2, "a proper". Do you mean "high"?

R: Yes, revised

7) P.4 line 9, "Yellow Sea". "the Yellow Sea". There are the same expressions in the manuscript. Please check in the manuscript

R: Revised

8) P.4 line 13-15, "The inertial navigation system is ...laser beam". How did you confirm to keep the constant relative angle?

R: I didn't explain it clearly.

"The inertial navigation system is rigidly mounted on the base of the scanner, instead of the deck of the ship, to keep constant relative angles with reference to the lidar coordinate system.

9) P.4 line 16-17, "Hard target calibration". How did you conduct out the hard target calibration? Please describe details about it and statistical results (bias and error)

R: The specific description can be seen in General comments question 3. Generally, the buildings near the wharf where there is no occlusion issue between the CDL and the candidate buildings can be chosen as the hard target. As shown in Fig.1, when the laser beam direction points to the hard target, the azimuth angle φ_{lidar} in Lidar coordinate system is recorded, meanwhile the azimuth angle φ_g in Earth Coordinate System can be obtained using the Google Earth software if the exact longitude and latitude of hard target is determined. According to the ship heading angle ψ, we can get the azimuth angle $\varphi_s = \varphi_g - \psi$ between ship heading and the hard target in Ship Coordinate System. So far, the misalignment angle between the ship and laser beam axes $\Delta\varphi = \varphi_s - \varphi_{Lidar}$ can be corrected using the geometrical relationship between these three angles. And then the standard ship attitude definition can be determined based on the relationship between Lidar and ship coordinate system, which will be used in the following ship motion correction process. It can be seen that there exists no laser direction error determined by misalignment between the ship and laser beam axes since the Lidar is considered to be relative static during field experiment.

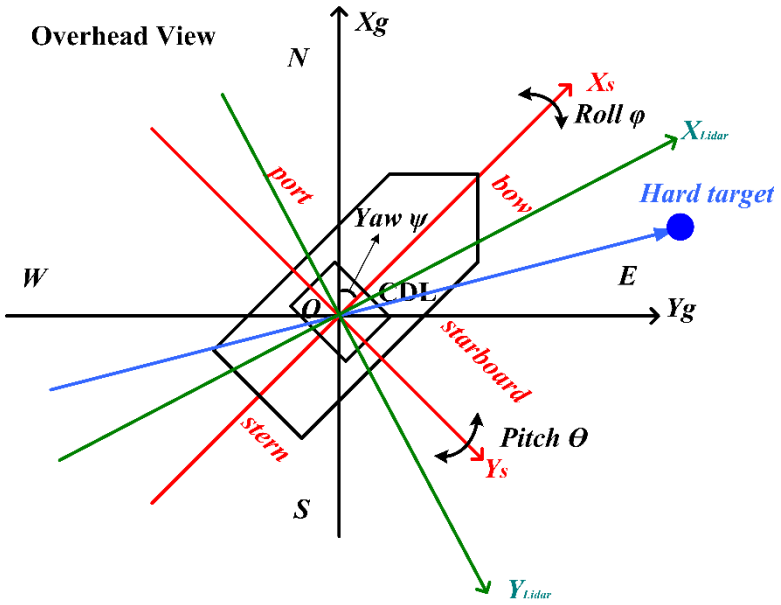

Figure 1. The overhead view of Lidar, ship and Earth coordinate system and corresponding hard target calibration.

10) P.4 line 19-20, "laser direction". Do you mean "laser beam direction"? What do you mean "between the ship and..."? Please explain it and show the axes in Figure 2.

R: Yes, the "laser direction" means "laser beam direction". The ship and Lidar coordinate system are shown in fig.2 in revised version with red and green arrowed lines, respectively. "between the ship and …" mean the the laser direction error determined by misalignment between the ship and Lidar is negligible since the Lidar is considered to be relative static compared with ship during the field experiment.

11) P.5 line 3, "the transmitting laser path". Do you mean "laser beam direction"?

R: Yes, revised

12) P.5 Eq. 3, (x, y, z) ->(xg, yg, zg)

R: Revised, see Appendix A

13) P.5 line 9, "Where" -> "where"

R: Revised

14) P.5 line 10, "Eq. (2)-(3)" -> "Eqs. (2) and (3)"

R: Revised

15) P.5 Eq. 4, (y/x) ->(yg / xg)

R: Revised

16) P.5 Eq. 5, z -> zg

R: Revised

17) P.7 line 3-4, please describe the definition of SNR using a figure. Does the definition of SNR have minus value?

R: The specific description of SNR can be seen in General comment question 1.

18) P.7 line 16-17, please give observation time to get each LOS wind speed profile.

R: Revised, the temporal resolution of radial velocity is 0.5 s.

19) P.7 line 24, How do you determine the wind measurement fluctuation?

R: In this study, the horizontal wind profile with 2-min temporal resolution will be retrieved for vertical velocity correction. Basically, the LOS velocities from N, S, E, and W direction after SNR quality control during the chosen 2-min interval are collected firstly. Then the procedure of filtration of reliable estimates of each radial velocity based on SNR threshold is used to obtain "good" speed estimates. The selected radial velocities and corresponding ship condition information in each radial direction are averaged and the averaged ship condition will be used for the removal of platform velocity effect. Finally, the horizontal with 2-min temporal resolution can be retrieved using modified 4-DBS mode. The vertical wind measurement has a temporal resolution of 0.5 s, the horizontal wind whose retrieved time is closest to vertical wind measured time will be used for vertical velocity correction.

The blue bars shown in Fig. 5 and 6 represent the standard deviation of CDL wind measurement from the 2-min temporal resolution results during the chosen analyzed period, which can effectively represent the atmospheric fluctuations.

20) P.7 line 28, "SNR threshold". Please add the threshold value.

R: Revised. Data quality control based on SNR threshold is used to remove the spikes higher than 2.4 km . The SNR threshold in this study is 8 dB and the reason has been analyzed in Sect. 3.3.

21) P.8 line 26, "measurement". "measurements"

R: Revised.

22) P.8 line 27, "multipath". I do not understand it. Please add explanations.

R: Since the drift of radiosonde is affected by atmospheric wind and turbulence perturbation, and the CDL detection volume is changing during cruising observation, the result discrepancy between radiosonde and CDL caused by different observation location, also called the multipath effect, is larger with increasing height.

23) P.11 line 1, "shipborne-based". "ship-based" or "shipborne".

R: Revised.

24) P.11 line 9-10, "assuming that the wind field has a constant horizontal and vertical velocity". Is the assumption always reasonable? What is the spatial and temporal scale of wind field when the assumption is reasonable.

R: Whether the assumption is reasonable or not depends on particular investigated process, land surface condition and atmospheric stratification stability. Specifically, under the assumption of homogeneous flow with little turbulence which would lead to a smooth sinusoidal behavior in the VAD scan, it can be expected that 4-DBS mode should be sufficient, along with one measurement in the vertical. It is faster and simpler both in the hardware and in the data evaluation algorithm, but lacks the goodness-of-fit information as a measure for the reliability of the results (Weitkamp 2005). This shortcoming is partially compensated by information about the temporal behavior of the data. Therefore, the parameters such as maximum range, range resolution, temporal resolution (or scan rate) need to be set carefully based on a given purpose (Weitkamp, 2005).

In this study, both the ship-induced shift and radial velocity have the same temporal resolution of 0.5 s, and the pulse repetition rate is 10 kHz, which is useful for the detection of small-scale turbulence. The temporal resolution of horizontal wind profile is 2-min, and it is reasonable for the knowledge of background wind field. The temporal resolution of vertical velocity is 0.5 s, which is necessary for atmospheric turbulence characteristics statistics. If the mean wind speed is 5 m/s, the corresponding smallest spatial and temporal scale of wind field for the homogeneous isotropic assumption is 600 m and 2 min, respectively.

25) P.11 line 13, "the lidar pointing angle". Do you mean the laser beam direction?

R: Yes, revised.

26) P.12 line 6-8, "In this case...2016).". Why do you have to use the Hamming window and zero-padding? Please clarify it. What is the difference between with and without Hamming window and zero-padding?

R: A 50 % window overlap factor, a Hamming window is used in order to reduce leakage in the spectra. A zero-padding of the missing values were applied to each window for each spectrum calculation to improve the frequency resolution. Figure 1 shows the results without and with Hamming window and zero-padding. It can be seen that the P(f) with Hamming window is more smoother and easier to find the constant frequency region for random error estimation.

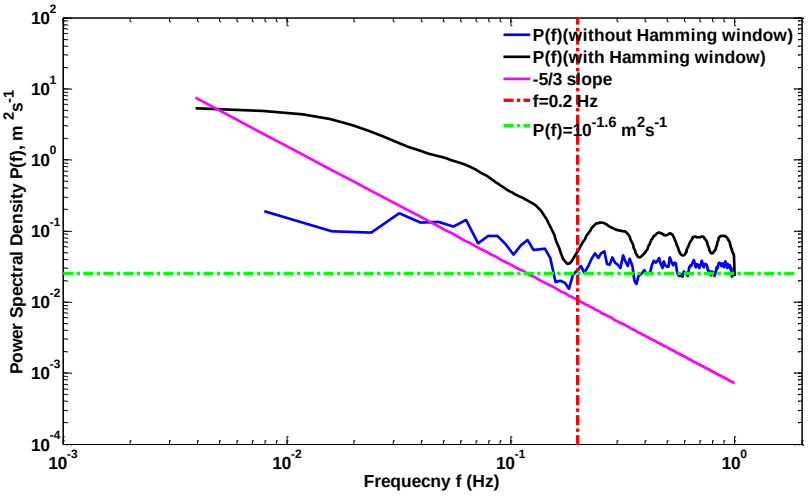

Figure 1: Power spectral density P(f) without and with Hamming window for the CDL measured vertical speed between 15:52 and 16:02 LST on 09 May and for an altitude of 1495 m (blue and black solid line, respectively). The expected spectral behaviour according to the Kolmogorov's−5/3 law (pink solid line), the noise frequency threshold (red dotted line) and the derived noise floor for the CDL (green dotted line) are shown.

27) P.12 line 16. "Eq.". "Eqs."

R: Revised.

28) P.12 line 21-23. "8dB." Why "8dB"? How do you determine the number? Please add explanation sentences. SNR looks the same value at 1 km as at 1.5 km. But different random errors at the altitudes are shown in the Figure 9. Why?

R: It can be seen that in the high SNR region above 8 dB, a constant random error range between 0.03 and 0.15 ms^{-1} is found because of the effect of the speckle-induced phase noise (Frehlich, 1997; Frehlich, 2001). At reduced values of the SNR, the errors increase as a result of increasing signal noise, rising to approximately 4 ms^{-1} at an SNR = 0 dB. It is confirmed that the choice of a conservative SNR threshold of 8 dB is robust for data quality control process.

The SNR at 1 km and 1.5 km are 7.3 dB and 7.2 dB, respectively. The Power spectrum density from 1 km and 1.5 km can be seen in figure 1, and figure 2 is the corresponding noise time domain signal. It can be seen that although the SNR has the same level, the standard deviation of velocity can be different because of specific signal.

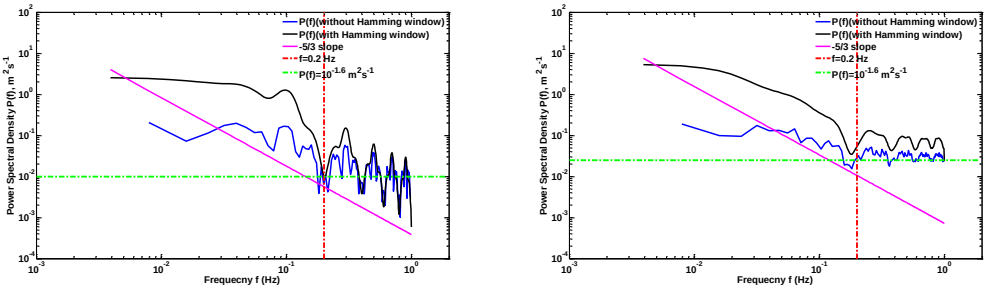

Figure 1: the power spectrum density at (left) h=1.002 km (right) h=1.495km

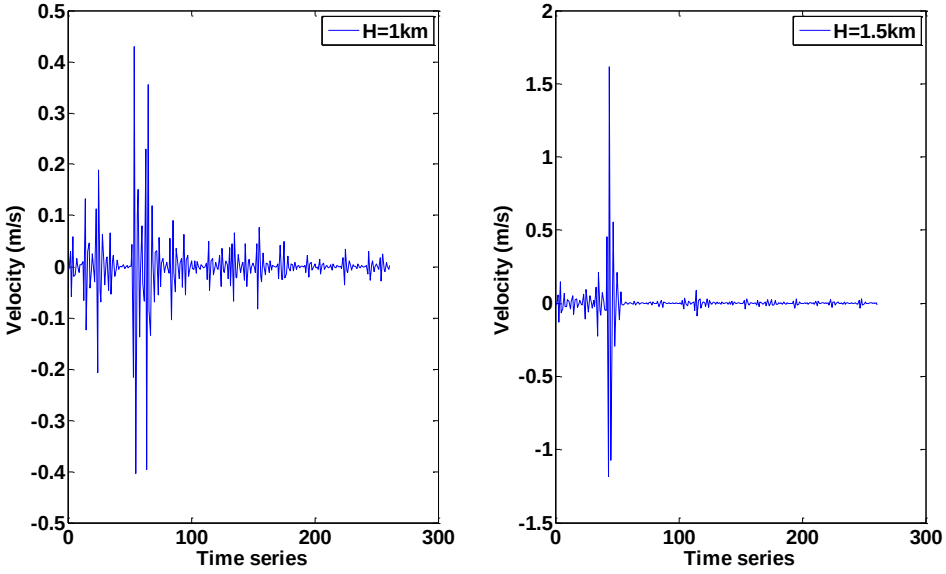

Figure 2: Time series of noise time domain signal at (left) h=1.002 km and (right) h=1.495km

5

29) P.12 line 23-25. "At reduced values...0 dB." Please plot results until SNR be 0dB in the Figures 9(a)-9(c). It is important for readers to identify the measurement performance of your CDWL. SNR=0 means the signal power equals to noise power (NEP), which is undetectable a true signal. Random errors would be large. "4 m/s" seems to be small.

R: The figure 13 shown in revised version shows the SNR profile from 0.15 km to 3.105 km. It is noted that the CDL blind
10 area is less than 0.15 km and the maximum detection range is 3.105 km. The minimum of SNR in Figure 1a is 1.08 dB at height of 3.105 km. The SNR=0 means that the peak value of spectrum equals to the mean RMS of background noise spectrum, see Eq.4, thus not representing the signal power equals to noise power. What's more, we didn't explain it clearly, figure 1b shows the random error of vertical velocity where 4 m/s is large for the order of vertical velocity.

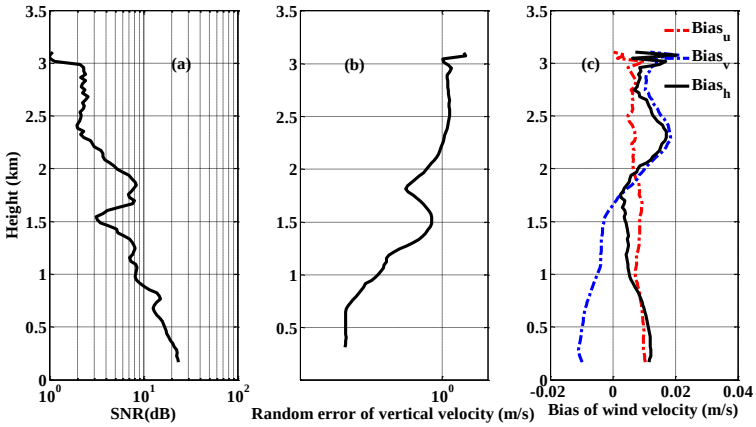

Figure 1: The averaged profile of (a) SNR (b) Random error of vertical velocity (c) bias of horizontal wind north-south component (u), east-west component (v) and horizontal wind velocity (h) measured by CDL from 15:52 to 16:02 LST on 09 May, 2014.

30) P.14 line 4. "Shipborne wind observation". This manuscript describes an algorithm to compensate for error of wind measurement due to the motion of the ship, not observation. Please modify explanation sentences to insist on the main purpose of the manuscript.

R: Revised. "Shipborne wind observation by a CDL during the 2014 Yellow Sea campaign are carried out to study the structure of the MABL. An algorithm to compensate for error of wind measurement due to the motion of the ship is presented in this paper."

31) P.14 line 12. "The correlation...respectively,". Please add details such as date, time, altitude range, and so on.

R: Revised. "In order to assess the accuracy of the shipborne lidar wind measurement, a comparison of the lidar measurement and 11-radiosonde dataset from 09 May 2014 to 19 May 2014 has been made. The total number of wind speed and direction dataset for comparison is 1062 and 951, respectively."

32) P.14 line 19-21. "random error...radiosonde data,". Please add explanation sentence about date, time and altitude.

R: Revised. "A case study during 15:52 to 16:02 LST on 09 May 2014 is presented. The height range is from 0.15 km to 3.105 km where the blind area of CDL is less than 0.15 km and the maximum detectable range is 3.105 km. It is found that the random error of vertical velocity is between 0.03 ms^{-1} and 1.2 ms^{-1} and is mainly determined by the SNR, while the bias was less than 0.02 ms^{-1}, which is negligible and consistent with the result of comparison between lidar and radiosonde data."

Reference:

1) P.14 line 12. Please add pages.

R: Banakh, V., and Smalikho, I.: Coherent Doppler wind lidars in a turbulent atmosphere: Artech House, 1-10, 2013.

2) P.14 line 23. Please add pages: 46754692. Figure and Tables

R: Chouza, F., Reitebuch, O., Jähn, M., Rahm, S., and Weinzierl, B.: Vertical wind retrieved by airborne lidar and analysis of island induced gravity waves in combination with numerical models and in situ particle measurements, Atmos. Chem. Phys., 16, 4675-4692, 2016.

3) P.19 Figure 4. Label and "(a)" , "(b)", "(c)" and , "(d)" are small. Please use larger fonts.

R: Revised.

4) P.19 Figure 5. Label and "(a)" , "(b)", "(c)" and , "(d)" are small. Please use larger fonts.

R: Revised.

5) P.20 Figures 6. "(a)" and "(b)" are small. Please use larger fonts.

R: Revised.

6) P.20 Figures 7. Label and "(a)" , "(b)", and "(c)" are small. Please add horizontal wind speed.

R: Revised.

7) P.20 Figures 7. Label and "(a)" , "(b)", and "(c)" are small. Please use larger fonts.

R: Revised.

8) P.21 Figures 8. "(a)" , "(b)", and "(c)" are small. Please use larger fonts.

R: Revised.

9) P.21 Figures 9. "(a)" , "(b)", and "(c)" are small. Please use larger fonts.

R: Revised.

Shipborne Wind Measurement and Motion-induced Error Correction of a~~by~~ Coherent Doppler Lidar over the Yellow Sea in 2014

Xiaochun. Zhai[1], Songhua. Wu[1, 2], Bingyi. Liu[1, 2], Xiaoquan. Song[1, 2], Jiaping. Yin[3]

[1]Ocean Remote Sensing Institute, Ocean University of China, Qingdao, 266100, China
[2]Laboratory for Regional Oceanography and Numerical Modelling, Qingdao National Laboratory for Marine Science and Technology, Qingdao, 266100, China
[3]Seaglet Environmental Technology, Qingdao, 266100, China

Correspondence to: S. Wu (wush@ouc.edu.cn)

Abstract. Shipborne wind observations by a~~the~~ Coherent Doppler Lidar (CDL) have been conducted to study the structure of the Marine Atmospheric Boundary Layer (MABL) during the 2014 Yellow Sea campaign. This paper evaluates uncertainties associated with the ship motion and presents the correction methodology regarding lidar velocity measurement based on modified 4-Doppler Beam Swing (DBS) solution. The errors of calibrated measurement, both for the anchored and the cruising shipborne observations, are comparable to those of ground-based measurements. The comparison between the lidar and radiosonde results in a ~~gives the~~ bias of -0.23~~1~~ ms^{-1} and a~~the~~ standard deviation of 0.87~~75~~ ms^{-1} for the wind speed measurement, and ~~shows the bias~~ 2.48° and ~~the standard deviation~~ 8.84° for the wind direction ~~measurement~~. The biases of horizontal wind speed and random errors of vertical velocity ~~of horizontal wind speed~~ are also estimated using the error propagation theory and frequency spectrum analysis, respectively. The results show that the biases are mainly related to the measuring error of the ship velocity~~,~~ and lidar pointing error, and the random errors are mainly determined by the Signal-to-Noise Ratio (SNR) of lidar backscattering spectral signal. It allows for the retrieval of vertical wind, based on one measurement, with random error below 0.15 ms^{-1} for appropriate SNR threshold and bias below 0.02 ms^{-1}. The combination of the CDL attitude correction system and the accurate motion correction process has the potential of continuous long-term high temporal and spatial resolution measurement for MABL thermodynamic and turbulence process.

1 Introduction

The vertical structure of atmospheric variables in the Marine Atmospheric Boundary Layer (MABL) plays an important role in the earth's climate system, governing exchanges of energy, sensible heat, water vapour and momentum between ocean and the overlying atmosphere (Rocers et al., 1995; Wulfmeyer and Janjic, 2005), and the turbulence characteristics are significant for understanding the driving and coupling mechanisms and for parameterizing ocean-atmosphere interaction process. There are a number of ~~many~~ studies on the turbulent fluxes measurement over the sea surface. Various motion sensing technique on the moving platform has been developed in the field of airborne (Axford, 1968), space-borne (Hawley et al., 1993) and shipborne observations (Fujitani, 1992; Song et al., 1996; Edson et al., 1998; Miller et al., 2008). Many shipborne field

experiments have been widely carried out over Pacific Oceanic area (Mitsuta et al., 1974; Bradley et al., 1991; Shao, 1995; Tsukamoto et al., 1995). (Axford, 1968; Mitsuta et al., 1974; Bradley et al., 1991; Fujitani, 1992; Hawley et al., 1993; Shao, 1995; Tsukamoto et al., 1995; Song et al., 1996; Edson et al., 1998; Miller et al., 2008). One of the most common direct techniques for measuring surface fluxes is eddy-correlation, which utilizes the covariance of mixing ratios and vertical wind velocity (Lenschow et al., 1981; Anctil et al., 1994; Fairaill et al., 2000), but the wind velocity retrieval is complicated by the contamination due to platform motion, representing a major source of uncertainty in measurement of turbulence and air-sea interaction. Several techniques have been used to correct the wind vector measured at sea for the influenceefforts of platform motion (Fujitani, 1992; Dunckel et al., 1974; Song et al., 1996; Edson et al., 1998; Schulz et al., 2005). Fujitani (1985) used a Stable Platform System (SPS) consisting of a vertical gyro-stabilized system and three accelerometers to measure the turbulent flux on the ship, and concluded that this system was applicable to measurement under the rough sea surface condition. A similar method was also used on a buoy (Anctil et al., 1994). This gyro-stabilized system can provide roll, pitch and yaw angles describing the ship's orientation in a fixed frame, which can be used directly in the total rotational coordinate transformation matrix. Song et al. (1996) used a Strapped-Down System (SDS) consisting of six accelerometers to measure the air-sea fluxes in the Western Tropical Pacific and estimated that the system appeared to be relatively robust for use at sea for extended period. In SDS, the attitude angles are should be calculated indirectly from the strapped-down angular rate sensors. Edson (1998) also used the SDS consisting of three orthogonal angle rate sensors and three orthogonal linear accelerometers to compute direct covariance fluxes from anemometers mounted on a moving platform at sea, and found that the results were in good agreement with fluxes derived using the bulk aerodynamic method. Miller et al. (2008) modified the procedure of Edson (1998)E98 procedure to explicitly account for misalignment between anemometers and motion sensors.

The Coherent Doppler Lidars (CDL) hashave proven to be powerful tools with high temporal and spatial resolution, providing nearly continuous particle backscatter, and wind profile observation in the cloud-freeclear atmosphere, which is vital for the vertical structure of turbulent characteristics measurement in MABL. Unlike the conventional in-situ wind measuring methods, CDL can only detect the line-of-sight (LOS) velocity which is the projection of the horizontal and vertical velocity along the laser beam direction, thus it is necessary to conduct measurement at three or more different directions of the probing beam to retrieve the wind vectorvelocity (Werner 2005; Cheong et al., 2008). More complicated attitude correction need to be should be considered when CDL is carried out at a moving platform such as ship or aircraft since the orientation of transmitting laser beam is not fixed and the speed of the ship itself and ocean wave will be stacked to the LOS velocity, which has a more serious detrimental obvious effect on vertical velocity. Several studies researches have been carried out to investigate study the CDL platform motion correction either by actively stabilizing the instrument based on robust mechanical compensation system or by accurately measuring platform motion and correcting for this in post-processingafter the fact. Wolfe et al. (2007) and Pichugina et al. (2012) deployed the NOAA High Resolution Doppler Lidar (HRDLHSRL) along with the first use of a motion compensation system at sea in 2004. The HRDL HSRL control computer can drive the scanner to actively stabilize the pointing of the scanner and modified Velocity Azimuth Display (VAD) technique are used in the mean-profile calculation. Hill et al.

(2005; 2008) used the NOAA HRDL ~~HSRL~~ with a SDS to compensate for the orientation of the lidar's scanning unit for the ship's motion and concluded that the attitude correction depends on the velocity of the seatainer and on the motion of the hemispheric scanner relative to the seatainer. Wulfmeyer et al. (2005) corrected the vertical velocity using LOS velocity in zenith stare mode and horizontal wind derived from VAD mode using NOAA- HRDL~~HSRL~~. Lacking real-time control of the scanning head orientation, Achtert et al. (2015) placed ~~a~~the CDL instrument on a motion-stabilization platform to remove the effect of ship motion, and the five-point geometrical wind solution and the four-point sinusoidal fit method were used to obtain wind profiles, showing that motion stabilization was successful for high wind speed in open water and the resulting wave condition. Reitebuch et al. (2001) presented the instrumental correction required for the ~~vertical~~ horizontal wind retrieval from an airborne CDL using conical scanning pattern measurement and recalculation of the lidar mounting angle based on the ground return speed and distance. It can be seen that actively mechanical compensation system is used in most of these studies. Especially, the improvements in technology along with decreasing costs and robust correction process are increasing needed. In order to simplify the mechanical structure and to ease installation of the CDL on the ship platform, an algorithm-based attitude correction method was developed for relaxing the requirements for mechanical stability and active compensation mechanisms. This method did not use any active stabilization method. Instead, only a relative simple but robust algorithm was used to achieve the motion correction in post-processing, which is very easy to use in limited space under the conditions of the shipborne measurements.

The experimental investigation was undertaken by *Dongfanghong-2* research vessel affiliated with Ocean University of China in 2014 over the Yellow Sea. The Yellow Sea, a marginal sea of the Pacific Ocean, is the northern part of the East China Sea. It is located between mainland China and the Korean Peninsula. There is seldom study on boundary layer dynamics study based on CDL in this region. As one of the main objectives, the CDL was deployed on the ship in this campaign to demonstrate the feasibility of the algorithm-based attitude correction method. The obtained accurate three-dimensional wind information can provide significant preparation for further studies on characteristics of dynamics and thermodynamics in the MABL and turbulence flux exchange over sea surface. In addition to CDL, as another important part of this campaign, a High Spectral Resolution Lidar (HSRL) and a Vaisala CL31 ceilometer were also deployed on the ship platform in order to detect the spatial-temporal evolution of the MABL height and to retrieve the aerosol and cloud optical characteristics such as extinction coefficient and backscatter ratio and so forth. It will help us to understand the complex behaviour of MABL and the aerosol cloud forcing characteristics over sea region and the impact on climate change. This paper focuses on CDL performance and gives a thorough analysis of the attitude correction for lidar velocity measurement. To illustrate the effect of ship motion on Doppler measurement, we focus on horizontal and vertical wind profile analysis. In Sect. 2, the specifications of CDL and especially its attitude correction system are described in detail, and the velocity correction method is discussed in. In Sect. 3, the corrected results of horizontal wind are analysed and compared with simultaneous radiosonde data. A case study is presented to analyse the effect of the ship velocity and horizontal wind on vertical velocity. Furthermore, the errors of horizontal and vertical velocity are analysed in Sect. 3. Finally, Sect. 4 provides a summary and concluding remark.

~~In order to simplify the mechanical structure and to easily install the CDL on the ship platform, our study did not use any active stabilization method. Instead, we only use a relative simple but robust algorithm to achieve the motion correction. This method is very easy to use in limited space under the conditions of the shipborne measurements.~~

~~With this method, we carried out the first cruise campaign. In order to measure the wind field and turbulence characteristics of MABL over the Yellow Sea, the experimental investigation was undertaken by *Dongfanghong 2* research vessel affiliated with Ocean University of China in 2014. The Yellow Sea, a marginal sea of the Pacific Ocean, is the northern part of the East China Sea. It is located between mainland China and the Korean Peninsula. Few studies have been devoted to measure the boundary layer dynamics in this region. This paper gives a thorough analysis of the attitude correction for lidar velocity measurement. To illustrate the effect of ship motion on Doppler measurement, we focus on horizontal and vertical wind profile analysis. In Sect. 2, the specifications of CDL and especially its attitude correction system are described in detail, and the velocity correction method is also discussed in Sect. 2. In Sect. 3, the corrected results of horizontal wind are analysed and compared with simultaneous radiosonde data. A case study is presented to analyse the effect of the ship velocity and horizontal wind on vertical velocity. Furthermore, the error analysis of horizontal and vertical velocity is also specifically analysed in Sect. 3. Finally, Sect. 4 provides a summary and concluding remark.~~

2 Lidar technology and methodology

The CDL system WindPrint S4000, manufactured by Seaglet Environmental Technology, is based on all-fibre laser technology and the heterodyne detection technology. Wu et al. (2016) and Zhai et al. (2017) provide~~have given~~ a comprehensive description of the CDL including a figure of the optical setup. The lidar has a semi-conductor single frequency seed laser that provides both the local oscillator reference beam for heterodyne detection as well as the transmitted beam. The laser operates at a wavelength of 1.55 μm with a linewidth (full width at half maximum of a~~from~~ Lorentzian function) of 1.6 kHz. Using the Acoustic Optic Modulator (AOM) and Master Oscillator Power-Amplifier (MOPA) configuration, the achieved pulsed energy is approximately 150 μJ ~~with~~ and the ~~a~~ pulse repetition frequency is~~of~~ 10 kHz. The number of laser shots used for each spectral accumulation is 5000. The pulse width produced by the modulation, which is also the width of time window for obtaining the lidar signal power spectrum, is adjustable from 100 ns to 400 ns, thus the spatial resolution can be varied from 15 m to 60 m. We typically operate the CDL with a pulse width of 200 ns for this study~~in this paper~~. The transmitted beam is directed into the atmosphere using the 3D scanner that contains an azimuth ~~mirror~~ and elevation mirror. The scanner allows the lidar beam to probe the hemisphere above the container by means of the "azimuth rotation" and "elevation rotation". The detection range of 4000 m (maximum 6000 m for high ~~at a proper~~ aerosol concentration) enables the system to monitor the complete MABL structure most of the time. A fibre optical circulator and a telescope are used as the optical transceiver. The atmospheric return beam passes through the 3D hemispheric scanner and the optical transceiver, and is combined ~~combines~~ with the local oscillator reference beam at the balanced detector. Using heterodyne detection, the frequency difference between

the atmospheric return beam and the local oscillator reference beam is detected, which is the measured Doppler shift caused by the relative motion of atmospheric scatters and the lidar system. The real-time analysis based on Fast Fourier Transform (FFT) is used with a Field Programmable Gate Array (FPGA) signal processer. Table 1 lists the general specifications of CDL.

Figure 1 shows the CDL setup on Dongfanghong-2 research vessel during the MABL field project over the Yellow Sea in 2014. It is located at the back of the upper deck and is around 8 m from the sea surface. The CDL scanner is mounted on the roof of the cabinet container with two fixed Global Navigation Satellite System (GNSS) antennas. Double antennas are used for determining the exact heading angle with accuracy of 0.1° when the ship is anchored. The attitude correction system uses XW-GI5651 MEMS Inertial/Satellite Integrated Navigation System. It is equipped with MEMS gyroscope, accelerometer, and multi-mode and multi-frequency GNSS receiver. It can realize single antenna dynamic alignment or double antenna auxiliary fast and high-precision orientation. The specifications are listed in Table 2. Generally, the attitude correction system uses GNSS to define ~~the Earth coordinate system~~ Earth coordinate system (ECS), where the ship speed, heading angle and earth location including the longitude and latitude in ECS ~~Earth coordinate system~~ can be obtained. Another important part of attitude correction system is the inertial navigation system (INS). The INS ~~inertial navigation system~~ is rigidly mounted on the base of the scanner within the cabinet container, instead of the deck of the ship, to keep constant relative angles with reference to the lidar coordinate system~~transmitting laser beam~~. It records the lidar motion angles in real time including pitch, roll, laser beam azimuth and elevation even when the GNSS is sheltered or disturbed, and ~~thus~~ the recorded information is the exact lidar itself attitude in lidar coordinate system. ~~After installation, a hard target calibration is firstly performed to determine the initial orientation of the laser beam in the Earth coordinate system, then the standard ship attitude definition can be determined based on the relationship between the lidar and the ship coordinate system, which will be used in the following ship motion correction process. It can be seen that there exists no laser direction error determined by misalignment between the ship and laser beam axis.~~ After installation, a hard target calibration is firstly performed to determine the misalignment between the ship and laser beam axes. Specifically, the buildings near the wharf where there is no occlusion issue between the CDL and the candidate buildings can be chosen as the hard target. As shown in Fig.2, the ECS, ship coordinate system (SCS) and Lidar coordinate system (LCS) are marked with black, red and green arrowed lines, respectively. When the laser beam direction points to the hard target, the azimuth angle φ_{lidar} in LCS is recorded, meanwhile the azimuth angle φ_g in ECS can be obtained using the Google Earth software if the exact longitude and latitude of hard target is determined. According to the ship heading angle ψ, we can get the azimuth angle $\varphi_s = \varphi_g - \psi$ between ship heading and the hard target in SCS. So far, the misalignment angle between the ship and laser beam axes $\Delta\varphi = \varphi_s - \varphi_{Lidar}$ can be corrected using the geometrical relationship between these three angles. And then the standard ship attitude definition can be determined based on the relationship between Lidar and ship coordinate system, which will be used in the following ship motion correction process. It can be seen that the laser direction error determined by misalignment between the ship and Lidar is negligible since the Lidar is considered to be relative static compared with ship during the field experiment.

Ship motion turns out to be an important error source for the determination of turbulence variables using shipborne CDL (Wulfmeyer and Janjic, 2005). To study boundary layer dynamics, the atmospheric wind velocity in ECS ~~Earth coordinate system~~ is required, so the compensation for the pointing error and along-beam platform velocity due to ship motion need to be determined using the attitude correction system. Figure 2 shows the specific definition of the parameters in SCS (X_s, Y_s, Z_s), ECS (X_g, Y_g, Z_g) and LCS ($X_{Lidar}, Y_{Lidar}, Z_{Lidar}$), respectively. Details on the motion-correction algorithm are given in Appendix A.

~~As can be seen in Fig. 2, the ship coordinate system (X_s Y_s Z_s) is defined as X_s axis along centre line of ship, positive toward bow, Y_s axis is perpendicular to X_s, and positive toward starboard, Z_s axis is positive toward the bottom. The attitude of the ship can be expressed by roll φ, pitch θ and heading angles ψ. The φ, θ and ψ refer to rotations about X_s, Y_s, and Z_s axes, respectively. Specifically, positive φ is defined when the port is up, and positive θ is defined when the bow is up. The ψ is defined 0° when the bow points to north in Earth coordination system. The Earth coordinate system (X_g Y_g Z_g) is defined as X_g axis along north-south direction, positive toward to north, Y_g axis is along east-west direction, and positive toward to east, Z_g axis is positive toward the bottom.~~

~~In the ship coordinate system, the recorded azimuth and elevation of the transmitting laser are φ_s and θ_s, respectively. φ_s is defined as the angle between the projection of transmitting laser path on X_s Y_s plane and the positive X_s axis. When looking downward, φ_s increases in a clockwise direction. θ_s is defined as the angle between the transmitting laser path and the X_s Y_s plane. Therefore, the direction of the transmitting laser in the ship coordinate system can be expressed by a unit vector $\vec{r}_s$ as (Hill, 2005; Liu et al., 2010).~~

~~$$\vec{r}_s = \begin{pmatrix} x_s \\ y_s \\ z_s \end{pmatrix} = \begin{pmatrix} \cos\theta_s \cos\varphi_s \\ \cos\theta_s \sin\varphi_s \\ -\sin\theta_s \end{pmatrix} \quad (1)$$~~

~~The coordinate transformation from the ship coordinate system to that of the Earth is needed. According to the transformation matrix from the product of three rotation matrixes shown in Eq. (2), the unit vector $\vec{r}_g$ of transmitting laser direction in Earth coordinate system can be expressed as Eq. (3)~~

~~$$H_2 = \begin{pmatrix} \cos\theta & 0 & -\sin\theta \\ 0 & 1 & 0 \\ \sin\theta & 0 & \cos\theta \end{pmatrix}, H_3 = \begin{pmatrix} \cos\psi & \sin\psi & 0 \\ \sin\psi & \cos\psi & 0 \\ 0 & 0 & 1 \end{pmatrix}, H_3 = \begin{pmatrix} 1 & 0 & 0 \\ 0 & \cos\varphi & \sin\varphi \\ 0 & -\sin\varphi & \cos\varphi \end{pmatrix}, \quad (2)$$~~

~~$\vec{r_g} = \begin{pmatrix} x \\ y \\ z \end{pmatrix} = (H_1 H_2 H_3)^{-1} \vec{r_s}$~~ ~~(3)~~

~~Where H_1, H_2, H_3 are the rotation matrices of roll, pitch and heading, respectively (Hill, 2005).~~

~~Once the unit vector $\vec{r_g}$ is calculated from Eq. (2) (3), the azimuth φ_g and elevation θ_g of LOS observation in Earth coordinate system can be calculated~~

~~$\varphi_g = \arctan(y / x)$~~ ~~(4)~~

~~$\theta_g = -\arcsin z$~~ ~~(5)~~

For a shipborne CDL, the recorded velocity corresponds to the relative velocity along the laser beam direction between the ship and the atmospheric target, where the ship platform motion will add to the measured LOS velocity in SCS ~~ship coordinate system~~. Therefore, the first step in the wind retrieval process is the removal of the along-beam platform velocity due to ship motion $\vec{V}_{LOS\_ship}$. It is noted that ~~the~~ wave-induced velocity perturbations would add to the ship's mean velocity when underway, which needs no correction independently in the correction procedure. During the experiment, the speed of the ship $\vec{V}_{ship}$ is acquired by GNSS with temporal resolution of 0.5 s, and is recorded as the horizontal component $\vec{V}_{ship\_horizontal}$ and vertical component $\vec{V}_{ship\_vertical}$, respectively thus the $\vec{V}_{LOS\_ship}$ can be calculated

$$\vec{V}_{LOS\_ship} = \vec{r_g} \cdot \vec{V}_{ship} = \vec{V}_{ship\_horizontal} \cos(\psi - \varphi_g) \cos\theta_g + \vec{V}_{ship\_vertical} \sin\theta_g \quad (16)$$

The LOS velocity $\vec{V}_{LOS}$ in ECS ~~Earth coordinate system~~ is the vector sum of the LOS velocity measured by CDL in SCS ~~ship coordinate system~~ $\vec{V}_{LOS\_measure}$ and the $\vec{V}_{LOS\_ship}$, that is ,

$$\vec{V}_{LOS} = \vec{V}_{LOS\_measure} + \vec{V}_{LOS\_ship} \quad (27)$$

and

$$\vec{V}_{LOS} = \vec{r_g} \cdot \vec{V} + \vec{r_g} \cdot \vec{W} = u\cos\varphi_g \cos\theta_g + v\sin\varphi_g \cos\theta_g + w\sin\theta_g \quad (38)$$

where $\vec{V} = [u, v, 0]$ and $\vec{W} = [0, 0, w]$ are the horizontal and vertical component of the wind speed respectively, u v and w are the north-south, east-west and vertical velocity in ECS ~~Earth coordinate system~~, respectively. The CDL measured LOS velocity has the same temporal resolution of 0.5 s as the $\vec{V}_{ship}$ parameters acquired by GNSS.

Profiles of the wind vector can be retrieved by scanning the lidar beam or stepping the lidar beam through a sequence of different angles or perspectives (Reitebuch et al., 2001; Frehlich, 2001; Werner 2005). For the ground-based CDL, the profile of horizontal wind velocity can be retrieved using 4-Doppler Beam Swing (DBS) mode which is faster and simpler both in the hardware and in the data evaluation algorithm (Werner 2005; Weitkamp, 2005~~2006~~; Wang et al., 2010). Specifically, the wind vector components at target altitude can be derived by measuring the LOS wind velocities in four directions (normally east, west, south and north) under the assumption of homogenous ~~cellular~~ flow with little turbulence. But for the shipborne platform,

the elevation θ_g in four directions (north, south, west and east in ship coordination system) may have slightly difference (see Eq. (A5)) due to ship rotation and movement during the time period of measuring different LOS directions. A conversion of $\vec{V}_{LOS}$ from real elevation θ_g to the expected elevation θ_0 is firstly processed, that is,

$$\vec{V}_{LOS}^{'} = \vec{V}_{LOS} \cos\theta_0 / \cos\theta_g \quad (49)$$

In this study $\theta_0 = 60^\circ$ is set for horizontal wind profile retrieval. During the experiment, each radial direction will take 5 s to obtain 10 measured LOS velocity for accumulation and average. In this sense, the highest temporal resolution of horizontal wind velocity using 4-DBS mode is 20 s. The recorded ship condition information has the same update rate of 0.5 s as radial velocity's, which can be averaged to remove the platform motion effect on radial velocity.

Furthermore, since the laser beam azimuth angle in ECS ~~Earth coordinate system~~ need to be determined using Eq. (A4), the conventional DBS formula ~~where four measurement at azimuth angle has an interval of 90° need to be modified. Then the u, v can be calculated using modified 4-DBS formula~~where four directions at an interval of azimuth-angle of 90° are detected need to be modified. Except for the extremely rough sea condition, the LOS velocity component from vertical velocity in different directions is assumed to be identical. Then the u, v can be calculated using a modified 4-DBS formula

$$\begin{pmatrix} \cos\varphi_N - \cos\varphi_S & \sin\varphi_N - \sin\varphi_S \\ \cos\varphi_E - \cos\varphi_W & \sin\varphi_E - \sin\varphi_W \end{pmatrix} \begin{pmatrix} u \\ v \end{pmatrix} = \begin{pmatrix} (\vec{V}_{LOS\_N}^{'} - \vec{V}_{LOS\_S}^{'}) / \cos\theta_0 \\ (\vec{V}_{LOS\_E}^{'} - \vec{V}_{LOS\_W}^{'}) / \cos\theta_0 \end{pmatrix} \quad (510)$$

$$u = \frac{a_4 b_1 - a_2 b_2}{a_1 a_4 - a_2 a_3} \quad (6)$$

$$v = \frac{a_1 b_2 - a_3 b_1}{a_1 a_4 - a_2 a_3} \quad (7)$$

where $a_1 = \cos\varphi_N - \cos\varphi_S$, $a_2 = \sin\varphi_N - \sin\varphi_S$, $a_3 = \cos\varphi_E - \cos\varphi_W$, $a_4 = \sin\varphi_E - \sin\varphi_W$, $b_1 = (\vec{V}_{LOS\_N}^{'} - \vec{V}_{LOS\_S}^{'}) / \cos\theta_0$, and ~~where~~ the subscript- N ~~N~~, S ~~S~~, E ~~E~~, and W ~~W~~ represent the north, south, east and west in SCS ~~ship coordinate system~~, respectively. ~~.~~It is noted that under extremely rough sea condition, the difference of elevation angle in different directions is significant, and the contribution of vertical velocity to LOS velocity needed to be treated carefully. In this case, the height interpolation of radial velocity can be used, and if three or more radial velocities at the same height are obtained, the horizontal and vertical velocity can be retrieved. But if the elevation angle in one direction is too small, the detectable height will be limited.

For the case of vertical wind measurement, small deviation from vertical pointing due to ship motion induces a projection of the horizontal wind on the laser beam direction. To exactly correct this effect, estimation of the horizontal wind using ~~Eq. (10~~Eq. (5) are used~~,~~ and then the vertical velocity w can be obtained using Eq. (~~8~~3), where in this formula $\vec{V}_{LOS}$ is the measurement in zenith stare mode in ship coordination system.

The SNR in this study is defined as the ratio of the peak value of FFT spectral signal in each range bin to the Root-Mean-Square (RMS) of background noise signal. Figure 3 shows the array of the spectral $S(l\Delta f;k\Delta R)$, where $l=0,1,2,3,...,L-1$ is the spectral channel number and $L=100$ and $k=1,2,3...,K$ is the range bin number and $K=104$. In this case the frequency resolution $\Delta f\approx 0.98$ MHz and the corresponding velocity resolution is $\Delta V=0.76$ ms^{-1}. The bandwidth $B_{100}=L\Delta f=97.65$ MHz, and the corresponding radial velocity measurement range is ± 37.5 ms^{-1}. Figure 3a shows the last 10 range bins' raw array of spectral in green line. We estimate the averaged background noise spectrum

$$\overline{S}_N(l\Delta f)=\frac{1}{10}\sum_{k=94}^{103}S(l\Delta f;k\Delta R) \quad (8)$$

Subtracting the background noise spectral $\overline{S}_N(l\Delta f)$ from the raw spectral array $S(l\Delta f;k\Delta R)$, the unnoisy array of spectral $S(l\Delta f;k\Delta R)$ can be obtained and shown in red line in Fig. 3. The peak value index l_{peak} from the $S(l\Delta f;k\Delta R)$ can be firstly obtained and thus the absolute signal power $P_s(k\Delta R)$ at various ranges $k\Delta R$ can be represented as:

$$P_s(k\Delta R)=S(l_{peak}\Delta f;k\Delta R)-\frac{1}{12}\left(\sum_{l_{peak}-20}^{l_{peak}-15}S(l\Delta f;k\Delta R)+\sum_{l_{peak}+15}^{l_{peak}+20}S(l\Delta f;k\Delta R)\right) \quad (9)$$

Replacing integration by summation and taking into account that the zero velocity point in one channel is $l_{zero}=50$, we estimate the noise power P_N as

$$P_N=\frac{1}{10}\sum_{k=94}^{k=103}\sqrt{\frac{1}{21}\sum_{l=l_{zero}-10}^{l_{zero}+10}\hat{S}_N(l\Delta f;k\Delta R)^2} \quad (10)$$

Finally, we obtain the range profile of the $SNR(k\Delta R)$ using the equation

$$SNR(k\Delta R)=\frac{P_s(k\Delta R)}{P_N} \quad (11)$$

It is noted that unlike the definition of SNR in previous studies (Banakh et al. 2013) where the SNR is defined as the ratio of the average heterodyne signal power to the averaged detector noise power in a 50-MHz bandwidth, the SNR in this study is

simpler and also indicates the CDL detection capability, data accuracy and atmospheric tracer particle relative intensity. In this sense, the SNR threshold value in this study is higher than the one in previous studies (Banakh et al., 2013; Achtert et al., 2015) for the same signal power spectrum.

Figure 4~~3~~ shows the flowchart of shipborne CDL data processing. Specifically, the LOS velocity and ~~Signal-to-Noise Ratio (~~SNR~~)~~ can be firstly determined using lidar data and FFT analysis. ~~It is noted that unlike the definition of SNR in previous studies (Banakh et al. 2013) where the SNR is defined as the ratio of the average heterodyne signal power to the averaged detector noise power in a 50-MHz bandwidth, the SNR in this paper is simpler and defined as the ratio of the peak value of FFT spectral signal in 50-MHz bandwidth in each range bin to the Root-Mean-Square Error (RMSE) of background noise signal, also indicating the CDL detection capability, data accuracy and atmospheric tracer particle relative intensity. In this sense, the SNR threshold value in this paper is higher than the one in previous studies (Banakh et al. 2013; Achtert et al 2015) for the same signal power spectrum.~~ After the data pre-processing including the quality control based on SNR threshold ~~and averaging process~~, the attitude transformation is then used to obtain the azimuth and elevation in each LOS velocity~~vector~~ in ECS ~~Earth coordinate system~~with temporal resolution of 0.5 s. The LOS velocity detected by the lidar is the atmosphere motion relative to SCS~~ship coordinate system~~, thus the removal of the along-beam platform velocity due to ship motion is needed. In this study, the horizontal wind profile with 2-min temporal resolution will be retrieved for vertical velocity correction. Basically, the LOS velocities from N, S, E, and W direction after SNR quality control during the chosen 2-min interval are collected firstly. Then the procedure of filtration of reliable estimates of each radial velocity based on SNR threshold is used to obtain "good" speed estimates. The selected radial velocities and corresponding ship condition information in each radial direction are averaged and the averaged ship condition will be used for the removal of platform velocity effect. ~~-~~Finally, the horizontal velocity with 2-min temporal resolution ~~and vertical wind profiles~~ can be retrieved using modified 4-DBS mode. The vertical wind measurement has a temporal resolution of 0.5 s, the horizontal wind whose retrieved time is closest to vertical wind measured time will be used for vertical velocity correction. ~~and zenith stare mode data correction, respectively.~~

3 Observation results and discussion

3.1 Horizontal wind evaluation

The modified 4-DBS method for horizontal wind profile retrieval is ~~has been~~ illustrated in Fig. 3~~4~~. Two examples of the comparison between uncorrected and corrected horizontal wind profiles ~~can be~~ are shown in Fig. ~~4~~ 5 for anchored measurement and Fig. ~~5~~ 6 for cruising observation, respectively.~~,~~ ~~where~~ The temporal resolution of radial velocity is 0.5 s and the lidar results (black curves) averaged over at least 10 min after the launch of the radiosonde are compared with the radiosonde data (red curves). ~~It is noted that the wind profile from lidar and radiosonde should be interpolated to the common height grid before comparison because of different spatial resolutions.~~ The type of radiosonde is Model GTS1 digital radiosonde with~~,~~ the basic parameters ~~of which are~~ listed in Table 3~~2~~ (Song et al., 2017).

Figure ~~4~~ 5 shows the horizontal wind profile during ~~with~~ anchored measurement (mean ship speed equals to 0.27 ms^{-1}) during 15:52-16:02 Local Standard Time (LST) on 9 May 2014 at 37.00° N, 122.86° E. The black line indicates the mean measurement by CDL during the 10-min period, and the red line shows the result from simultaneous radiosonde data. The blue bars represent the standard deviation of CDL wind measurement from the 2-min temporal resolution results during the chosen analysed period, which can effectively represent the atmospheric fluctuations. It can be seen that the wind is approximately southerly through the measurement altitude, but slightly southeasterly below 1.6 km, and then shifts to southwesterly above 1.6 km. The wind speed ~~slightly increases below 0.2 km and~~ gradually decreases with height till 1.6 km and then increases above. ~~The blue bars represent the wind measurement fluctuation during analysed period, showing that the atmospheric condition is relative stable below 1.6 km whereas it is more changeable above 1.6 km where the wind direction has a continuous variation.~~ The standard deviation of wind speed and direction below 1.4 km are less than 0.5 ms^{-1} and 5°, respectively, showing that the atmospheric condition is relative stable below 1.4 km. While there are higher fluctuations in the height of 1.4 – 1.6 km. The higher SNR in the layer of 1.4 – 1.6 km shown in Fig. 5a implies the existence of a cloud or aerosol layer, more active and complex atmospheric movement in this layer may result in higher fluctuations. The specific ship condition parameters are listed in Table ~~3~~4. The time series of ship horizontal speed, pitch and roll angles are shown in Fig.7a and 7b, respectively. It can be seen that the mean pitch and roll are -0.17° and 0.63° with standard deviation 0.06° and 0.11°, respectively, thus the swing of the ship is not obvious. It is noted that the standard deviation of the angles is determined from the variability during the 10 min period using N=1200 raw data with temporal resolution of 0.5 s, which is shown in Fig. 7b. Since lower SNR makes the data ~~invalid~~unavailable, data quality control based on SNR threshold is used to remove the spikes higher than 2.4 km. The SNR threshold in this study is 8 dB and the reason will be analysed in Sect. 3.3. The Root- Mean-Square-Error (RMSE) in speed between lidar and radiosonde below 2 km is~~are~~ 0.49 ms^{-1} for the uncorrected measurement and 0.45 ms^{-1} for the corrected measurements, both showing consistent with the radiosonde wind speed. It is reasonable since the effect of ship motion speed on LOS velocity is less obvious in anchored measurement. Moreover, the variation of lidar elevation and azimuth in ECS ~~Earth coordinate system~~ is small, and in this case, for instance, when the lidar points to bow with elevation of 60° in SCS~~ship coordinate system~~. If the ship's pitch, roll and heading are -0.17°, 0.63°, 5.28°, respectively, according Eq. (A4) and (A5), the lidar azimuth and elevation in Earth coordinate are $\varphi_s = 6.37^{\circ}$ and $\theta_s = 59.82^{\circ}$, respectively. Similarly, when the lidar points to starboard, stern and port, the corresponding azimuth are 94.99°, 184.18° and 275.58°, and the elevation are 59.37°, 60.16° and 60.63°, respectively, resulting in less difference of horizontal wind speed retrieved from the SCS ~~ship~~ and ECS ~~Earth coordinate system~~. However, the RMSE in wind direction between lidar and radiosonde is~~are~~ 84.43° for uncorrected measurement and 5.27° for corrected measurement. The obvious difference of the wind direction results from two aspects. The first one is the definition in different coordinate

systems, where the heading has an important effect on lidar azimuth. The second aspect is that because of the experimental field limitation, the direction of GNSS master antenna is perpendicular to the ship bow, meaning that the "real" heading is the recorded heading plus 90°, and this angle offset due to placement problem is fixed and calibrated using hard target detection before the campaign. Generally, attitude correction is necessary, especially for the wind direction retrieval even though the ship is anchored with slight shake.

Figure ~~5~~ 6 shows the results of the cruising observation from 07:44 to 07:54 LST on 13 May 2014 when the mean ship speed is 4.84 ms^{-1} with standard deviation of 0.03 ms^{-1}. It can be seen that the wind is constantly southwesterly through the available measurement altitude, and there is a low-level-jet at around 0.3 km where the wind speed exceeds 25 ms^{-1}. What's more, the fluctuation in wind speed and direction above 1 km is more severe than the result below 1 km. The specific ship condition parameters are also listed in Table ~~3~~4. The time series of ship horizontal speed, pitch and roll angles are shown in Fig.7c and 7d, respectively. It can be seen that the mean pitch and roll are -0.43° and 2.06° with standard deviation 0.05° and 0.87°, respectively. Generally, the ship roll has a more effect on the lidar elevation when it points to the port or starboard, on the contrary, the lidar elevation in bow or stern direction is more sensitive to ship pitch. In this case, the lidar mean elevation in bow, starboard, stern and port direction after attitude transformation are 59.51°, 57.84°, 60.30° and 62.49°, respectively, and the mean heading is 75.86° with standard deviation 1.22° where the ship sails downwind. In this condition, the horizontal wind speed without motion correction will be underestimated compared with the radiosonde result. The RMSE in speed between lidar and radiosonde data below 1.0 km are 4.42 ms^{-1} for uncorrected measurement and 0.88 ms^{-1} for corrected measurements, and the corresponding RMSE in wind direction are 48.71° and 9.52°, respectively. Therefore, the attitude correction algorithm has obviously improved the wind profile result when the ship is in cruising observation. ~~It can been seen that the discrepancies in wind profile above 1 km between the radiosonde and lidar measurement are significant~~The difference in mean wind speed and direction between radiosonde and CDL above 1 km is about 3.4 ms^{-1} and 15.2°, respectively, showing significant discrepancy. On the one hand, the random error of the corrected CDL estimation of the wind due to the low SNR shown in Fig. 6a contributes to this discrepancy. On the other hand, according to the recorded information, the mean heading angle and cruising speed of the ship is 75.86° and 4.84 ms^{-1}, respectively, and the mean wind speed and direction above 1 km is 255° and 18.4 ms^{-1}, respectively. Since the drift of radiosonde is affected by atmospheric wind and turbulence perturbation, and the CDL detection volume is changing during cruising observation, the result discrepancy between radiosonde and CDL caused by different observation location, also called the multipath effect, is larger with increasing height. ~~due to the multipath effect at the ship platform and decrease in collocation of the measurement.~~

In order to assess the accuracy of the shipborne lidar wind measurement, a ~~the~~ comparison of the lidar measurement and 11-radiosonde dataset during the experiment are ~~has been~~ made. It is noted that the range resolution of lidar in this study is 30 m,

and the corresponding vertical resolution with elevation angle of 60° is about 26 m. The vertical resolution of radiosonde is 10 m. During the comparison, the wind profile of radiosonde should be interpolated to the common height grid with finer resolution of 2 m firstly, and then the data point closest to height point of lidar will be chosen for comparison. Figure ~~6~~ 8 shows a ~~the~~ scatter plot of wind speed and direction for radiosonde and lidar measurement based on modified 4-DBS solution. ~~-~~The radial measurement range in this study is between 150 m and 3240 m (corresponding to the 104th range bin), thus the altitude range between 130 m and 2806 m are used for the statistical comparison shown in the Fig. 8. The red trend line plotted through these points represents an ordinary linear least square regression for the data excluding $|ydata - xdata| > 2 * SD$, where ~~*fdata* is the fitted value, *ydata* is the corresponding lidar result~~ *ydata* and *xdata* is the lidar and corresponding radiosonde data, respectively, and SD represents the standard deviation of the difference of $ydata - xdata$. According to the distribution of difference of $ydata - xdata$ and fitted Gaussian distribution, the criteria of excluding data with $2 * SD$ is reasonable for gross outliers. The excluded data-pair number and proportion is 62 and 6% for wind speed, respectively, 56 and 5.9% for wind direction, respectively. ~~-~~The wind speed linear regression shows a~~the~~ correlation coefficient of 0.982 ~~(the coefficient of determination of 0.96), and~~ SD of 0.87~~0.75~~ ms^{-1} and RMSE of 0.90 ms^{-1}. The wind direction linear regression shows the correlation coefficient of 0.995, ~~(the coefficient of determination of 0.98) and~~ SD of 8.84° and RMSE of 9.50°. ~~Both wind speed and direction show negligible biases~~The bias of wind speed and direction is -0.23 ms^{-1} and 2.48°, respectively, demonstrating the feasibility and reliability of the modified 4-DBS solution.

Table ~~4~~ 5 lists a height-resolved view (from 0.2 km to 1.6 km) of the linear fit parameters between lidar and radiosonde. The correlation coefficient R for wind direction is approximately 0.99 and almost constant with altitude up to 1.6 km. The correlation coefficient for wind speed is minimum at the lowest altitudes, and improves with height to values comparable to those for wind direction, the trends of which compare well with the results from Achtert et al. (2015). ~~On the one hand, the flow distortion around the ship would affect the low-level measurement from lidar and radiosonde with different effect on each due to different locations. On the other hand, the blind area of lidar is 150 m, meaning that too few data points are available below 200 m with effective comparison.~~ An obvious feature in SD, RMSE, normalized RMSE for wind speed and direction is found at the lowest levels where the discrepancies between lidar and radiosonde data are larger than the higher levels. ~~-~~On the one hand, the relative height between CDL and the highest building on ship is about 18 m shown in Fig.1b. When the strong wind blows from the ship bow, the building and experimental setups on ship have an important effect on CDL lower-level detection volume where the induced-turbulence may cannot meet the assumption of homogeneous isotropic atmosphere for 4-DBS retrieval. On the other hand, the blind area of the CDL is 150 m and corresponds to the height of 129.9 m when laser beam elevation angle is 60°, meaning that less data points are available below 200 m with effective comparison. Whether the flow distortion around the ship is the main reason for the discrepancies in the lower part measurement or not is yet unclear. Further study, especially focused on the CFD model, needs to be used to the assess the potential effects on turbulent flow and

wind field analysis (Achtert et al., 2015). It is also significant for assessing turbulence fluxes exchange from sea-air interface. ~~The source of discrepancies is likely from flow distortion around the ship, which influences the lower-level measurement from lidar and radiosonde with different effects due to different locations.~~ Furthermore, SD, RMSE, normalized RMSE for wind speed and direction increase with altitude from 0.4~~1.2~~ km , which are mainly caused by the lower SNR and ~~the drift of the radiosonde and~~ increasing spatial separation because of the multipath effect mentioned above. ~~between each other.~~

3.2 Vertical wind evaluation

The motion correction of vertical velocity, which is more challenging ~~obvious~~ compared with the horizontal wind component, has been specifically described in Sect. 2. A typical measurement case study on 14 May 2014 is presented in Fig. ~~7~~9. Figure ~~7a~~ 9a shows the whole series of time-height cross section of the SNR. ~~It is noted that the data analysis below 0.15 km is not reliable because of the lidar blind area, and the data above 2.5 km is also removed since the SNR is less than its threshold value.~~According to the Vaisala CL31 ceilometer recorded result, an aerosol layer is presented at around 2.1 km during 07:33 – 08:40 LST. ~~In this paper, the SNR gradient method is used to retrieve the MABL height, and the height of the first strong negative gradient in SNR is regarded as the MABL height on the basis of the fact that the boundary layer has higher aerosol concentrations than the free troposphere above. The temporal and spatial variations of MABL height marked with black solid circles can be seen in Fig. 7a, where the marine stratocumulus structure is also presented at around 2.1 km during 07:33-08:40 LST. It can be seen that diurnal variation of MABL height is less obvious within 1.0 km - 1.5 km, consistent with the mixing layer height retrieved from the radiosonde potential temperature profile.~~ The MABL height has been retrieved and compared using different instruments such as the CDL, radiosonde, and Vaisala CL31 ceilometer during this campaign (Wang et al., 2016). Many papers have discussed the use of backscatter signal of Lidar for mixing height estimation, assuming that the boundary layer has higher aerosol concentrations than the free troposphere above. In this study, the SNR, representing the relative aerosol backscatter profiles, were used and two common methods includes thresholding SNR to determine MABL height (Melfi et al., 1985) and finding the height of the first strong negative gradient (White et al., 1999; Hennemuth and Lammert, 2005) in SNR. The temporal and spatial variation of MABL height from threshold and gradient methods can be seen in Fig. 9a marked with black and red solid circles, respectively. The radiosonde data during 12:00 LST on 14 May 2014 and corresponding MABL height using the gradient of potential temperature and relative humidity are also shown in Fig. 10. It can be seen that diurnal variation of MABL height is less obvious within 1.0 km - 1.5 km, consistent with the mixing layer height retrieved from the radiosonde potential temperature and relative humidity profile. ~~Figure 7b shows the time series of ship heading, CDL laser beam azimuth and elevation, and horizontal wind direction at 0.4 km, respectively. The hemispherical scanner maintains the pointing of the lidar beam to zenith stare mode with an averaged elevation of $88.6^{\circ} \pm 0.35^{\circ}$ because of the ship motion. During the zenith stare mode, the mean angle between ship heading and the laser azimuth is 66° with standard deviation of 7°, thus the projection of ship velocity on vertical velocity is always positive, the results of which are shown in~~

~~Fig. 8a. Furthermore, the estimation of the horizontal wind speed and direction (black line in Fig. 7b) from modified 4-DBS solution is used to remove the horizontal wind speed projection $\vec{r_g} \cdot \vec{V}$ from the relative speed measured by CDL. In this case, the $\vec{r_g} \cdot \vec{V}$ is positive and negative in downwind and headwind, respectively, causing the overestimate and underestimate of the vertical velocity, the effect of which is shown in Fig. 8b.~~ The corrected vertical velocity wind speed is presented in Fig. ~~7c~~9b. It is noted that the data analysis below 0.15 km is not reliable because of the lidar blind area, and the data above 2.5 km is also removed since the SNR is less than its threshold value. The red and blue colour indicate positive (upward) and negative (downward) movement of the atmosphere parcels along the laser beam, respectively. It can be seen that the vertical velocity has a significant diurnal variation. Specifically, the downdraft dominants mixing layer in the morning and amounted to about 0.5 ms^{-1}, and small-scale convective activity can be observed at the top of mixing layer. As the solar radiation strengthens, the atmospheric convection becomes more active and extends to the whole mixing layer, the strengths of updrafts and downdrafts are weakly stronger than before and the atmospheric vertical alternation becomes more frequent. The mixing layer recovers to descending motions with a continuous and long period after 13:11 LST. ~~The difference between the corrected and uncorrected vertical velocity can be shown in Fig. 8c, obviously showing the temporal and spatial variation of the contribution of ship motion and horizontal wind on vertical velocity.~~

Figure 11a shows the time series of ship heading, CDL laser beam azimuth and elevation, and horizontal wind direction at 0.4 km, respectively. Figure 11b shows the time series of elevation angles in zenith stare mode from SCS and ECS, respectively. It can be seen that the hemispherical scanner maintains the pointing of the lidar beam to zenith stare mode with an averaged elevation of $88.6^{\circ} \pm 0.35^{\circ}$ because of the ship motion. During the zenith stare mode, the mean angle between ship heading and the laser azimuth is 66° with standard deviation of 7°, thus the projection of ship velocity on vertical velocity is always positive, the results of which are shown in Fig. 12a. Furthermore, the estimation of the horizontal wind speed and direction (black line in Fig. 11a) from modified 4-DBS solution is used to remove the horizontal wind speed projection $\vec{r_g} \cdot \vec{V}$ from the relative speed measured by CDL. In this case, the $\vec{r_g} \cdot \vec{V}$ is positive and negative in downwind and headwind, respectively, causing the overestimate and underestimate of the vertical velocity, the effect of which is shown in Fig. 12b. The difference between the corrected and uncorrected vertical velocity can be shown in Fig. 12c, obviously showing the temporal and spatial variation of the contribution of the ship motion and horizontal wind on the vertical velocity.

3.3 Measurement uncertainty and error analysis

Error analysis is useful in assessing the accuracy and precision of the lidar wind measurements (Wang et al., 2010). They also shed light on the potential improvements of this CDL. According to the definition of error for measurement of a random wind field, the measured velocity is represented as (Frehlich, 2001):

$$\hat{V} = V_{truth} + e_V + bias_V \quad (12)$$

where V_{truth} is the desired or true wind measurement, e_V is the random error with zero mean, representing the precision of wind measurements, and $bias_V$ is the systematic error, representing the accuracy of the wind measurements.

As for radial velocity, for instance, the north radial velocity $\hat{V}_{LOS\_N}$ with azimuth angle φ_N and elevation angle θ_N, the measurement can be represented as:

$$\hat{V}_{LOS\_N} = c_1\bar{u} + c_2\bar{v} + c_3\bar{w} + e_N + bias_N \quad (13)$$

where $\bar{h} = [\bar{u}, \bar{v}]$ and $\bar{w}$ are the spatially averaged horizontal and vertical velocity, respectively, $c_1 = \cos\varphi_N \cos\theta_N$, $c_2 = \sin\varphi_N \cos\theta_N$, $c_3 = \sin\theta_N$, e_N and $bias_N$ are the random error and bias of the north radial velocity measurements, respectively.

For shipborne ~~-based~~ measurement, the ship platform velocity $\vec{V}_{ship}$ produces a large contribution $\vec{V}_{LOS\_ship}$ to the total radial velocity (see ~~Eq. (6~~Eq. (1)). The bias in the radial velocity measurement comes from errors in the knowledge of $\vec{V}_{ship\_horizotnal}$, $\vec{V}_{ship\_vertical}$, ψ_N, φ_N, θ_N,

$$\begin{aligned} bias_{LOS\_N} &= \Delta\vec{V}_{ship\_horizontal}\cos(\psi_N - \varphi_N)\cos\theta_N + \Delta\vec{V}_{ship\_vertical}\sin\theta_N - \\ &\Delta\psi_N \vec{V}_{ship\_horizontal}\cos\theta_N \sin(\psi_N - \varphi_N) + \Delta\varphi_N \vec{V}_{ship\_horizontal}\cos\theta_N \sin(\psi_N - \varphi_N) \\ &+\Delta\theta_N(\vec{V}_{ship\_vertical}\cos\theta_N - \vec{V}_{ship\_horizontal}\cos(\psi_N - \varphi_N)\sin\theta_N) \end{aligned} \quad (14)$$

where $\Delta\vec{V}_{ship\_horizontal}$, $\Delta\vec{V}_{ship\_vertical}$, $\Delta\psi_N$ are the errors in the determination of the ship speed and direction, and equal to 0.1 ms^{-1}, 0.1 ms^{-1}, 0.1°, respectively. $\Delta\theta_N$, $\Delta\varphi_N$ are the pointing angle knowledge errors of the north direction lidar beam. In this case, $\Delta\varphi$ and $\Delta\theta$ are related to the servo system, and the scanner pointing accuracy is 0.1°, thus $\Delta\varphi = \Delta\theta = 0.1^\circ$ in all directions. It is noted that the knowledge error of the ship velocity and lidar pointing angle mentioned above are systematic part and it is assumed that the random error of these quantities is zero, which is reasonable and robust for horizontal wind retrieval.

Similarly, to derive the $\vec{V}'_{LOS}$ bias, we take the derivatives of ~~Eq. (9~~Eq. (4)

$$bias_{LOS\_N'} = bias_{LOS\_N}\cos\theta_0 / \cos\theta_N + \Delta\theta_N \vec{V}_{LOS\_N}\cos\theta_0 \sin\theta / \cos^2\theta_N \quad (15)$$

~~Estimation for the horizontal velocity are produced by solving Eq. (10) assuming that the wind field has a constant horizontal and vertical velocity, that is,~~

$$u = \frac{a_4 b_1 - a_2 b_2}{a_1 a_4 - a_2 a_3} \quad (15)$$

$$v = \frac{a_1 b_2 - a_3 b_1}{a_1 a_4 - a_2 a_3} \quad (16)$$

~~where $a_1 = \cos\varphi_N \quad \cos\varphi_S$, $a_2 = \sin\varphi_N \quad \sin\varphi_S$, $a_3 = \cos\varphi_E \quad \cos\varphi_W$, $a_4 = \sin\varphi_E \quad \sin\varphi_W$, $b_1 = (\vec{V}'_{LOS\_N} - \vec{V}'_{LOS\_S})/\cos\theta_0$, $b_2 = (\vec{V}'_{LOS\_E} - \vec{V}'_{LOS\_W})/\cos\theta_0$.~~

~~Since the error in the lidar pointing angle should be very small, one can assume perfect knowledge of the coefficient a_i~~ Because of the requirement for small bias in the radial velocity measurements, the error in the laser beam direction must be very small and one can assume perfect knowledge of the coefficient a_i . (Frehlich, 2001), so the biases of u and v from the radial velocity estimation can be described:

$$bias_u = \frac{a_4 bias_{b_1} - a_2 bias_{b_2}}{a_1 a_4 - a_2 a_3} \quad (16~~7~~)$$

$$bias_v = \frac{a_1 bias_{b_2} - a_3 bias_{b_1}}{a_1 a_4 - a_2 a_3} \quad (17~~8~~)$$

It can be seen that the dominant source of bias of the horizontal velocity estimates come from the biases of the radial velocity estimates ($bias_N$, $bias_S$, $bias_E$ and $bias_W$), which are determined by the error in the ship velocity $\vec{V}_{ship\_horizontal}$, $\vec{V}_{ship\_vertical}$ and heading angle ψ and lidar pointing knowledge errors $\Delta\varphi$ and $\Delta\theta$ (see Eq. 13).

~~which are determined by the error in the ship velocity and lidar pointing errors.~~

~~Following the approach of Frehlich (Frehlich, 2001; Frehlich, 1996), a method based on the frequency spectrum of the retrieved velocity has been used to determine the random error of horizontal and vertical wind measurements, which assumes that the estimation error is uncorrelated with the random variations in the velocity field and aerosol backscatter.~~ Various methods of estimating the magnitude of the random error of Doppler Lidar velocity measurements have been introduced (Frehlich, 2001). A method based on the frequency spectrum of the retrieved velocity has been used to determine the random error of vertical wind measurements. A 50 % window overlap factor, a Hamming window is used in order to reduce leakage in the spectra (Chouza et al., 2016). A zero-padding of the missing values were applied to each window for each spectrum calculation to improve the frequency resolution. The constant high-frequency region of velocity spectrum higher than 0.2 Hz, shown in Fig.

13 at height of 1495 m, represents uncorrelated random error contribution, which is departing from the Kolmogorov's -5/3 law. The random error of vertical velocity is estimated as the standard deviation of the measured signal after high-pass filter

Figure 9 14 shows the error analysis of horizontal and vertical wind during 15:52-16:02 LST on 09 May 2014. In this case, a 50 % window overlap factor, a Hamming window and a zero-padding of the missing values were applied to each window for each spectrum calculation (Frehlich, 2001; Chouza et al., 2016). The resulting spectrum shows that the frequencies higher than 0.2 Hz tend to be a constant value, and the high frequency region represents the spectrum of the random noise. The observed SNR is illustrated in the Fig. 9a14a, and there is an aerosol layer at around 1.5 km , consistent with the higher value in SNR. The random errors of vertical velocity from the standard deviation of the random noise signal, shown in Fig. 149b, are less than 0.1 ms^{-1} below 1 km with SNR< 8 dB , and a peak value appears at around 1.3 km and decreases with altitude till at around 1.5 km . Then the random errors increase with altitude as the SNR decrease, and reach about 1.2 ms^{-1} at 2.3 km . It is clear that the random error is mainly determined by the SNR. Figure 9c 14c shows the $bias_u$, $bias_v$ and corresponding bias of horizontal wind velocity $bias_h$. The $bias_h$ is less than 0.02 ms^{-1} below 2.5 km , which is negligible and consistent with the result shown in Sect. 4.1section 4.1. According to Eqs. (1316) and (1718), the dominant source of bias of horizontal wind velocity is mainly from the ship velocity and lidar pointing errors in different direction. In this case, the $\vec{V}_{ship\_horizotnal}$ provides the highest contribution has the most effect on the bias of the radial velocity. The bias of horizontal wind speed is typically less than the random error which is determined from the frequency spectrum of the retrieved horizontal velocity

The observed random error of the vertical velocity as a function of SNR is presented in Fig. 150, which is retrieved from the frequency spectrum of the retrieved vertical velocity during 07:33 to 15:29 LST on 14 May 2014. It can be seen that in the high SNR region above 8 dB , a constant random error range between 0.03 and 0.15 ms^{-1} is found because of the effect of the speckle-induced phase noise (Frehlich, 1997; Frehlich, 2001Achtert et al., 2015), which is much smaller than the standard deviation discrepancy between the mean wind speed derived from lidar and radiosonde of 0.75 ms^{-1} (see Sect. 3.1). At reduced values of the SNR, the errors increase as a result of increasing signal noise, rising to approximately 4 ms^{-1} at an SNR = 0 dB . It is confirmed that the choice of a conservative SNR threshold of 8 dB is robust for data quality control process.

4 Summary

Shipborne wind observation by a the CDL during the 2014 Yellow Sea campaign are has been presented carried out to study the structure of the MABL. An algorithm to compensate for error of wind measurement due to the motion of the ship is presented in this paper. The algorithm-based attitude and velocity correction methods greatly relax the requirements for mechanical stability and compensation mechanisms. The attitude correction system of the CDL consists of GNSS and INS inertial navigation system to directly measure the speed and the attitude of the ship. According to the transformation matrix from the product of roll, pitch and heading rotation matrix, the azimuth and elevation of the LOS velocity in the ECS Earth

~~coordinate system~~ can be firstly determined. Then the removal of the along-beam platform velocity due to ship motion is needed to obtain the "real" LOS velocity in the~~-~~ ECS ~~Earth coordinate system~~. The horizontal wind profiles can be retrieved by a modified 4-DBS method. For the case of vertical velocity, small deviations from vertical pointing due to ship motion induces a projection of the horizontal wind on the LOS vector, thus estimation of the horizontal wind speed contribution are used to correct the vertical velocity.

In order to assess the accuracy of the shipborne lidar wind measurement, a comparison of the lidar measurement and 11-radiosonde dataset from 09 May 2014 to 19 May 2014 are made. The total number of wind speed and direction dataset for comparison is 1062 and 951, respectively. The comparison of the CDL and~~to~~ radiosonde shows that attitude correction is essential for the wind retrieval in cruising measurement. The correlation coefficients of wind speed and direction are 0.982, 0.995, respectively, both of which show negligible bias and demonstrate the feasibility and reliability of the modified 4-DBS method. A case study of 8-h time series observation on 14 May 2014 is presented to compare uncorrected and corrected vertical velocity, additionally showing the specific temporal and spatial variation of the contributions of ship motion and horizontal wind on vertical velocity.

The bias of horizontal wind velocity is~~was~~ estimated using error propagation analysis and concluded that the dominant source comes from the radial velocity estimates, which are determined by the error in the ship velocity and lidar pointing errors. The random error is~~was~~ estimated based on the frequency spectrum of the retrieved velocity. ~~Based one measurement case,~~ A case study during 15:52 to 16:02 LST on 09 May 2014 is presented. The radial measurement range is from 0.15 km to 3.105 km where the blind area of CDL is less than 0.15 km and the maximum detectable range is 3.105 km.~~-~~ ~~the~~ It is found that the random error of vertical ~~horizontal wind~~ velocity is~~was~~ between 0.03 ms^{-1} and 1.2 ms^{-1} ~~in different heights,~~ and ~~it~~ is mainly determined by the SNR, while the bias was less than 0.02 ms^{-1}, which is negligible and consistent with the result of comparison between lidar and radiosonde data. The fundamental random error of the lidar vertical wind obtained from 07:33 to 15:29 LST on 14 May 2014 in all height range is ~~was~~ found to be in the range of 0.03 to 0.15 ms^{-1} for SNR above 8 dB, which is much smaller than the standard deviation ~~discrepancy~~ between the mean wind speed derived from lidar and radiosonde of 0.75 ms^{-1}. The choice of a conservative SNR threshold of 8 dB is ~~was~~ also confirmed by the error analysis results of vertical velocity. Overall, combining a CDL with attitude correction system and accurate motion correction process as presented here forms a reliable and autonomous set-up that could be placed on mobile platform to provide~~-~~ more detailed, higher spatial and temporal resolution view of three-dimensional wind field information. It will be further validated and improved under different sea conditions using CFD model simulation in further field campaign. More specific studies are being carried out or prepared, including atmospheric turbulence characteristics statistics and multi-scale wind field observation in MABL, wind turbine wake and atmospheric turbulence interaction over offshore wind power field (Wu et al., 2016; Zhai et al., 2017), mass transport and flux analysis in MABL with combination of CDL and Multi-wavelength Polarization Raman Lidar (Wu et al., 2016).

~~measurement for MABL thermodynamic process, air-sea interaction and so forth, providing much more detailed, higher spatial and temporal resolution view of MABL process.~~

Appendix A:

As can be seen in Fig. 2, the SCS (X_s, Y_s, Z_s) is defined as X_s axis along centre line of ship, positive toward bow, Y_s axis is perpendicular to X_s , and positive toward starboard, Z_s axis is positive toward the bottom. The attitude of the ship can be expressed by roll φ , pitch θ and heading angles ψ . The φ , θ and ψ refer to rotations about X_s , Y_s , and Z_s axes, respectively. Specifically, positive φ is defined when the port is up, and positive θ is defined when the bow is up. The ψ is defined 0° when the bow points to north in ECS. The ECS (X_g, Y_g, Z_g) is defined as X_g axis along north-south direction, positive toward to north, Y_g axis is along east-west direction, and positive toward to east, Z_g axis is positive toward the bottom.

In the SCS, the recorded azimuth and elevation of the transmitting laser are φ_s and θ_s , respectively. φ_s is defined as the angle between the projection of transmitting laser path on $X_s - Y_s$ plane and the positive X_s axis. From the top view, φ_s increases in a clockwise direction during 4-DBS mode operation. θ_s is defined as the angle between the laser beam direction and the $X_s - Y_s$ plane. Therefore, the direction of the transmitting laser in the SCS can be expressed by a unit vector $\vec{r_s}$ as (Hill, 2005; Liu et al., 2010).

$$\vec{r_s} = \begin{pmatrix} x_s \\ y_s \\ z_s \end{pmatrix} = \begin{pmatrix} \cos\theta_s \cos\varphi_s \\ \cos\theta_s \sin\varphi_s \\ -\sin\theta_s \end{pmatrix} \quad \text{(A1)}$$

The coordinate transformation from the SCS to that of the ECS is needed. According to the transformation matrix from the product of three rotation matrixes shown in Eq. (A2), the unit vector $\vec{r_g}$ of transmitting laser direction in ECS can be expressed as Eq. (A3)

$$H_2 = \begin{pmatrix} \cos\theta & 0 & -\sin\theta \\ 0 & 1 & 0 \\ \sin\theta & 0 & \cos\theta \end{pmatrix}, H_3 = \begin{pmatrix} \cos\psi & \sin\psi & 0 \\ -\sin\psi & \cos\psi & 0 \\ 0 & 0 & 1 \end{pmatrix}, H_3 = \begin{pmatrix} 1 & 0 & 0 \\ 0 & \cos\varphi & \sin\varphi \\ 0 & -\sin\varphi & \cos\varphi \end{pmatrix}, \quad \text{(A2)}$$

$$\vec{r_g} = \begin{pmatrix} x_g \\ y_g \\ z_g \end{pmatrix} = (H_1 H_2 H_3)^{-1} \vec{r_s} \quad \text{(A3)}$$

Where H_1, H_2, H_3 are the rotation matrices of roll, pitch and heading, respectively (Hill, 2005).

Once the unit vector $\vec{r}_g$ is calculated from Eqs. (A2) and (A3), the azimuth φ_g and elevation θ_g of LOS observation in ECS can be calculated

$$\varphi_g = \arctan(y_g / x_g) \quad \text{(A4)}$$

$$\theta_g = -\arcsin z_g \quad \text{(A5)}$$

Acknowledgements

This work was partly supported by the National High Technology Research and Development Program of China under grant 2014AA09A511, the National Natural Science Foundation of China under grant 41471309 and 41375016, and the National Key Research and Development Program of China under grant 2016YFC1400904.

References

Achtert, P., Brooks, I., Brooks, B., Moat, B., Prytherch, J., Persson, P., and Tjernström, M.: Measurement of wind profiles by motion-stabilised ship-borne Doppler lidar, Atmos. Meas. Tech., 8, 4993-5007, 2015.

Axford, D.: On the accuracy of wind measurements using an inertial platform in an aircraft, and an example of a measurement of the vertical mesostructure of the atmosphere, J. Appl. Meteorol., 7, 645-666, 1968.

Anctil, F., Donelan, M. A., Drennan, W. M., and Graber, H. C.: Eddy-correlation measurements of air-sea fluxes from a discus buoy, J. Atmos. Oceanic. Technol., 11, 1144-1150, 1994.

Banakh, V., and Smalikho, I.: Coherent Doppler wind lidars in a turbulent atmosphere: Artech House, 1-10, 2013.

Banta, R. M., Pichugina, Y. L., and Brewer, W. A.: Turbulent velocity-variance profiles in the stable boundary layer generated by a nocturnal low-level jet, J. Atmos. Sci., 63, 2700-2719, 2006.

Bradley, E. F., Coppin, P., and Godfrey, J.: Measurements of sensible and latent heat flux in the western equatorial Pacific Ocean, J. Geophys. Res.: Oceans, 96, 3375-3389, 1991.

Cheong, B., Palmer, R., Yu, T., Yang, K., Hoffman, M., Frasier, S., and Lopez-Dekker, F.: Effects of wind field inhomogeneities on Doppler beam swinging revealed by an imaging radar, J. Atmos. Oceanic. Technol., 25, 1414-1422, 2008.

Chouza, F., Reitebuch, O., Jähn, M., Rahm, S., and Weinzierl, B.: Vertical wind retrieved by airborne lidar and analysis of island induced gravity waves in combination with numerical models and in situ particle measurements, Atmos. Chem. Phys., 16, 4675-4692, 2016.

Dunckel, M., Hasse, L., Krügermeyer, L., Schriever, D., and Wucknitz, J.: Turbulent fluxes of momentum, heat and water vapor in the atmospheric surface layer at sea during ATEX, Boundary-Layer Meteorol., 6, 81-106, 1974.

Edson, J. B., Hinton, A. A., Prada, K. E., Hare, J. E., and Fairall, C. W.: Direct covariance flux estimates from mobile platforms at sea*, J. Atmos. Oceanic. Technol., 15, 547-562, 1998.

Fairaill, C., Hare, J., Edson, J., and McGillis, W.: Parameterization and micrometeorological measurement of air-sea gas transfer, Boundary-Layer Meteorol., 96, 63-106, 2000.

Frehlich, R.: Simulation of coherent Doppler lidar performance in the weak-signal regime, J. Atmos. Oceanic. Technol., 13, 646-658, 1996.

Frehlich, R.: Effects of wind turbulence on coherent Doppler lidar performance, J. Atmos. Oceanic. Technol., 14(1), 54-75, 1997.

Frehlich, R.: Errors for space-based Doppler lidar wind measurements: Definition, performance, and verification, J. Atmos. Oceanic. Technol., 18, 1749-1772, 2001.

Frehlich, R.: Estimation of velocity error for Doppler lidar measurements, J. Atmos. Oceanic. Technol., 18(10), 1628-1639, 2001.

Fujitani, T.: Method of turbulent flux measurement on a ship by using a stable platform system, Papers in Meteorol. Geophys., 36, 157-170, 1985.

Fujitani, T.: Turbulent transport mechanism in the surface layer over the tropical ocean, J. Meteorol. Soc. Jpn., 70, 795-811, 1992.

Hawley, J. G., Targ, R., Henderson, S. W., Hale, C. P., Kavaya, M. J., and Moerder, D.: Coherent launch-site atmospheric wind sounder: theory and experiment, Appl. Opt., 32, 4557-4568, 1993.

Hennemuth, B., and Lammert, A.: Determination of the atmospheric boundary layer height from radiosonde and lidar backscatter, Boundary-Layer Meteorol., 120(1), 181-200, 2006.

Hill, R. J.: Motion compensation for shipborne radars and lidars, US Department of Commerce, National Oceanic and Atmospheric Administration, Office of Oceanic and Atmospheric Research, Earth System Research Laboratory, Physical Sciences Division, 2005.

Hill, R. J., Brewer, W. A., and Tucker, S. C.: Platform-motion correction of velocity measured by Doppler lidar, J. Atmos. Oceanic. Technol., 25, 1369-1382, 2008.

Lenschow, D., Pearson, R., and Stankov, B.: Estimating the ozone budget in the boundary layer by use of aircraft measurements of ozone eddy flux and mean concentration, J. Geophys. Res.: Oceans., 86, 7291-7297, 1981.

Lenschow, D.: Aircraft measurements in the boundary layer, Probing. Atmos. Boundary. Layer., 39-55, 1986.

Liu, B.-Y., Liu, Z.-S., Song, X.-Q., Wu, S.-H., Bi, D.-C., Wang, X.-T., Yin, Q.-W., and Reitebuch, O.: Modifications and Moving Measurements of Mobile Doppler LIDAR, ESA Special Publication, 2010, 30.

Menut, L., Flamant, C., Pelon, J., and Flamant, P. H.: Urban boundary-layer height determination from lidar measurements over the Paris area, Appl. Opt., 38(6), 945-954, 1999.

Miller, S. D., Hristov, T. S., Edson, J. B., and Friehe, C. A.: Platform motion effects on measurements of turbulence and air-sea exchange over the open ocean, J. Atmos. Oceanic. Technol., 25, 1683-1694, 2008.

Mitsuta, Y., and Fujitani, T.: Direct measurement of turbulent fluxes on a cruising ship, Boundary-Layer Meteorol., 6, 203-217, 1974.

Pichugina, Y. L., Banta, R. M., Brewer, W. A., Sandberg, S. P., and Hardesty, R. M.: Doppler lidar-based wind-profile measurement system for offshore wind-energy and other marine boundary layer applications, J. Appl. Meteorol. Clim., 51, 327-349, 2012.

Reitebuch, O., Werner, C., Leike, I., Delville, P., Flamant, P. H., Cress, A., and Engelbart, D.: Experimental Validation of Wind Profiling Performed by the Airborne 10-μ m Heterodyne Doppler Lidar WIND, J. Atmos. Oceanic. Technol., 18, 1331-1344, 2001.

Rocers, D. P., Johnson, D. W., and Friehe, C. A.: The stable internal boundary layer over a coastal sea. Part I: Airborne measurements of the mean and turbulence structure, J. Atmos. Sci., 52, 667-683, 1995.

Schulz, E., Sanderson, B., and Bradley, E. F.: Motion correction for shipborne turbulence sensors, J. Atmos. Oceanic. Technol., 22, 55-69, 2005.

Shao, Y.: Correction of Turbulent Wind Measurements Contaminated by Irregular Motion of a Ship, TOGA-COARE Project, CSIRO Center for Environmental Mechanics, Canberra, Australia, Technical Report, 1995.

Song, X., Friehe, C. A., and Hu, D.: Ship-board measurements and estimations of air-sea fluxes in the western tropical Pacific during TOGA COARE, Boundary-Layer Meteorol., 81, 373-397, 1996.

Song, X., Zhai, X., Liu, L., and Wu, S.: Lidar and Ceilometer Observations and Comparisons of Atmospheric Cloud Structure at Nagqu of Tibetan Plateau in 2014 Summer, Atmosphere, 8(1), 9, 2017.

Tsukamoto, O.; Ishida, H.: Turbulent flux measurements and energy budget analysis over the equatorial Pacific during TOGA-COARE IOP. J. Meteorol. Soc. Jpn., 73, 557-568, 1995.

Tucker, S. C., Senff, C. J., Weickmann, A. M., Brewer, W. A., Banta, R. M., Sandberg, S. P., Law, D. C., and Hardesty, R. M.: Doppler lidar estimation of mixing height using turbulence, shear, and aerosol profiles, J. Atmos. Oceanic. Technol., 26, 673-688, 2009.

Wang, D., Song, X., Feng, C., Wang, X., and Wu, S.: Coherent Doppler Lidar Observations of Marine Atmospheric Boundary Layer Height in the Bohai and Yellow Sea, Acta Opt. Sin., 35(A01), 1-7, 2015.

Wang, Z., Liu, Z., Liu, L., Wu, S., Liu, B., Li, Z., and Chu, X.: Iodine-filter-based mobile Doppler lidar to make continuous and full-azimuth-scanned wind measurements: data acquisition and analysis system, data retrieval methods, and error analysis, Appl. Opt., 49, 6960-6978, 2010.

Weitkamp, C.: Lidar: range-resolved optical remote sensing of the atmosphere, Springer Science & Business, 2005~~2006~~.

Werner, C.: Doppler Wind Lidar, edited by: Weitkamp, Springer, New York, 325–353, 2005.

White, A. B., Senff, C. J., and Banta, R. M.: A comparison of mixing depths observed by ground-based wind profilers and an airborne lidar, J. Atmos. Oceanic. Technol., 16(5), 584-590, 1999.

Wolfe, D., Brewer, W., Tucker, S., White, A., White, D., Welsh, D., Ruffieux, D., Fairall, C., Ratterree, M., and Intrieri, J.: Shipboard multisensor merged wind profiles from the New England Air Quality Study 2004, J. Geophys. Res.: Atmos.112, 2007.

Wu, S., Liu, B., Liu, J., Zhai, X., Feng, C., Wang, G., Zhang, H., Yin, J., Wang, X., Li, R., and Gallacher, D.: Wind turbine wake visualization and characteristics analysis by Doppler lidar, Opt. Express, 24(10), A762-A780, 2016.

Wu, S., Dai, G., Song, X., Liu, B., Liu, L.: Observations of water vapor mixing ratio profile and flux in the Tibetan Plateau based on the lidar technique, Atmos. Meas. Tech., 9(3), 1399-1413, 2016.

Wulfmeyer, V., and Janjic, T.: Twenty-four-hour observations of the marine boundary layer using shipborne NOAA high-resolution Doppler lidar, J. Appl. Meteorol., 44, 1723-1744, 2005.

Zhai, X., Wu, S., and Liu, B.: Doppler lidar investigation of wind turbine wake characteristics and atmospheric turbulence under different surface roughness, Opt. Express, 25, A515-A529 2017.

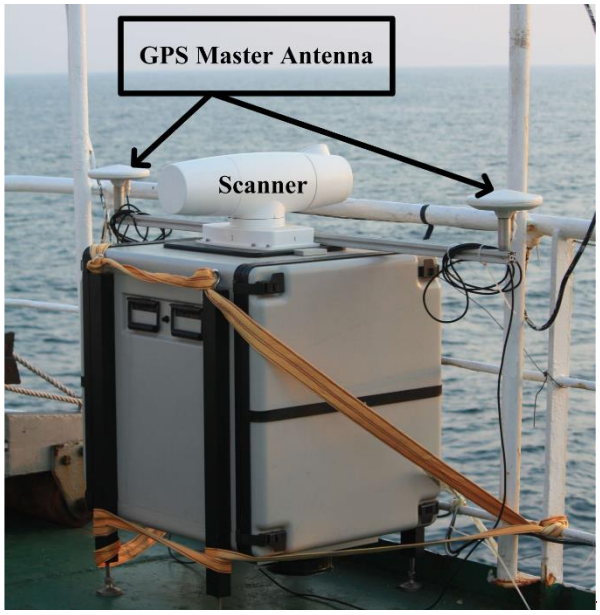

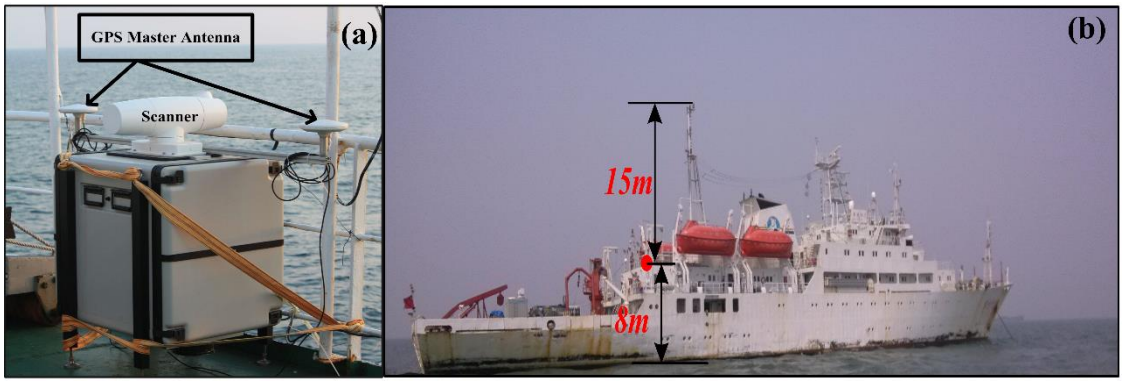

Figure 1: (a) The Coherent Doppler Lidar setup on Dongfanghong-2 research vessel. (b) The Dongfanghong-2 research vessel during 2014 Yellow Sea Campaign. The red solid dot represents the CDL position.

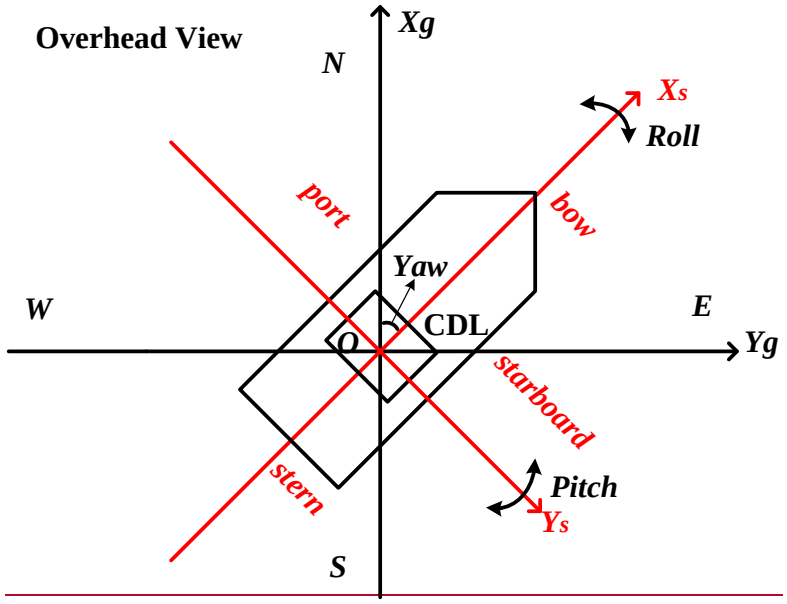

Figure 2. The overhead view of Lidar, ship and Earth coordinate system and corresponding hard target calibration.

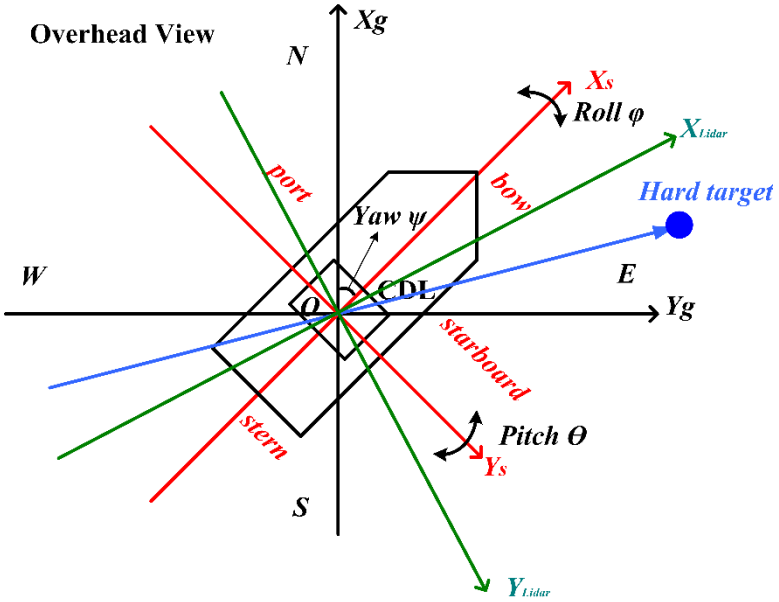

~~Figure 2: The overhead view of ship and Earth coordinate system.~~

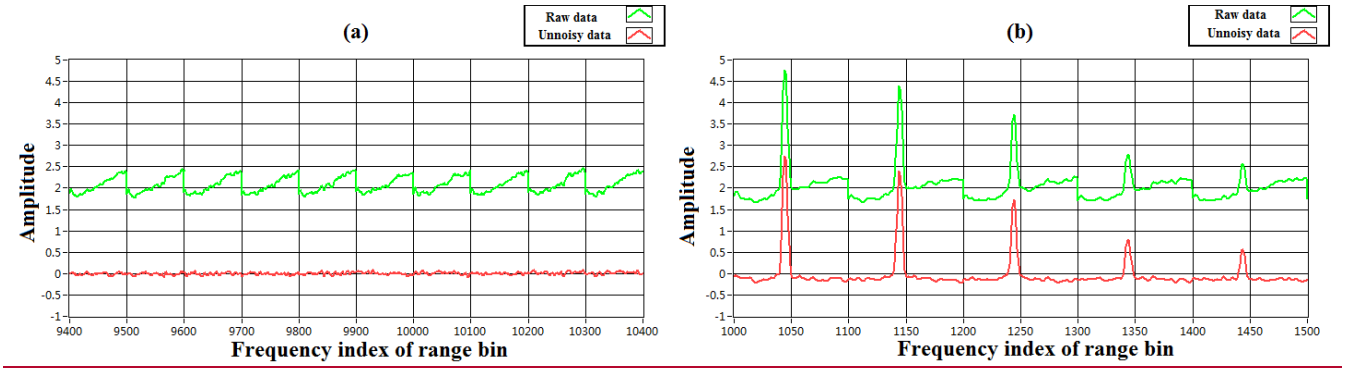

Figure 3: The CDL measured array of the FFT spectra (a) the last 10 range gates spectra for background noise spectrum estimation (b) the 1st – 5th range gates (150 m – 270 m, range resolution is 30 m) spectrum.

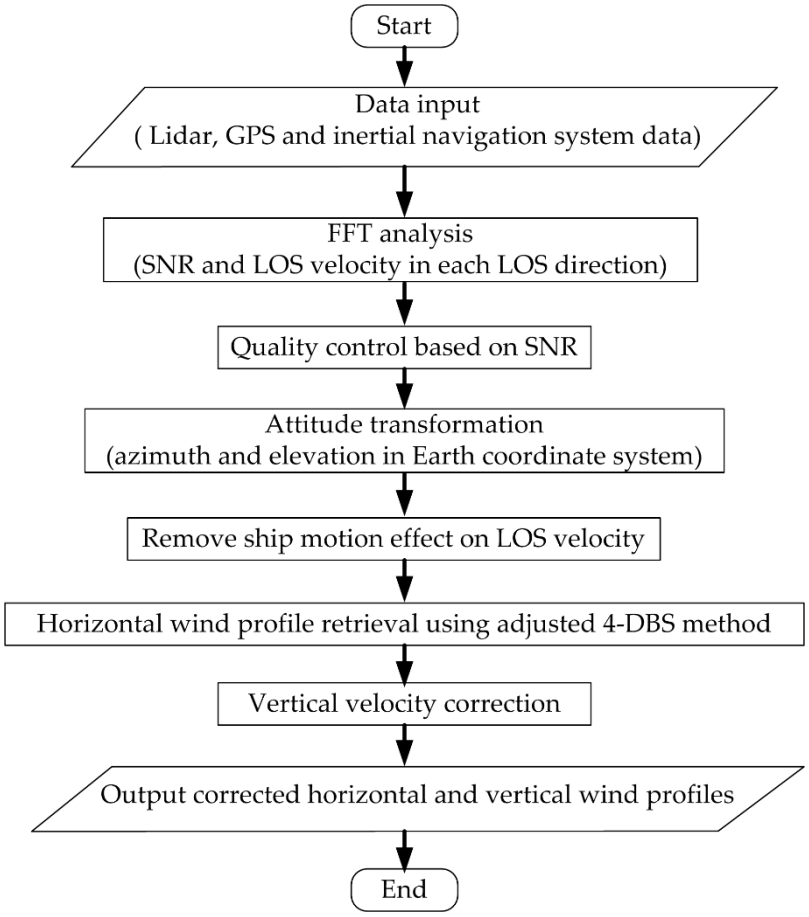

Figure 43: Flow chart of ship motion correction algorithm based on CDL.

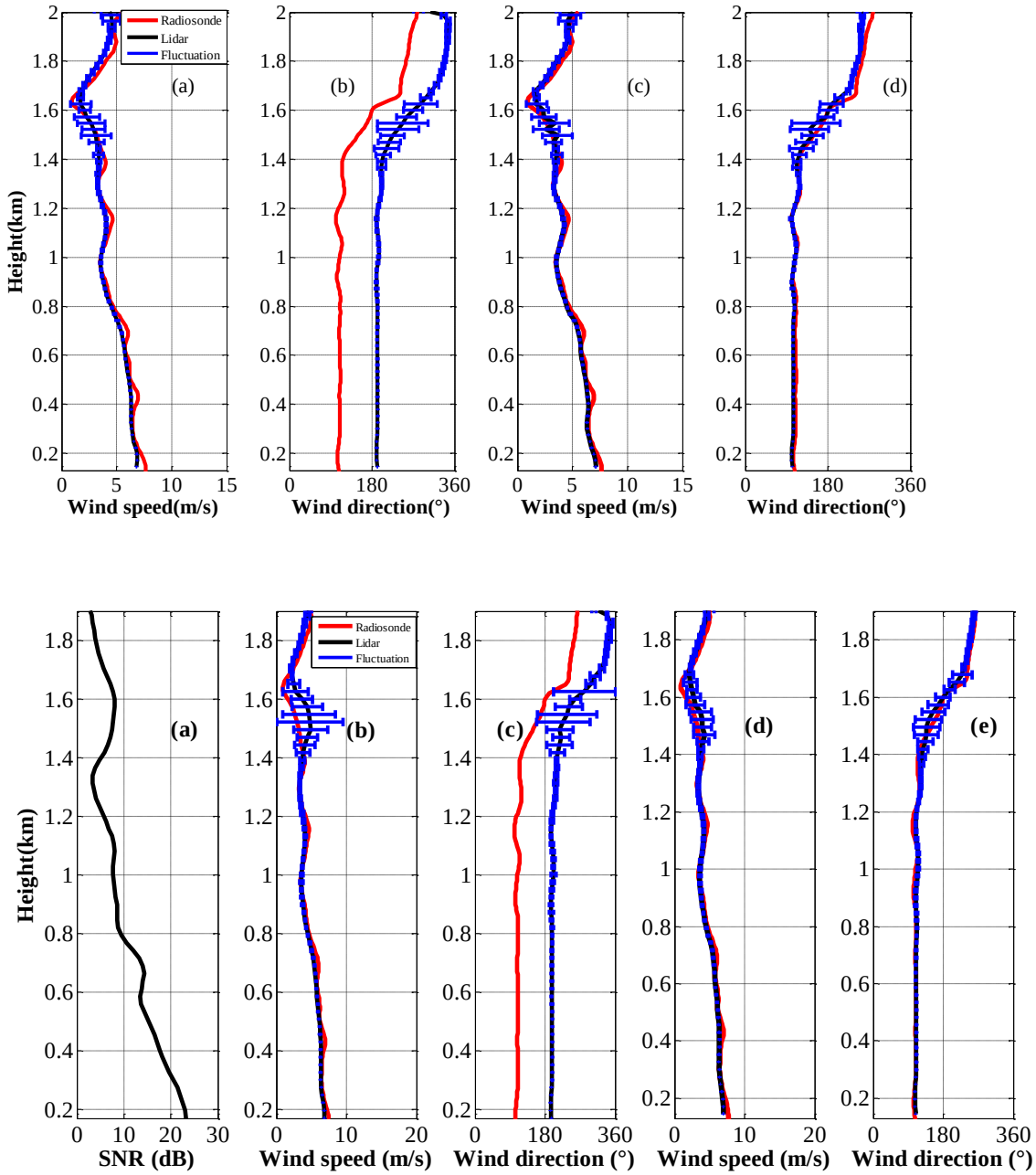

Figure 54: Anchored observation: (a) SNR profile (ba) (ce) wind speed and (db) (ed) wind direction measured by CDL (blackue line) before and after attitude correction, respectively. The simultaneous radiosonde data is shown asin red line. The blue bars represent the sampling fluctuations from 15:52 to 16:02 LST on , 09 May, 2014.

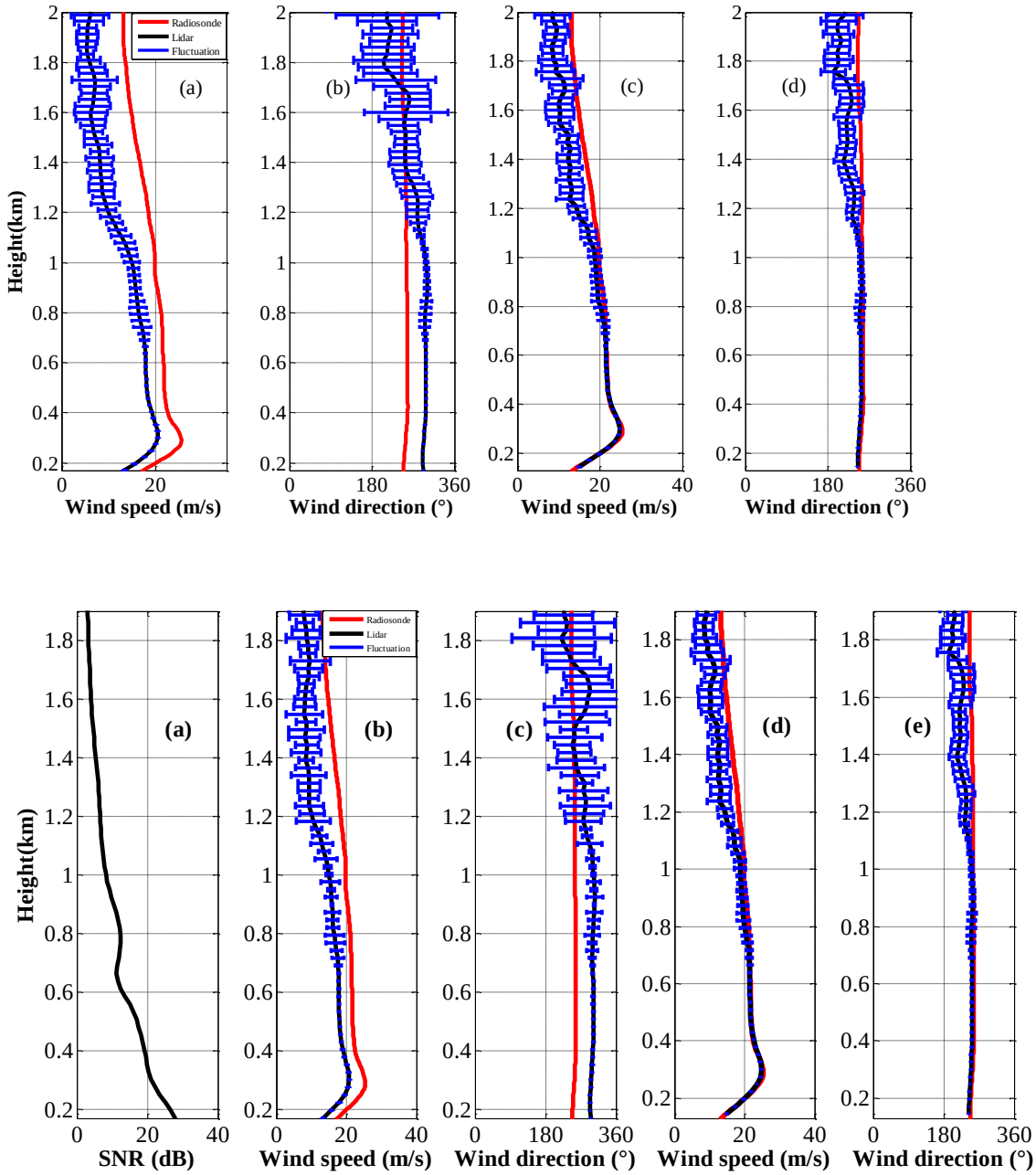

Figure 65: As Fig. 54, but for 07:44 to 07:54 LST on 13 May, 2014 in cruising observation.

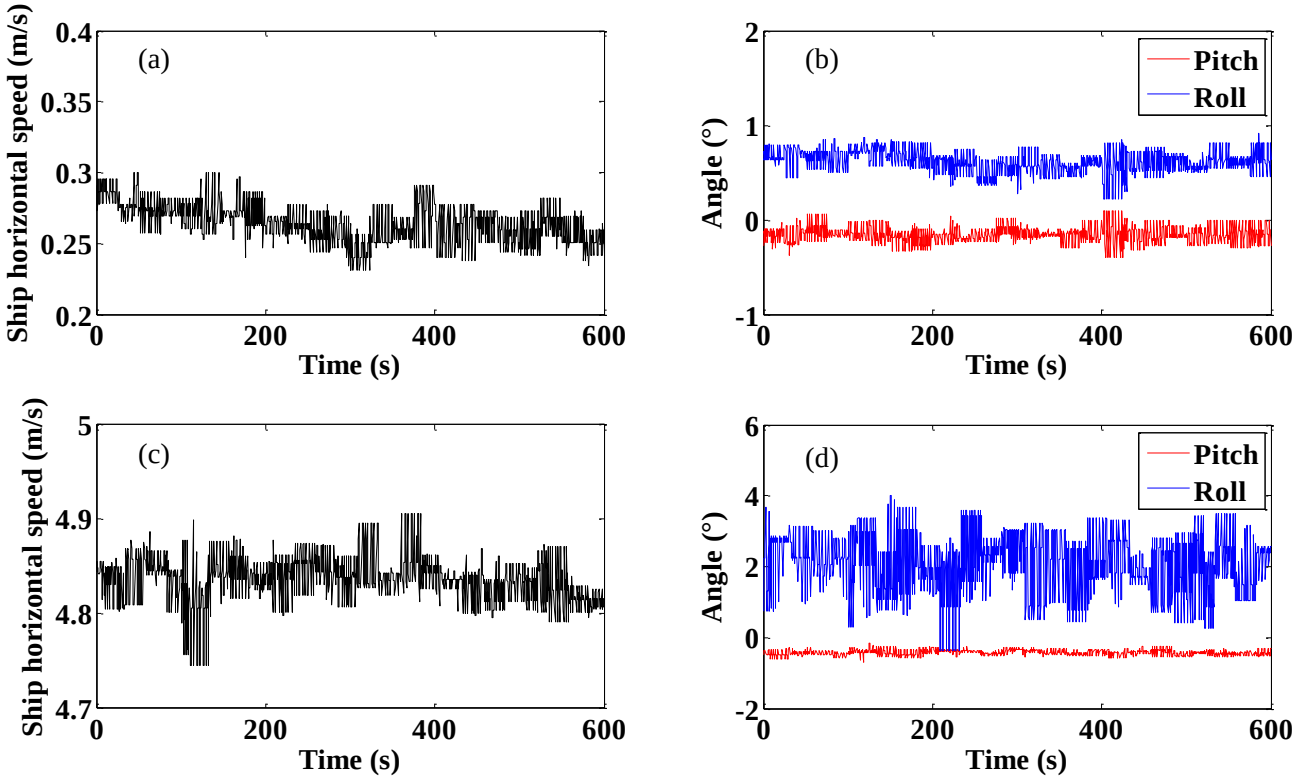

Figure 7: (a) Time series of ship horizontal speed and (b) pitch and roll angles on 09 May 2014 (15:52-16:02) during anchored measurement, (c) Time series of ship horizontal speed and (d) pitch and roll angles on 13 May 2014 (07:44-07:54) during cruising measurement.

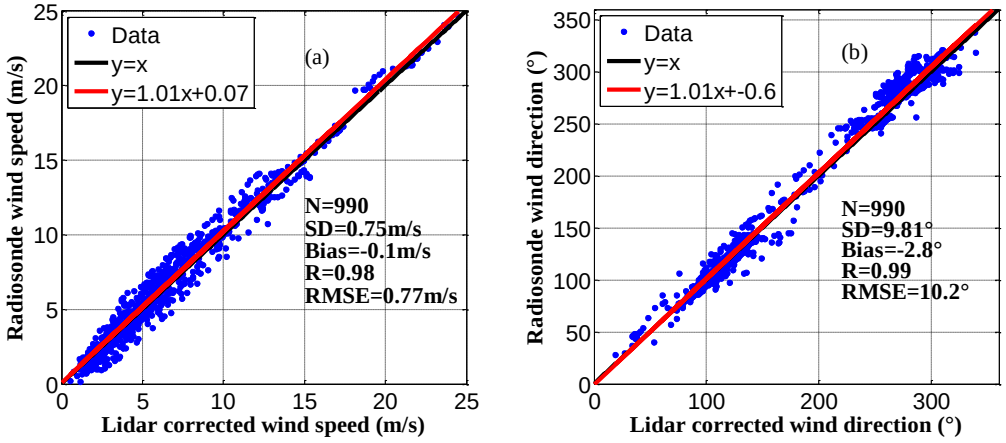

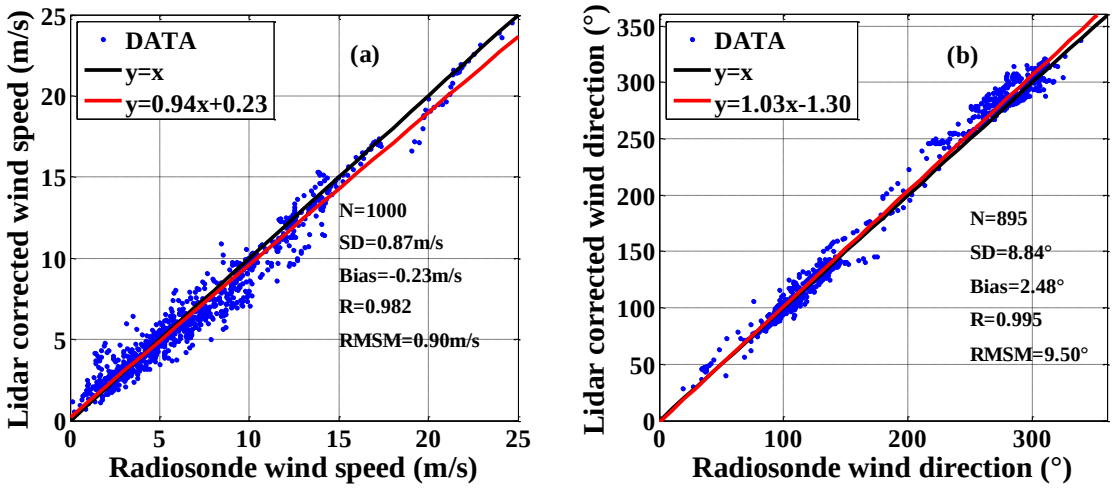

Figure ~~86~~: Comparison of (a) wind speed and (b) wind direction between CDL and radiosonde data from 09 May 2014 to 19 May 2014. The number of points (N), standard deviation (SD), bias, correlation coefficient (R), and root-mean-square-error (RMSE) are also listed.

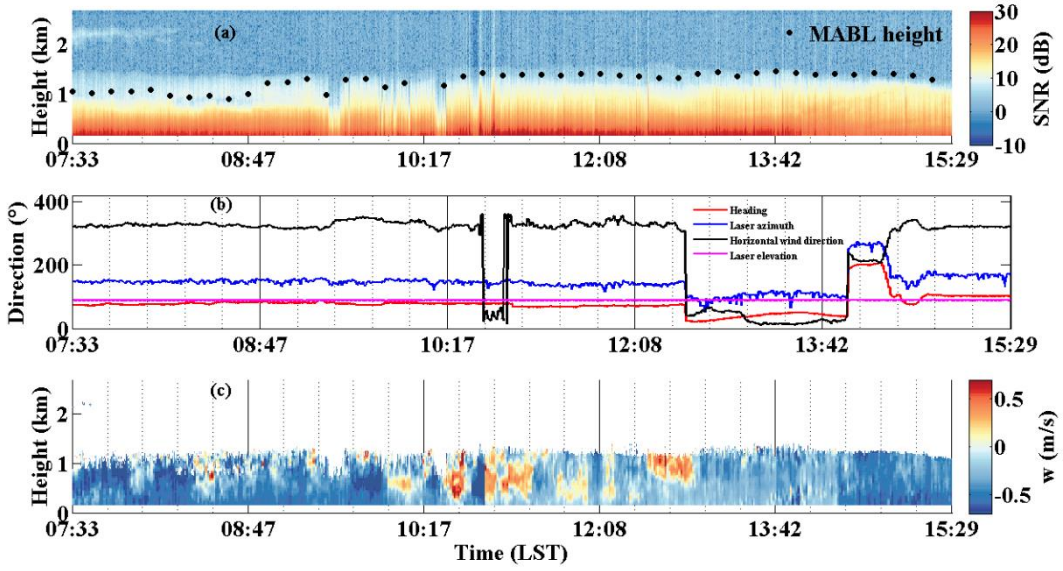

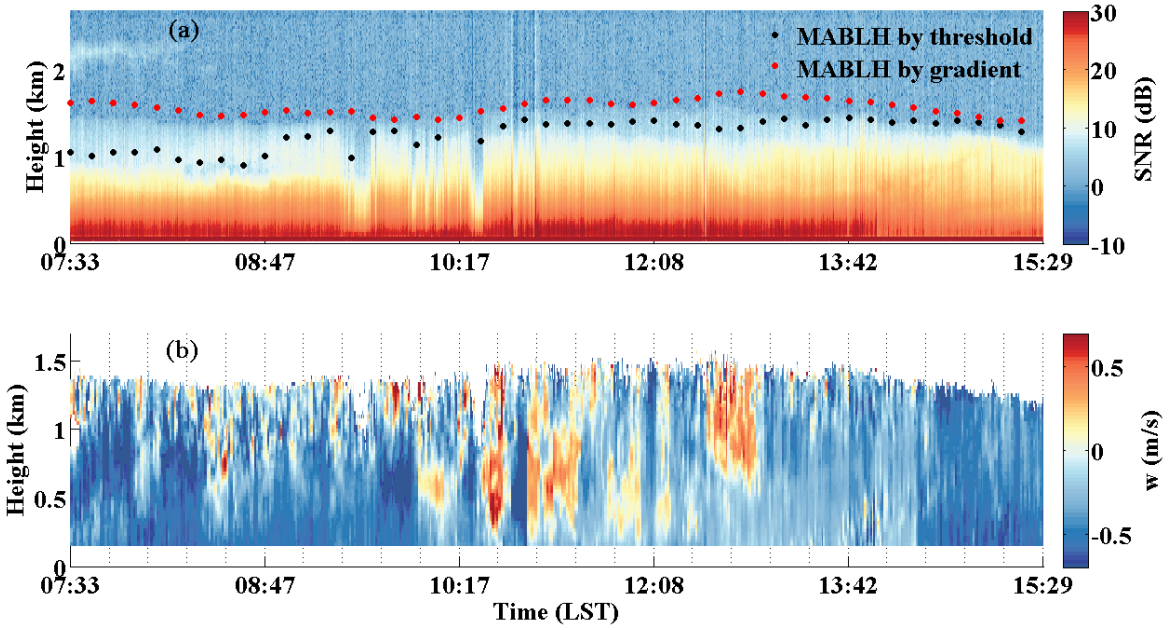

Figure 9~~7~~: Example measurement from 07:33 to 15:29 LST on 14 May 2014: (a) Time-Height-Intensity of SNR and retrieved MABL height using SNR threshold and gradient method (black and red solid circles, respectively). ~~(b) time series of ship heading, CDL laser beam azimuth and elevation in the Earth coordinate system, and horizontal wind direction at 0.4 km.~~ (b~~c~~) Time-Height-Intensity of vertical velocity after attitude correction.

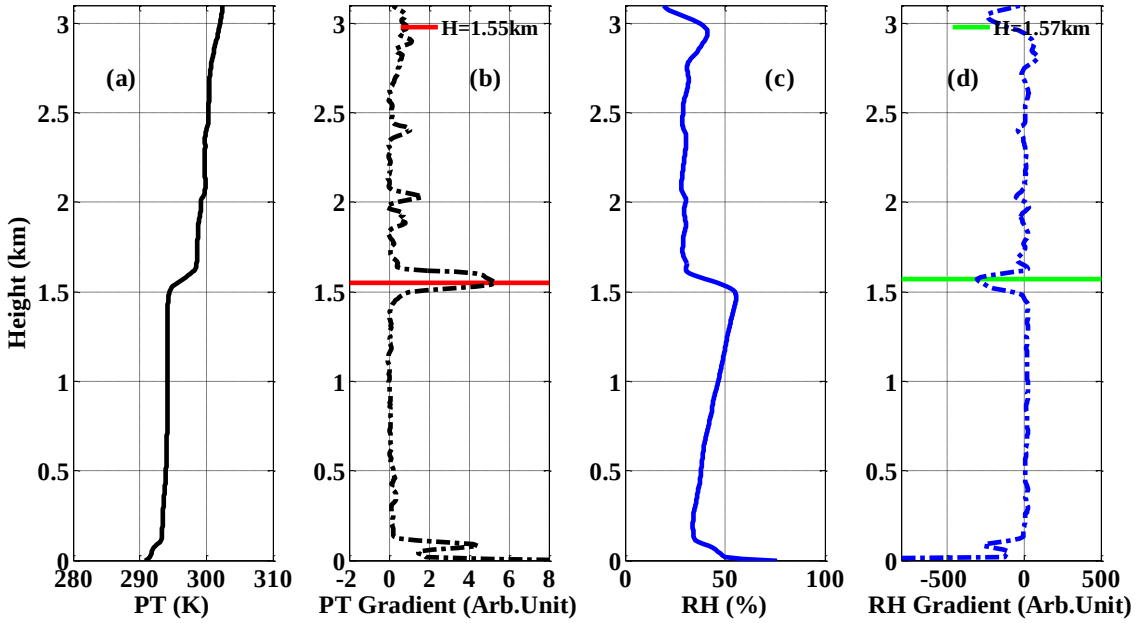

Figure 10: Radiosonde profiles of (a) potential temperature (K) (b) the gradient of potential temperature (c) relative humidity (%) and (d) the gradient of relative humidity at 12:00, LST on 14 May 2014. The horizontal red and green lines in (b) and (c) stand for MABL height retrieved from potential temperature and relative humidity, respectively.

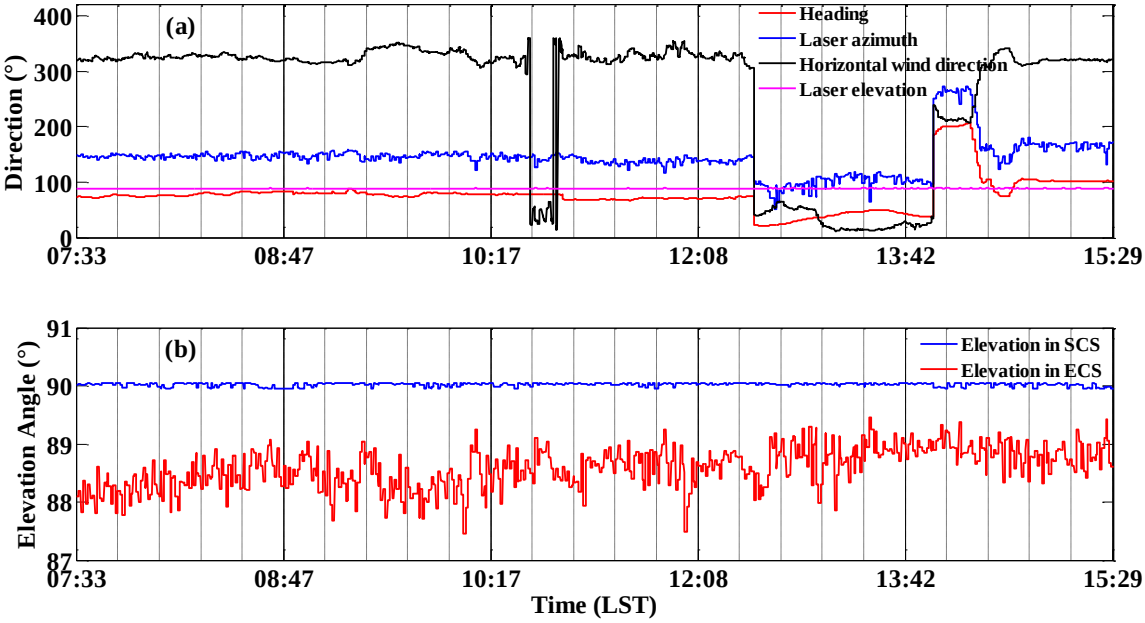

Figure 11: Measurement from 07:33 to 15:29 LST on 14 May 2014: (a) Time series of ship heading, CDL laser beam azimuth and elevation in the Earth coordinate system, and horizontal wind direction at 0.4 km. (b) Elevation angle in zenith stare mode in Ship Coordinate System and Earth Coordinate System.

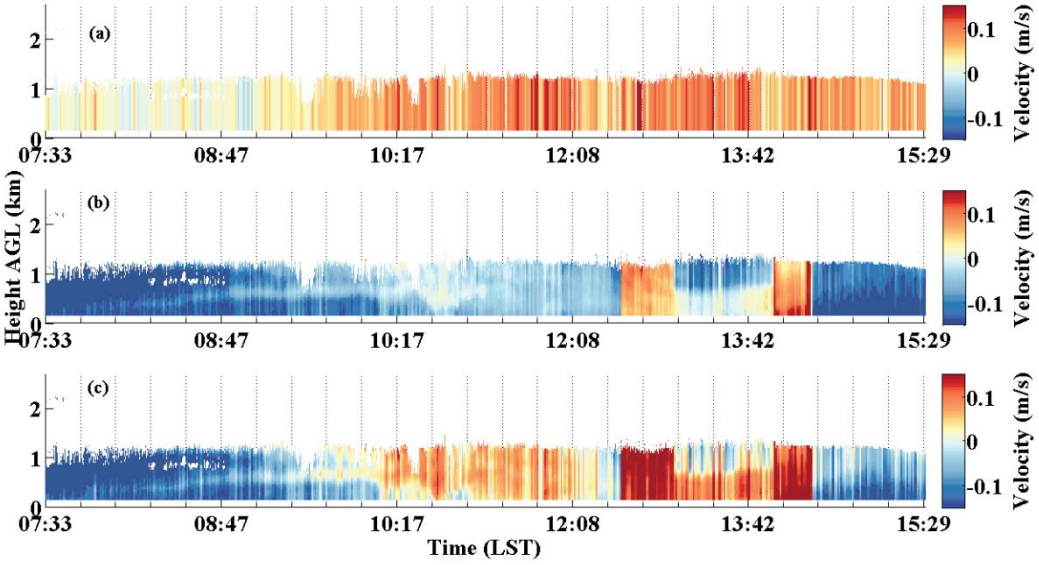

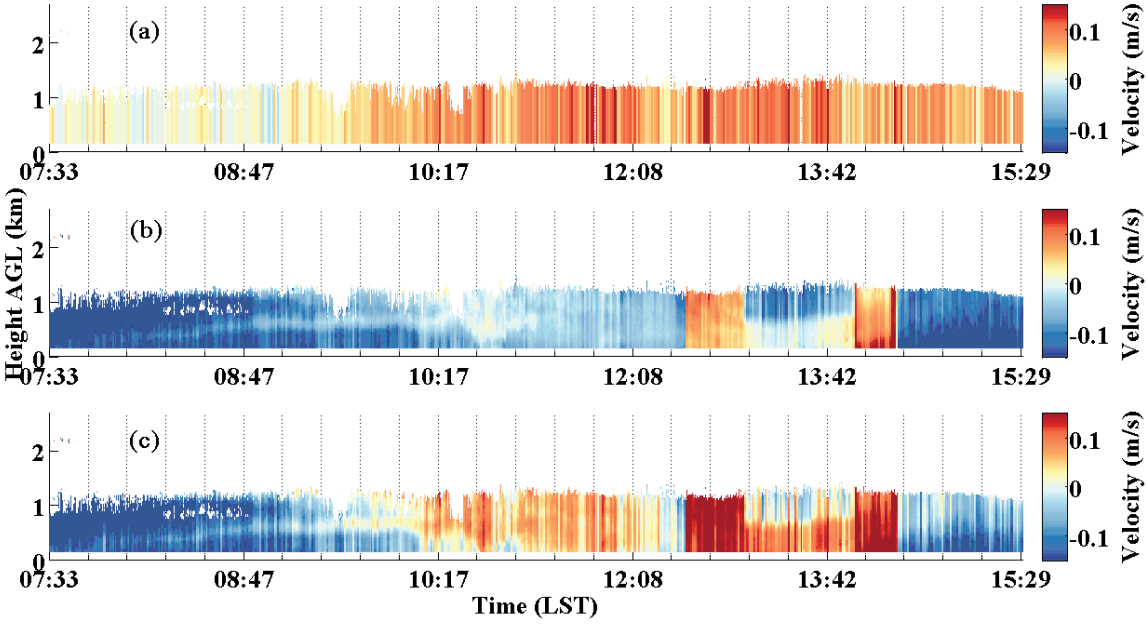

Figure 128: Vertical velocity correction analysis: (a) projection of ship velocity on vertical velocity: $\vec{V}_{LOS\_ship}$ (b) the effect of horizontal wind on vertical velocity: $-\vec{r_g}\cdot\vec{V}$ (c) difference between vertical velocity after attitude correction and vertical velocity before attitude correction.

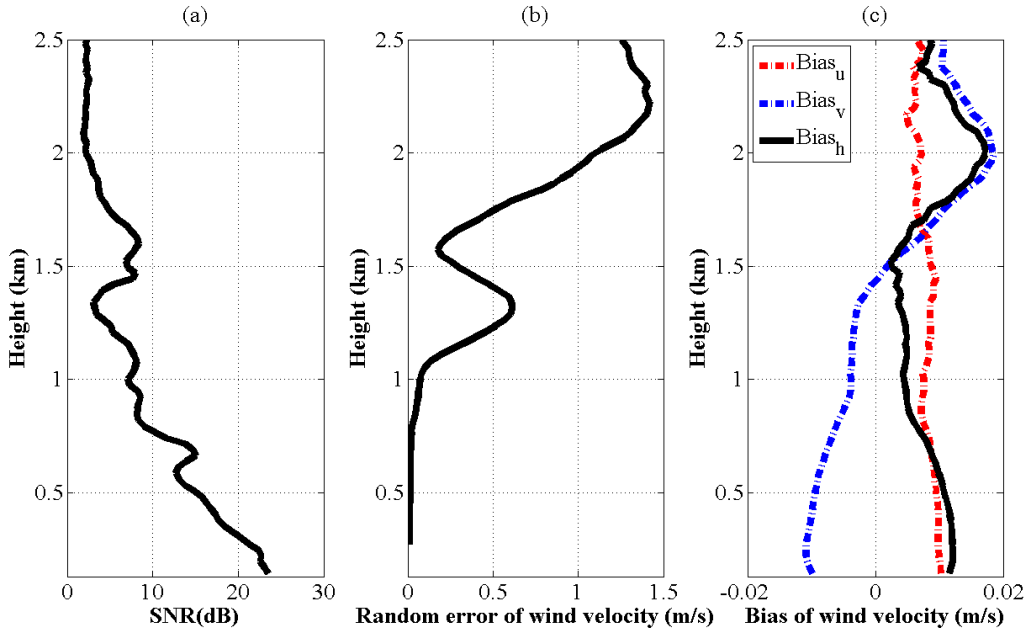

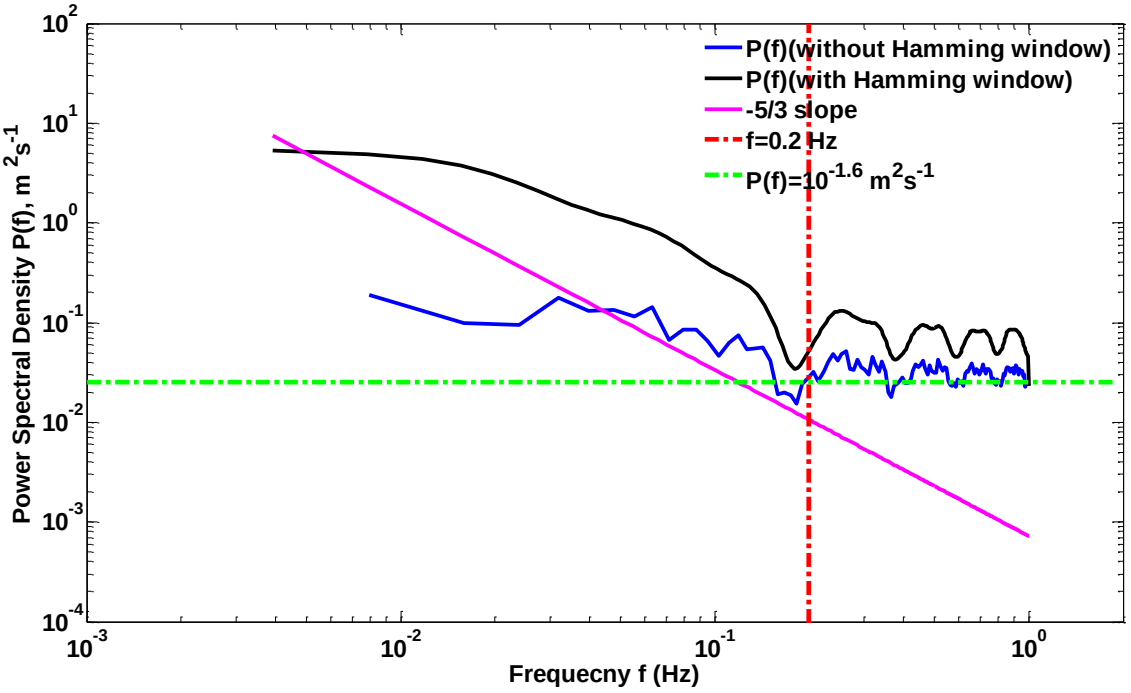

Figure 13: Power spectral density P(f) without and with Hamming window for the CDL measured vertical speed between 15:52 and 16:02 LST on 09 May and for an altitude of 1495 m (blue and black solid line, respectively). The expected spectral behaviour according to the Kolmogorov's−5/3 law (pink solid line), the noise frequency threshold (red dotted line) and the derived noise floor for the CDL (green dotted line) are shown.

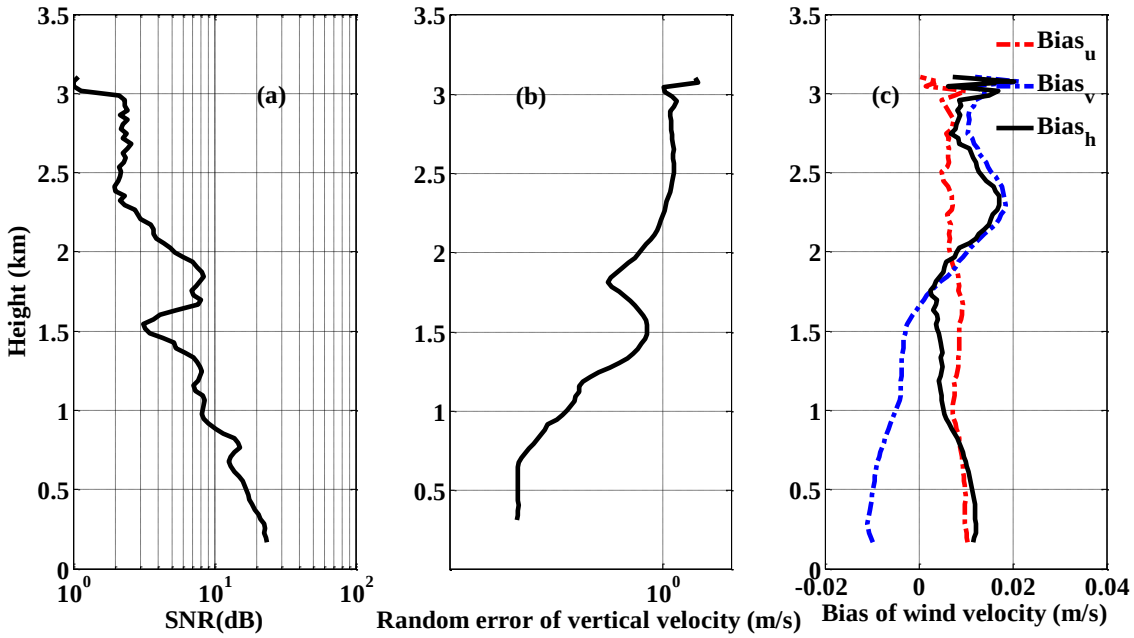

Figure 14~~9~~: The averaged profile of (a) SNR (b) Random error of vertical ~~horizontal wind~~ velocity (c) bias of horizontal wind north-south component (u), east-west component (v) and horizontal wind velocity (h) measured by CDL from 15:52 to 16:02 LST~~,~~ on 09 May, 2014.

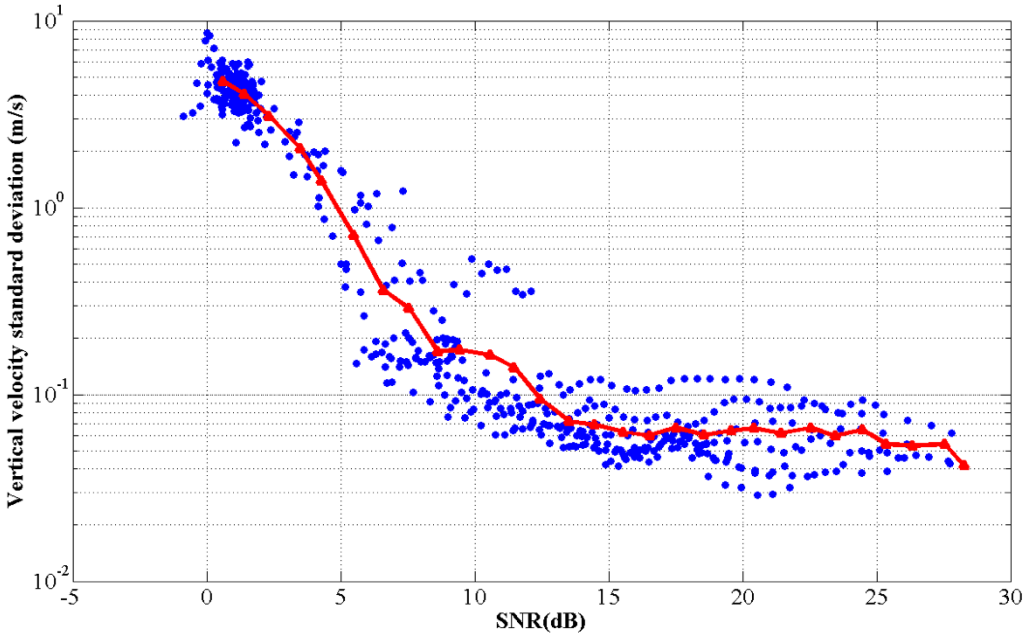
Vertical velocity standard deviation (m/s)
SNR(dB)

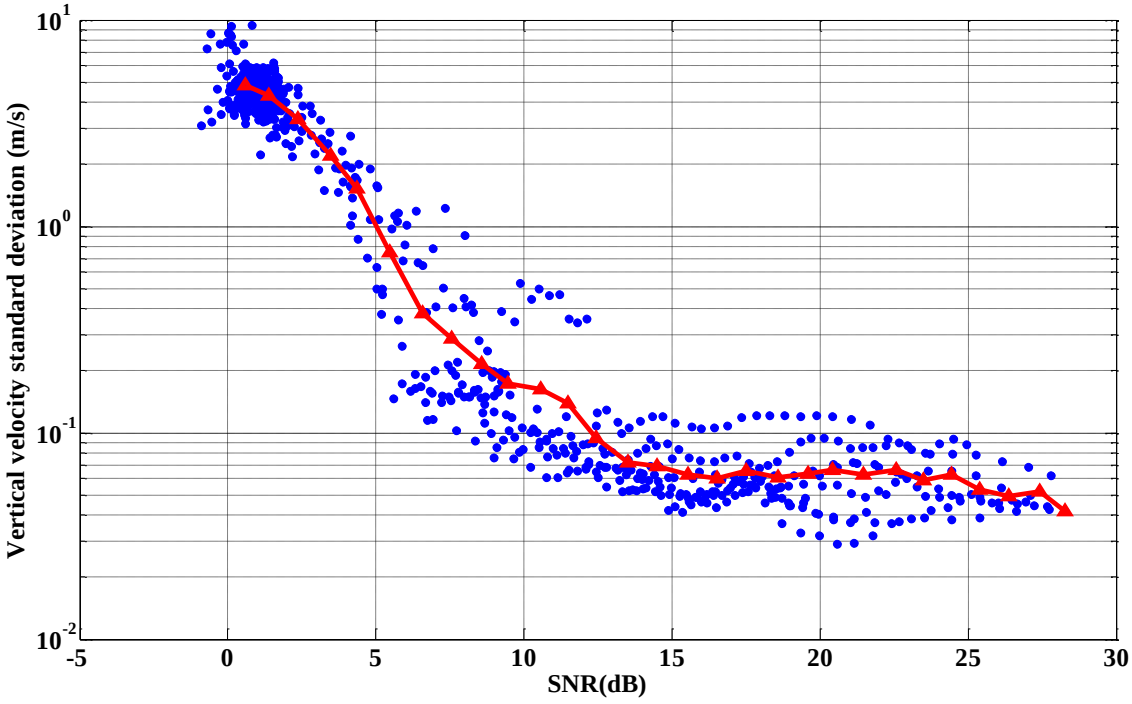
Vertical velocity standard deviation (m/s)
SNR(dB)

Figure 15~~0~~: Random error of the CDL vertical velocity from 07:33 to 15:29 LST on 14 May 2014 in all height range, which is determined as from the frequency spectrum of the retrieved vertical velocity. The averaged random error per SNR bin is shown in red-tringle line.

Table 1: Component Parameters of the CDL system

Qualification	Specification
Wavelength	1.55 μm
Pulse repetition rate	10 kHz
Pulse width	100 ns - 400 ns
Pulse energy	150 μJ
Measurement range	80 m - 4000 m (6000 m maximum)
Range resolution	15 m - 60 m
Speed measurement uncertainty	≤ 0.1 ms^{-1}
Radial velocity measurement range	± 37.5 ms^{-1}
Power Consumption~~dissipation~~	<300 W
weight	~75 kg
Telescope diameter	3 inches
Beam effective diameter	60 mm
Focal length	290 mm

5

Table 2: Component Parameters of the XW-GI5651 MEMS Inertial/Satellite Integrated Navigation system.

System real-time precision	
Heading	0.1° (double antenna mode, baseline length ≥ 2 m)
	0.1° (single antenna, speed > 10 ms^{-1})

Attitude		0.1°				
Position		Single point positioning ≤ 5 m				
		RTK 2 cm + 1 ppm (CEP)				
Data updating rate		200 Hz (configurable)				
Starting time		≤ 10 s				
Alignment time		1~2 min (depending on dynamic maneuvering mode)				
		Double antenna aided orientation time ≤ 1 min				
Post-processing precision						
Heading		0.05°				
Attitude		0.05°				
Position precision	Time to lose lock	0 s	10 s	60 s	300 s	600 s
	Position	0.02 m	0.04 m	3 m	20 m	60 m
Physical properties						
Power consumption		< 7 W				
Working temperature		-40 °C ~ 80 °C				
Overall size		100 mm × 90 mm × 50 mm				
Weight		< 500 g				

Table ~~2~~3: Component parameters of the GTS1 radiosonde

Meteorological Sensor	Specification	Technical Parameter
Temperature	Range	-90 - 50 °C
		0.2 °C (-80 - 50 °C)

	Accuracy (standard deviation)	0.3 °C (-90 - -80 °C)
	Resolution	0.1 °C
Humidity	Range	0% RH - 100% RH
	Accuracy (standard deviation)	5% RH ($T \geq 25^{\circ}C$)
		10% RH ($T \leq 25^{\circ}C$)
	Resolution	1% RH
Pressure	Range	1060 hPa - 5 hPa
	Accuracy (standard deviation)	2 hPa (1050 hPa - 500 hPa)
		1 hPa (500 hPa - 5 hPa)
	Resolution	0.1 hPa

Table ~~3~~4: Ship motion parameters during anchored (first line) and cruising (second line) observations, respectively.

Date period	pitch	Roll	heading	Ship speed
2014.05.09 15:52-16:02	$-0.17^{\circ} \pm 0.06^{\circ}$	$0.63^{\circ} \pm 0.11^{\circ}$	$5.28^{\circ} \pm 1.22^{\circ}$	$0.27 ms^{-1} \pm 0.01 ms^{-1}$
2014.05.13 07:44-07:54	$-0.43^{\circ} \pm 0.05^{\circ}$	$2.06^{\circ} \pm 0.87^{\circ}$	$75.86^{\circ} \pm 1.22^{\circ}$	$4.84 ms^{-1} \pm 0.03 ms^{-1}$

Table ~~4~~5: Statistics of the comparison between CDL and radiosonde at heights of 0.2, 0.4, 0.8, 1.2 and 1.6 km. Normalized RMSE is defined as RMSE divided by the maximum range of the measured values (maximum-minimum).

	Wind speed					Wind direction				
Height (km)	0.2	0.4	0.8	1.2	1.6	0.2	0.4	0.8	1.2	1.6
Number points	84	104	104	87	65	89	93	96	90	88
SD (ms^{-1})/($^{\circ}$)	0.83	0.49	0.46	0.67	0.77	9.77	6.71	8.23	9.39	10.8
Bias (ms^{-1})/($^{\circ}$)	0	-0.1	-0.3	0.26	-0.5	-3.4	-2.7	0	-0.1	-6.3

R	0.97	0.99	0.99	0.98	0.98	0.99	0.99	0.99	0.99	0.98
RMSE (ms^{-1})/($^{\circ}$)	0.83	0.50	0.59	0.72	0.94	10.3	7.22	8.18	9.34	12.5
Normalized RMSE (%)	4.64. 55	2.32. 31	3.33. 32	5.95. 93	7.47. 44	4.34. 27	3.23. 17	3.23. 18	3.4	6.86. 81
Slope	1	0.99	1.04	1.09	1.10	0.99	1.01	1.01	1.09	1.10
Intercept (ms^{-1})/($^{\circ}$)	0	0.2	0.01	-0.9	0.03	4.23	0.77	-1.7	-4.9	5.1